THE UNIVERSITY OF MANITOBA

EFFECT OF PRECIPITATE PARTICLE SIZE ON THE STEADY STATE CREEP DEFORMATION OF INCONEL 718 SUPERALLOY

by

YAFANG HAN

A DISSERTATION SUBMITTED TO THE FACULTY OF GRADUATE STUDIES OF THE UNIVERSITY OF MANITOBA IN PARTIAL FULFILLMENT OF THE REQUIREMENTS OF THE DEGREE OF

DOCTOR OF PHILOSOPHY

DEPARTMENT OF MECHANICAL ENGINEERING

METALLURGY

Winnipeg, Manitoba

October, 1984

EFFECT OF PRECIPITATE PARTICLE SIZE ON THE STEADY STATE CREEP DEFORMATION OF INCONEL 718 SUPERALLOY

BY

YAFANG HAN

A thesis submitted to the Faculty of Graduate Studies of the University of Manitoba in partial fulfillment of the requirements of the degree of

DOCTOR OF PHILOSOPHY

ABSTRACT

The creep deformation behaviour of underaged, peak aged and overaged Inconel 718 superalloy, which is strengthened by coherently ordered disc shaped BCT (DO_{22}) γ'' and spherical FCC (LI_2) γ' precipitates, has been studied in the stress and temperature ranges of 620 - 865 MN/m^2 and 853 - 943 K, respectively. Constant stress, tensile creep tests were used to measure the values of steady state creep rate, $\dot{\varepsilon}_s$, and the consecutive stress reduction method was used to determine the values of back stress. Transmission electron microscopy was used to measure the particle sizes of the γ'' and γ' phases and to observe the dislocation structures of crept specimens.

The dependence of $\dot{\varepsilon}_s$ on particle size, $d\gamma''$ shows that the steady state creep rate decreases with increase in particle size until a critical particle size is reached. Upon further increase in particle size the creep rate increases with particle size. The minimum secondary creep rate, $\dot{\varepsilon}_s$, is obtained when the particle sizes are $d\gamma'' = 23.2$ nm and $d\gamma' = 13.7$ nm.

The creep deformation mechanism of peak aged material has been studied in the above stress and temperature ranges by determining the values of effective stress exponent and

activation energy. The values of n_e and Q_e suggest that the creep deformation mechanism changes from diffusional creep ($n_e \simeq 1$) at 853 - 873 K to dislocation power law creep (n_e = 5.12) at 943 K in the stress range of 620 - 720 MN/m^2. On the other hand at the temperature of 873 K the creep mechanism changes from diffusional or linear creep ($n_e \simeq 1$) at applied stresses below 720 MN/m^2 to power law creep (n_e = 5.10) in the stress range 765 - 840 MN/m^2. The values of n_e also show that there exists a transition region between linear creep and homogeneous power law creep since the values of n_e change from 1.12 to 5.65 continuously when either the temperature or the applied stress increases.

The values of back stress in the stress range of 620 - 865 MN/m^2 and the temperature range 873 - 923 K have also been determined. The results show that the values of back stress are as high as 0.6 - 0.9 σ_a, where σ_a is the applied stress. In the diffusional creep region, there exists a threshold stress, $\sigma_{o(th)}$. While in the high stress region or power creep region ($\sigma_a \geq 746$ MN/m^2), the back stress, σ_o, is proportional to the applied stress, σ_a. The dependence of threshold stress, $\sigma_{o(th)}$, on particle size, dγ", in the stress range $\sigma_a < 720$ MN/m^2 and at a temperature of 873 K reveals that in the underaged region $\sigma_{o(th)}$ increases with increase in particle size until a maximum $\sigma_{o(th)}$ is reached. $\sigma_{o(th)}$ then decreases with further increase in particle size.

The comparison of experimentally measured threshold stress, $\sigma_{o(th)}$ with theoretically calculated values of σ_o suggests that in the small particle size region Harris model involving the formation and punching of prismatic dislocation loops operates the diffusional creep process, while in the large particle size region Ashby's model of grain boundary edge dislocation climb controls the diffusional creep process.

ACKNOWLEDGEMENTS

I would like to express my appreciation to my supervisor, M.C. Chaturvedi, for his precious guidance and genuine help and his financial support.

I am also grateful to Dr. J. Cahoon for his helpful suggestion and discussion, and I would like to express my thanks to Mr. John Van Dorp, Mr. Don Mardis and Mr. Roy Hartle for their generous technical assistance. I would also like to thank the University of Manitoba for providing me a university graduate fellowship, and the Government of the People's Republic of China and Institute of Aeronautical Materials, Beijing, China for giving me leave-of-absence.

Finally, I would like to express my appreciation to my husband Mr. Xiaobao Huang for his patience and endless encouragement during my study.

CONTENTS

CHAPTER 4 RESULTS

CHAPTER 5 DISCUSSION

LIST OF SYMBOLS

b	Burgers vector or lattice spacing
C_o	equilibrium vacancy concentration
$\dot{c}$	climb rate of dislocations
D	diffusion coefficient of atoms
d	particle size (diameter)
E	Young's modulus
ε	plastic strain
$\dot{\varepsilon}_s$	Steady state creep rate
G	shear modulus
γ	stacking fault energy
$\bar{h}$	strain hardening coefficient
k	Boltzmann's constant, $k = 1.38 \times 10^{-23}$ joule/°C
L	grain size
L_F	length of Frank-Read Source
L_p	average free path of dislocation motion
ℓ	subgrain size
λ	interparticle spacing
M	mobility of dislocations
n_a	apparent stress exponent of creep rate equation
n_e	effective stress exponent of creep rate equation
Q_c	apparent activation energy for creep process
Q_e	effective activation energy for creep process
Q_d	activation energy for self diffusion

r	recovery rate during creep
R	gas constant R = 8.31 Joule/mol, °C
r_p	radius of precipitate particles
ρ	dislocation density
σ_a	applied stress
σ_e	effective stress
σ_o	back stress or threshold stress
σ_i	internal stress due to strain hardening
T	absolute temperature
T_m	melting point
Γ	dislocation line tension
V	volume fraction of precipitates
X	length of dislocation pile-up
y	distance between two adjacent pile-ups

LIST OF TABLES

LIST OF FIGURES

CHAPTER 1 INTRODUCTION

Components for high temperature operation usually require creep resistance and one or more of such material properties as stress rupture resistance, high and low frequency fatigue resistance, oxidation and corrosion resistance, and other specific physical and mechanical properties. Creep resistance is nearly always required because a significant average stress is usually maintained for prolonged periods during most high temperature applications. Therefore the study of creep behaviour and mechanisms is of great importance.

Creep is the continuing plastic deformation of materials subjected to a constant load or constant stress. Theoretically, above absolute zero, any stress will cause polycrystalline material to flow. At lower temperatures substantial plastic deformation occurs only when the applied stress exceeds the yield strength. However, at higher temperatures creep plastic flow can take place with time at stresses well below the yield strength. This is due to the fact that as temperature increases more thermal energy is available to assist the applied mechanical energy in causing dislocations to move and grain boundaries to slide, resulting in creep deformation. Therefore, creep can be defined as thermally assisted, time-dependent plastic deformation of materials. Creep in an engineering sense refers to the slow

and time dependent plastic deformation caused by prolonged loading below the yield stress at high temperature, generally above 0.5 T_m where T_m is the melting point.

There are several ways to decrease the creep rate, including increasing the general resistance to plastic flow by strengthening, decreasing the diffusion coefficient, decreasing the stacking fault energy or increasing the elastic modulus. Solid solution strengthening by solute additions is therefore one way of increasing creep resistance. However, a more effective method of improving the creep resistance of a metal is to introduce finely dispersed second phase particles. The development of these two-phase alloys along with advanced processing techniques such as unidirectional solidification and high strength fibre reinforcing composite materials has made possible an average increase of 10 K per year in operating temperature over the last 40 years[1].

Many of the successful creep resistant alloys are nickel and cobalt base superalloys strengthened by coherent precipitates of γ' and γ'' phases or by oxide dispersoids. The creep behaviour and mechanisms of dispersed oxide and ordered coherent γ' precipitate strengthened superalloys have been extensively studied. However there seems to be no published work in this field on superalloys strengthened by coherent ordered BCT γ'' precipitate particles. The

commercial alloy Inconel 718 is a nickel base superalloy precipitation hardened by ~ 17% volume fraction of disc shaped coherent ordered BCT γ'' phase and spherical FCC γ'' phase particles. This alloy is widely used as hot end parts for gas engines, such as turbine blades, discs or cases. The creep crack growth behaviour of Inconel 718 has been studied earlier[2], and the coarsening behaviour of γ'' and γ' precipitates, the room temperature deformation behaviour and strengthening mechanism have been investigated recently[3-5]. Therefore, research was initiated to study the creep deformation behaviour of Inconel 718 alloy.

The main objectives of this investigation were to study:

1. the creep behaviour and deformation mechanism in the steady state creep stage of Inconel 718 containing various particle sizes;

2. the effect of particle size on creep rate;

3. the effect of particle size, temperature and applied stress on back stress or threshold stress.

This dissertation presents a review of the relevant literature in Chapter 2 and the details of the experimental techniques used in Chapter 3. In Chapter 4 the results of the creep deformation of this alloy are presented.

In Chapter 5 the results are discussed in light of various theories developed to explain the creep deformation behaviour of precipitation hardened alloys.

CHAPTER 2. LITERATURE REVIEW

2.1 General view of elevated temperature creep.

2.1.1 Typical creep curves.

The shapes of creep curves, which are shown schematically in Figure 1 depend on many factors, such as, composition and structure of materials, heat-treatment schedule and deformation history of samples, testing temperature and applied stress level.[6,7] In general, there are three stages during the creep process. The first stage of creep is known as primary creep where the material is

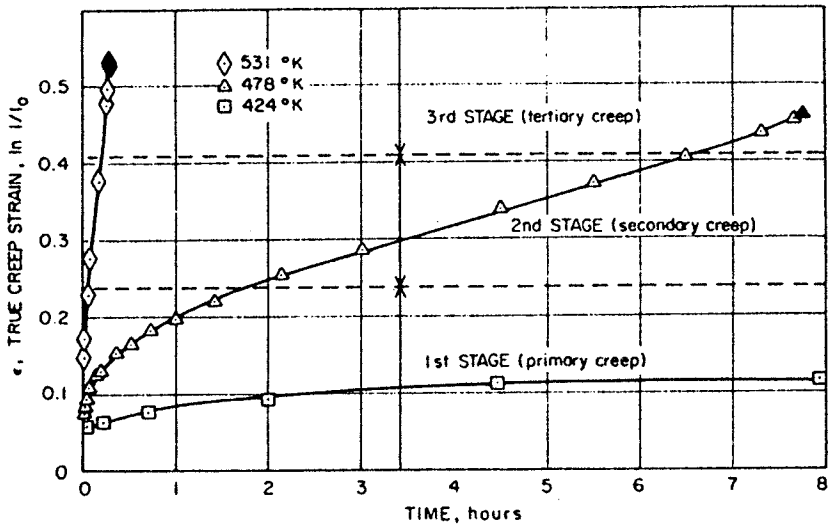

Figure 1. Typical creep cures for high purity aluminum in tension and the tests performed under constant stress of σ = 20.7 MN/m^2 (3000psi)[6].

strain hardening and the creep rate is decreasing with time. At the beginning of the first stage the strain rate is usually very high for annealed metals since barriers to

dislocation motion are very few and largely ineffective i.e., most of the initial dislocations are not impeded and move easily. Upon loading, deformation proceeds and dislocation entanglements and cells are produced. These lead to strain hardening and hence the strain rate decreases with time. The cells and entanglements disperse later either through recrystallization or dynamic recovery processes, such as cross-slip and climb of dislocations.

In the second stage of creep, known as steady state creep, the creep rate remains constant. This steady state creep is obtained when a balance is reached between the rate of strain hardening, (i.e. generation of creep-resistant substructure) and the rate of thermal recovery, by such processes as cross-slip, climb or recrystallization under an applied stress.

The third stage, tertiary creep, represents the regime of runaway creep rate which is quite often associated with localized necking due to the stress concentration, the formation of cavities (especially at grain boundaries which are at right angle to the tensile stress) and also with structural instabilities such as overaging, grain growth or harmful second phase formation in some alloys.

Secondary creep is the most important stage as most elevated temperature materials are designed so that they spend their service lives in this stage. In fact, the term creep strength generally refers to the steady state creep

rate. Therefore the mechanical behaviour and micromechanism of steady state creep only will be discussed in this chapter.

2.1.2 General law of secondary creep.

The overall steady state creep rate, $\dot{\varepsilon}_s$, consists of rates of diffusional creep, $\dot{\varepsilon}_{diff}$, grain boundary sliding creep, $\dot{\varepsilon}_{gbs}$, and dislocation or intragranular creep, $\dot{\varepsilon}_{disl}$ [1], i.e.

$$\dot{\varepsilon}_s = \dot{\varepsilon}_{diff} + \dot{\varepsilon}_{gbs} + \dot{\varepsilon}_{disl}. \qquad (2.1)$$

Depending on the testing temperature and stress, one or two of these mechanisms will be predominant. The dependence of the secondary creep rate, $\dot{\varepsilon}_s$, on applied stress and temperature is basic to an understanding of creep.

2.1.2.1 Temperature dependence of creep and activation energy for the creep process.

As mentioned earlier, creep is a thermally activated process and accordingly the temperature sensitivity should essentially obey an Arrhenius type expression with a characteristic activation energy for the rate controlling process, i.e.

$$\dot{\varepsilon}_s = f(\sigma)\exp(-Q_c/RT) \qquad (2.2)$$

where σ_a is the applied stress, Q_c is the activation energy for the creep process, T is the absolute temperature and R is

the gas constant. It has been experimentally established that the activation energy for creep, Q_c, is a function of temperature [9,10] and stress or strain rate[11,12] and is generally independent of strain unless a change in deformation mode occurs[8].

A typical relationship between temperature and activation energy, Q_c, is shown in Figure 2[6]. At lower

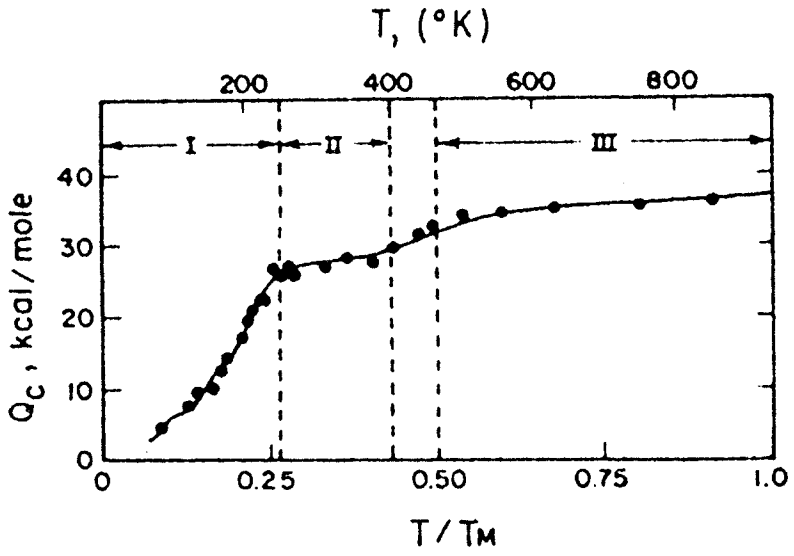

Figure 2. Activation energy for creep of pure aluminum as a function of temperature(6).

temperatures, i.e., $T < 0.25\ T_m$, where T_m is the melting point, Q_c decreases with decreasing temperature and the most likely mechanism (rate controlling process) of creep is considered to be the dislocation intersection process or the process of overcoming the Peierls-Nabarro stress. In the temperature range $0.25 - 0.5\ T_m$, the activation energy for creep is less than that for self diffusion and the rate controlling process of creep has been generally considered to

be the cross-slip of screw dislocations and the interaction of dislocations with other dislocations and interstitials[10,13]. When the temperature increases to above 0.5 T_m the activation energy for creep appears insensitive to temperature and for many metals and solid solution alloys has been found to be nearly equal to the activation energy for self diffusion i.e., $Q_c \simeq Q_d$[8,14-16]

Figure 3 shows a one-to-one relation between Q_c and Q_d for a number of pure materials. This suggests that the most likely mechanism of creep at a temperature above 0.5 T_m is dislocation climb which is rate-controlled by the self diffusion of atoms. An alternative mechanism of creep at high temperature has been considered to be the nonconservative motion of jogs in screw dislocations, which is also rate-controlled

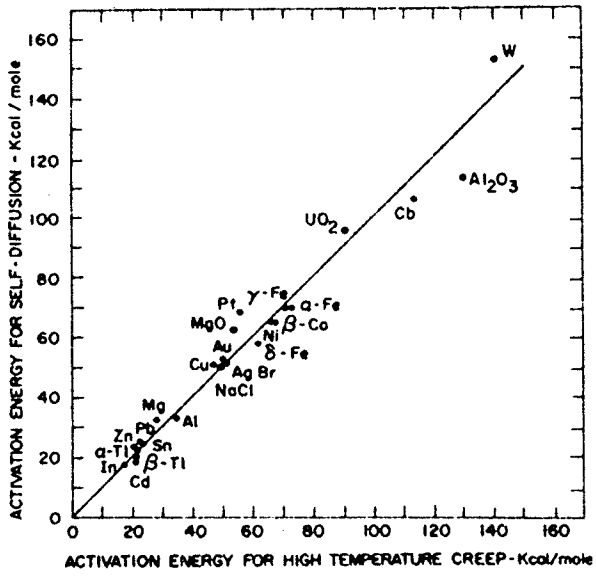

Figure 3. Relation between activation energy for creep, Q_c and activation energy for self-diffusion, Q_d, for pure materials, where Q_c were obtained near 0.5 T_m[6].

by the self diffusion of atoms. Therefore the steady state creep rate can be expressed as:

$$\dot{\varepsilon}_s = K\ D\ f(\sigma_a)\ . \qquad (2.3)$$

In equation (2.3), D is the diffusion coefficient given by $D = D_o \exp(-Q_d/RT)$ where $D_o \simeq a_o^2 V$, a_o being the lattice parameter and V the vibrational frequency of atoms.

The effect of creep strain rate on activation energy, Q_c, is shown in Figure 4. As the strain rate increases, the plot of Q_c vs. T shifts to the right. This suggests that dislocation climb does not control the deformation process at high strain rates and temperatures > 0.5 T_m. The reason for

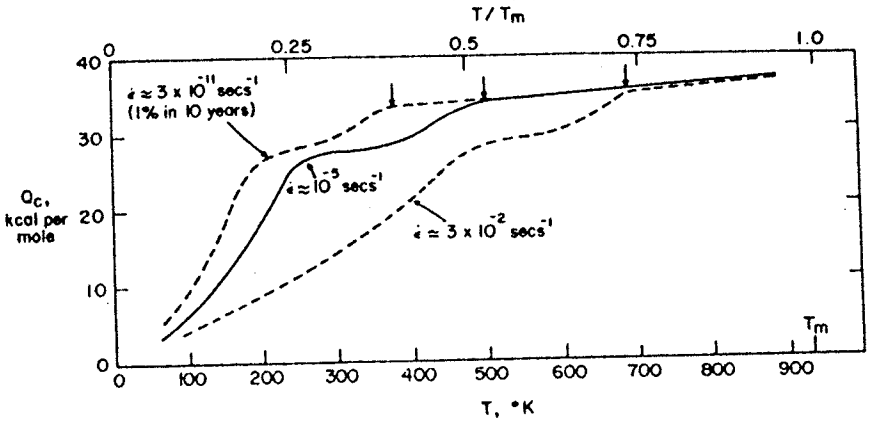

Figure 4. The effect of creep rate on the activation energy which has been shown in Figure 3(6).

this is that there is little time available (since the rupture life is very short) for a diffusion controlled process to contribute to deformation at such high strain rates. Therefore other deformation mechanisms, such as cross-slip will be preferred. At sufficiently high temperatures, however, atomic mobility will be high enough to permit dislocation climb to be the rate controlling process again, hence $Q_c \simeq Q_d$ when the temperature is higher than a critical value.

2.1.2.2. Stress-dependence and influence of material parameters on steady state creep rate.

Stress has a major effect on the creep rate. The stress-dependence of the creep rate for typical polycrystal metals at temperature above 0.5 Tm is schematically shown in Figure 5. At the low stress level (region I), where $\dot{\varepsilon}_s/D \leq 10^2$, $\dot{\varepsilon}_s$ is proportional to the applied stress, i.e. $\dot{\varepsilon}_s \alpha \sigma$. The intermediate stress law (region II), $\dot{\varepsilon}_s \alpha \sigma^n$, where n = 3-7, is valid for the values of $\dot{\varepsilon}_s/D = 10^2 \sim 10^9$. In the high stress range (region III) where $\dot{\varepsilon}_s/D > 10^9$, $\dot{\varepsilon}_s$ can be expressed as $\dot{\varepsilon}_s \alpha e^{\beta\sigma}$, where β is a material constant.

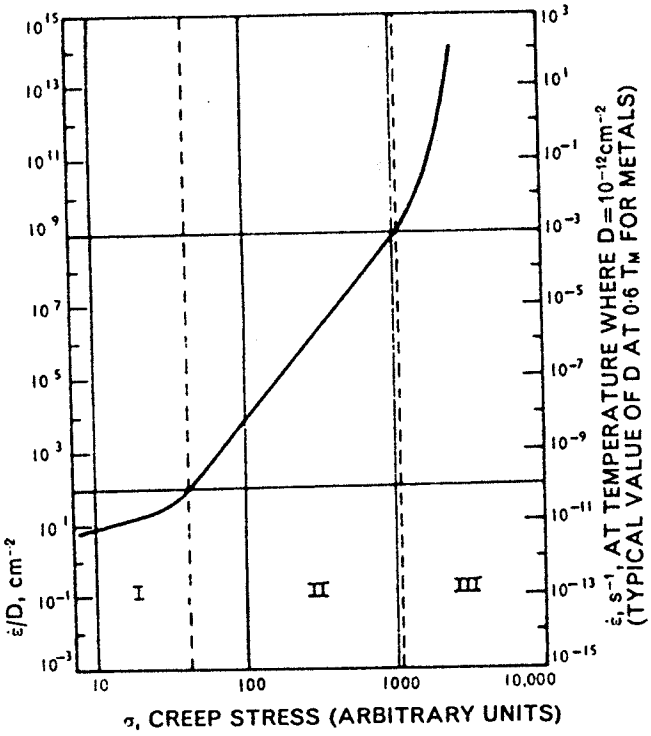

Figure 5. Influence of stress on the diffusion-compensated steady state creep rate for a typical polycrystalline metal[6,8].

1. Low stress creep range (Diffusional creep)

The steady state creep rate, $\dot{\varepsilon}_s$, varies linearly with stress at low stresses. This type of creep results from a stress-directed atom migration process; i.e., the diffusion of vacancies from regions of high chemical potential at grain boundaries subjected to normal tensile stress to regions of

lower chemical potential where the average tensile stress across the grain boundaries is near zero. The migration of atoms in the opposite direction of the migration vacancies accounts for the creep strain as shown in Figure 6. The

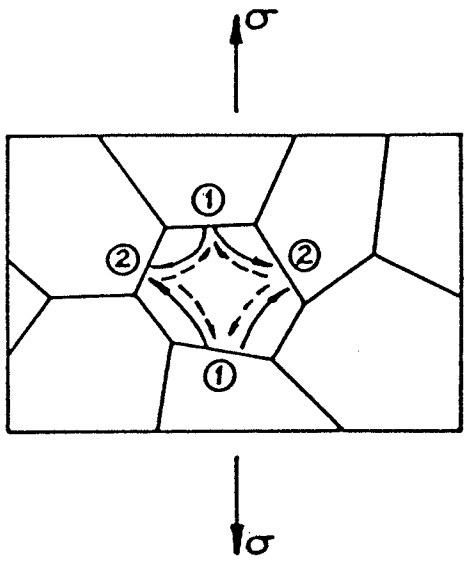

Fig. 6. Schematic showing stress-biased flux of vacancies (-) and atoms (----) resulting in diffusional creep[1].

volume-diffusion controlled process is known as Nabarro-Herring creep and the grain boundary diffusion controlled process is termed Coble creep[17]. The expression for the creep rate as a consequence of this stress-directed diffusional flux have been derived by Nabarro[18], Herring[19] and Coble[20]. The general form of the expressions is given by[1]

$$\dot{\varepsilon}_s = \dot{\varepsilon}_{diff} = C\, D_{v.g}\, b^3\, \sigma_a / KT\, L^n \qquad (2.4)$$

where L is the grain size, n = 2 for volume diffusion and n=3 for diffusion along grain boundaries. $D_{v.g}$ is the volume or grain boundary self-diffusion coefficient, b is the lattice

spacing and C is a geometrical constant having estimated values of 8[18] to 5[21] depending on the grain boundary condition. As stated earlier, the Nabarro-Herring and Coble creep processes involve the migration of atoms through grains or along grain boundaries and dislocation slide or climb at grain boundaries. Therefore, diffusional creep predominates in fine-grained materials.

2. Intermediate stress creep range (power law creep)

In this stress range, creep is believed to be controlled by either climb of edge dislocations or the non-conservative motion of jogs in screw dislocations which are further controlled by the recovery of dislocation structures for most metals and many solid solution alloys[6,7,22,23]. Although several empirical expressions have been suggested for the steady state creep rate in this stress range, $\dot{\varepsilon}_s$ can usually be represented as a power of the applied stress,[1,6-8,17,24-29]

$$\dot{\varepsilon}_s = A_1 \sigma_a^{n_a} \exp(-Q_c/RT) \qquad (2.5)$$

where n_a is a constant with a value of 3-7 for various solid solution alloys and pure metals.

McLean and Hale[40] made the important observation that the value of the constant A_1 for various metals and alloys depends on their elastic moduli, E, and give the following expression for $\dot{\varepsilon}_s$

$$\dot{\varepsilon}_s = A_2 (\sigma_a/E)^{n_a} \exp(-Q_c/RT) \qquad (2.6)$$

where E is Young's modulus.

Extensive experimental studies on creep deformation of polycrystalline metals[2,30,31] and creep theories developed by Weertman[15,32,33] and Sherby[6] indicate that the creep rate in this stress range is proportional to the diffusion coefficient and is a function of elastic modulus and stacking fault energy, i.e.

$$\dot{\varepsilon}_s = A_3 D\gamma^{3.5}(\sigma_a/E)^5 \qquad (2.7)$$

where γ is the stacking fault energy. The decrease in creep rate with decreasing SFE has been attributed to the fact that the more widely separated dislocations (due to the lower SFE) have a greater difficulty in climb because the partials must combine before their climb becomes possible, and the creep rate is reduced proportionately[6]. Weertman[32] suggested that climb is easy in high SFE materials, such as aluminum and nickel, where the dislocations are not extented, because diffusion is rapid along such a dislocation line (because of the high distortion in a perfect dislocation) and hence dislocation climb is relatively easy. The steady state creep rate in the power law creep range is not very sensitive to the grain size although $\dot{\varepsilon}_s$ increases with decreasing grain size in the small grain size region, say $d \leq 0.1$mm[6,34]. This effect is attributed to the increasing importance of grain boundary sliding.

After comparing all equations on creep rate and further considering the dimension of the equations and

taking the temperature effect into account, Mukherjee et al[7,35] suggested the relationship

$$\dot{\varepsilon}_s = A' (\sigma_a/G)^n a^{-1} (\sigma_a \Omega/KT) \exp(-Q_c^*/RT) \qquad (2.8a)$$

where G is the shear modulus, Q_c^* is the activation energy for creep and Ω is an activation volume for creep. Since high temperature creep is diffusion-controlled, the secondary creep rate can be written as

$$\dot{\varepsilon}_s = A'' (\sigma_a/G)^n a(GbD/KT) \qquad (2.8b)$$

or $$\dot{\varepsilon}_s = A (\sigma_a/G)^n a(Gb/KT)\exp(-Q_c/KT) \qquad (2.8c)$$

where b is Burgers vector, A', A" and A are constants, and $Q_c \simeq Q_d$ for most pure metals and solid solution alloys.

3. High stress creep range

High stress creep, region III in Figure 6, begins at stresses where the power law breaks down, and the stress dependence of the creep rate is greater than that predicted by the power law creep equation. Such a high strain rate may be attributed to the following two factors. Firstly, at high stress levels, many excess vacancies might be generated by the dislocation intersection process. Such excess vacancies will enhance dislocation climb and therefore make creep easier. Weertman[15] and Barrett and Nix[23] proposed that the rate of creep is proportional to the vacancy concentration gradient, i.e. $\dot{\varepsilon}_s = KC_o[\exp(n\sigma b^3/KT) - \exp(-n\sigma b^3/KT) = K'\sinh(n\sigma b^3/KT)$. $C_o \exp(n\sigma b^3/KT)$ and $C_o \exp(-n\sigma b^3/KT)$ are the concentrations of vacancies at a vacancy generating dislocation and a vacancy absorbing dislocation

respectively, C_o is the equilibrium vacancy concentration, n is a stress concentration factor equal to 1.0 in the Barrett - Nix theory and equal to $\sigma x/bGT$ in Weertman theory. X is the length of dislocation pile-up ($X \alpha \sigma^{1/2}$) and K and K' are constants. Secondly, deformation at high strain rates can lead to adiabatic heating. Under such conditions the deforming materials may become continually weaker with straining since the testing temperature increases with rapid deformation.

Garofalo[26] has proposed an empirical relation of the form

$$\dot{\varepsilon}_s = K(\sinh \beta\sigma)^n \qquad (2.9)$$

for both stress range II and III although different creep mechanisms control these two stress ranges. In this expression β and K are constants. It can be shown that equation (2.9) becomes $\dot{\varepsilon}_s = K'\sigma^n$ at low stress levels and becomes $\dot{\varepsilon}_s = K'' \exp(\beta\sigma)$ at higher stress levels.

2.2 Mechanisms of secondary creep

2.2.1 Structural characteristics during creep

The dislocations produced during creep are arranged in the form of a complex three dimensional network, as shown in Figure 7.

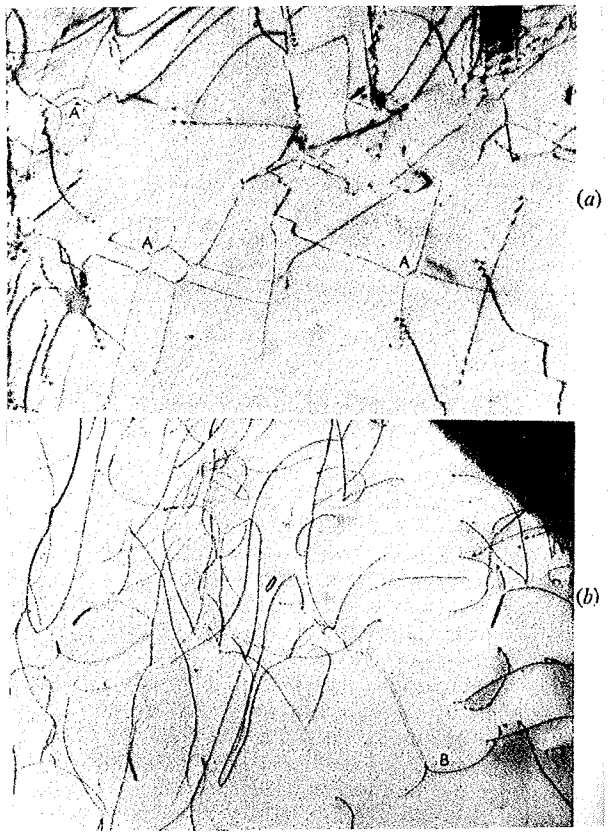

Figure 7 Dislocation Structure during creep of a 20% Cr - 35% Ni steel at 973K. (a) 110 MN/m^2; (b) 150 MN/m^2. Where sites marked A are dislocation attractive junctions and site marked B is dislocation repulsive junction[8].

The density of dislocations in this network-like structure increases gradually in the primary creep stage and takes a constant value in the secondary stage.

Subgrain formation is the typical structural feature of high temperature creep for pure metals and single phase alloys. This is a well defined structure and different from the cell walls comprising tangled dislocations observed during lower temperature deformation. Analogous to the dislocation network, the subgrain structure forms during the primary stage and is fully developed at the transition

between the primary and secondary stages. The subgrain size remains constant during the entire secondary stage[36]. The subgrain size, ℓ, decreases with creep rate, i.e., $\sigma = \sigma_c + K\ell^{-m}$, where $m \approx 1$[6,8,36], and K and σ_c are material constants. It is believed[8] that the stacking fault energy has a marked influence on the formation of subgrains. The higher the stacking fault energy the easier the subgrain formation, hence the finer the subgrain size.

2.2.2 Origin of strain hardening and thermal recovery during creep

As mentioned before, primary and steady state creep are the result of work-hardening and recovery. Therefore these two phenomena will be discussed next.

1. Strain hardening

The strain hardening coefficient h, or $\bar{h}$, is defined as $h = \partial\sigma_i/\partial\varepsilon$ or $\bar{h} = \partial\rho/\partial\varepsilon$[8,37,38], where σ_i is the internal stress due to strain hardening, ρ is the dislocation density, and ε is the strain. There are three sources of resistance to the movement of dislocations which contribute to strain hardening during creep[22]. The first one is the stress field arising from other dislocations. The magnitude of this stress for unextended dislocations is about $(0.1 - 0.2)\ Gb\sqrt{\rho}$. The second factor is due to the subgrain boundaries, which contribute to the stress field to resist the movement of dislocations. Subgrain boundaries continually receive fresh dislocations during creep. Since only part of these fresh

dislocations can be immediately absorbed in subgrain boundaries a long-range stress will be produced by those dislocations which cannot be absorbed. The resistance due to this effect for unextended dislocations is also equal to ~ $0.2\ Gb\sqrt{\rho}$. The third source of resistance is the generation of lattice defects, such as, dislocations, stacking fault, vacancies, interstitials and jogs. All these defects carry extra energy, which can be supplied only by an applied stress. The rate of production of most of these defects depends on the frequency of dislocation intersections and therefore depends on the density of dislocations. This suggests that the resistance from this source also has a value of $\sim 0.2\ Gb\sqrt{\rho}$.

2. Thermal recovery

The Thermal recovery rate, r, is given by $r = -\partial\sigma_i/\partial t$. There are two basic recovery processes during creep i.e., cross-slip of screw dislocations and climb of edge dislocations. Both these processes lead to dislocations with opposite signs in nearest planes which annihilate each other. Both cross-slip and climb are accelerated by an increase in stress and temperature. It has been found that the rate of climb varies with stress, and the frequency of cross-slip is considerably more sensitive to stress. Since climb involves self diffusion and the activation energy for creep at temperatures higher than $0.5\ T_m$ equals that for self diffusion in most pure metals and solid solution alloys, it

is believed that climb is the most important process during high temperature creep and is thus rate controlling.

2.2.3 Theoretical models of secondary creep

1. Dislocation climb model

Among all the high temperature creep models, the climb of dislocations may be the most important step as it must necessarily play a role in any model for high temperature creep although it need not be the rate controlling mechanism[7].

The dislocation climb model was first proposed by Weertman[33]. Since this model was not applicable to hexagonal systems he later modified it. In the first model[33] Weertman assumed that Frank-Read dislocation sources exist and that slip can occur on more than one slip system. As shown in Figure 8A, with application of an external stress many dislocation loops are produced from a F-R source. These dislocation loops move until they are stopped by some natural obstacle such as a grain boundary, thus producing a pile-up group. The stress produced by the pile-up induces other F-R sources on different slip systems to produce other dislocations which combine with those of the pile-up, creating Lomer dislocations (circles in Figure 8A). The obstacle blocking the movement of the dislocations from the original F-R source is now the closest Lomer lock (marked as A). Dislocation between the closest Lomer dislocation and natural obstacle disperse through climb. Those dislocations that are between the F-R source and the closest Lomer

dislocation climb out of the original slip plane, but are

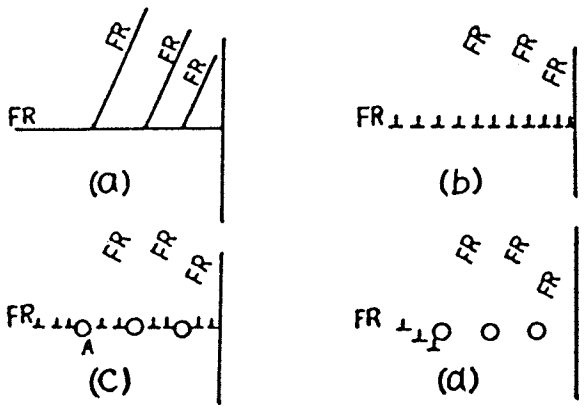

Figure 8A. Process leading up to a F-R source being blocked by a Lomer dislocation[33]. (a) before application of stress, (b) after application of stress, (c) after creation of immobile dislocation, (d) dislocation between Lomer locks have moved away by climb.

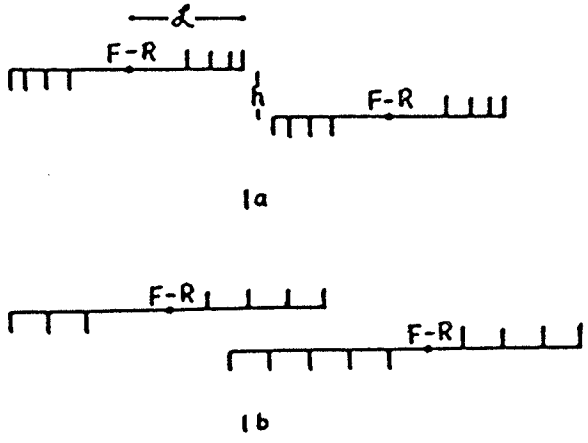

Figure 8B. (1a) Pile-up of dislocations on neighbouring slip planes (1b). A more stable arrangement than (1a)[15].

continually replaced by newly created dislocations. Based on this model Weertman proposed the creep rate to be given by $\dot{\varepsilon}_s = \alpha\sigma_a^n$, where n = 3 - 4 and α is a constant. As stated earlier, since this model is not applicable to the creep of hexagonal crystals Weertman proposed a second model which more closely corresponds to experimental results.

In the second model[15] it is considered that dislocations generated from a F-R source are arrented and pile-up as a consequence of a strong interaction from the pile-ups of neighbouring dislocation sources on parallel slip planes, i.e., pile-ups can exist in the manner shown in Figure 8B. For a material subjected to a constant stress this situation would rapidly lead to a discontinuation of dislocation motion and therefore of deformation if the leading dislocation of pile-ups could not climb and be annihilated. However, at high temperature vacancy diffusion makes dislocation climb possible, and therefore when the processes of climb and annihilation of leading dislocations have occurred, a new dislocation loop may be emitted from the F-R source. This expands over an area A and then stops when the old configuration of pile-ups is restored. For such a process the creep rate has been expressed as(8)

$$\dot{\varepsilon}_s = b\ A\ N\ \dot{C}/y \qquad (2.10)$$

where N is the number of F-R sources, $\dot{C}$ is the climb rate of the dislocation and y is the distance between two adjacent pile-ups.

It is suggested that the climb of leading dislocations occurs in the stress concentration at the tip of a pile-up. The stress concentration is given by $2x\sigma^2/Gb$, where x is the length of pile-up. Therefore, the vacancy concentration in equilibrium with the leading dislocation is given by $C_e = C_o \exp(\pm 2 \times \sigma^2 b^2/GKT)$ which yields a climb rate of $\dot{C} = 2D_s\sigma^2 \times b^4/GKT$[33,8]. The value of x and y have been estimated as $x \alpha \sigma^{1/2}$ and $y = Gb/4\pi\sigma$, respectively. The final expression for creep rate can therefore be written as[8]

$$\dot{\varepsilon}_s = B\, D_s \sigma^{4.5}/b^{1/2} N^{1/2} G^{3.5} KT \qquad (2.11)$$

where B is of the order of 0.2.

Although equation (2.11) is of the same form as the empirical stress/creep rate relation for pure metals and solid solution alloys, there are some shortcomings in this theory[8,25] 1) it has neglected the possible variation of N with stress; 2) the assumption of $x \alpha \sigma^{1/2}$ might not be true; 3) it is questionable whether dislocation of opposite sign on parallel slip planes will be held up by mutual interaction to form a pile-up.

2. Dislocation-jog model.

In general, jogs on edge dislocations will not restrain the motion of an edge dislocation. On the other hand, jogs on a screw dislocation are always edge jogs and therefore, if the screw dislocation is forced to move, jogs can not maintain their positions in the dislocations by glide in their own slip plane since cross-slip of screw

dislocations usually occurs. This cross-slip is possible only by climb of jogs. The thermally activated motion of jogged screw dislocations has been considered as a possible mechanism controlling plastic deformation during high temperature steady state creep[23-30, 32].

According to the dislocation-jog model, when a screw dislocation containing vacancy-emitting or-absorbing jogs moves under an applied stress, the jogs can accompany the dislocation only by emission and absorption of vacancies. In both cases this requires diffusion of vacancies for the dislocation motion to be maintained. The dislocation velocities for the two types of jogs (V_e and V_a) can be calculated by the following expressions:

$$V_e = 4\pi b^2 C_o D_v [\exp(\sigma b^2 s/KT)-1] \qquad (2.12a)$$

$$V_a = 4\pi b^2 C_o D_v [1-\exp(-\sigma b^2 s/KT)] \qquad (2.12b)$$

where s is the spacing between two jogs and is given by $(b/q) \exp(\varepsilon/KT)$. $q = 5-10$, ε is strain, and D_v is the vacancy diffusion coefficient.

Since $\dot{\varepsilon} = bV\rho$ and assuming that the number of the two types of jogs are equal, the creep rate can be expressed by[23]

$$\dot{\varepsilon} = B'D\rho \sinh(\sigma b^2 s/KT), \qquad (2.13a)$$

ρ is a function of σ and since ρ is usually $\alpha \sigma^m$, the creep rate is given by

$$\dot{\varepsilon} = BD\sigma^m \sinh(\alpha\sigma) \qquad (2.13b)$$

where $m = 2 \sim 3$, B is a temperature dependent constant and

$\alpha = b^2 s/KT$.

There is some experimental support for this theoretical model. The fact that the obvious restraints to the motion of edge dislocations, i.e. the long range stress fields from dislocation tangles and pile-ups, have not been observed in creep substructures during secondary creep adds some support to this model[23]. However, there also exists some imperfections in this model. For example, the exact dependence of the mobile dislocation density, ρ, on stress is uncertain, and the stress-dependence of s is not considered.

3. Recovery creep models

The recovery models for steady state creep are based on the ideas of Bailey[37] and Orowan[38] and include the dislocation climb model of Weertman[33]. Two consecutive events occur during high temperature creep; one is strain hardening due to dislocation glide and the other is recovery, i.e., softening with time by means of climb. According to this theory, a balance between strain-hardening and recovery will exist in the secondary creep stage, and the creep rate is given by[8]

$$\dot{\varepsilon}_s = \left(-\frac{\partial \sigma_i}{\partial t} \Big/ \frac{\partial \sigma_i}{\partial \varepsilon}\right) = r/\bar{h} \qquad (2.14)$$

However, recent theoretical analyses have centered upon the dislocation network growth models of McLean[39,40] and Lagneborg et al[41]. According to these models, the creep process consists of consecutive events of recovery and strain-

hardening. The strength is provided by the attractive and repulsive junctions of networks. Some of these junctions will break as a result of thermal fluctuations, and the junctions connected with the longest dislocations will glide and expand into loops and thereby move a certain distance until they are arrested by the surrounding network. This process provides strain and also increases the dislocation density and internal stress, which is the strain hardening process. Simultaneously, recovery of the dislocation networks take place, i.e., the growth of dislocation meshes by the process where large meshes grow at the expense of small ones. The driving force of the dislocation motion in the recovery process is due to the line tension of the curved dislocation meshes. This recovery process will decrease the dislocation density and eventually some links will be sufficiently long for their junctions to break under the influence of thermal flucuations and applied stress. Thus the glide and recovery processes will repeat themselves. Since the glide process is directly dependent on the recovery event and they have an opposite effect on dislocation production, they will tend to balance each other.

The network growth models are confirmed by the observation of an incubation or delay time whenever the stress during a creep test is reduced. During steady state creep when the stress is reduced by a small amount, $\Delta\sigma$, there will be an incubation time with zero creep rate, and then a new steady state is attained. The delay time is the time

required for the network to grow to its new steady state size, at which time the reduced stress is again able to free dislocation segments from their pinning points[8,39].

The creep rate of the dislocation recovery models is given by

$$\dot{\varepsilon}_s = 2b\ L_p\ M\tau\rho^2 \qquad (2.15)$$

where L_p is the average free path of dislocation motion, M is the mobility of the climbing dislocations and hence contains the self-diffusion coefficient, and τ is the dislocation line tension.

2.3 Creep in particle-hardened alloys

2.3.1 Improvement of creep resistance by second phase particles

As stated in Chapter 1, a very effective way of improving high-temperature creep resistance is by the introduction of second phase particles. This improvement is schematically shown in the two creep maps illustrated in Figures 9a and 9b. Figure 9a is the creep map of pure nickel and the other is that of the γ' containing nickel base superalloy, Mar-M200. It is observed that under the same service conditions, i.e., same temperature and applied stress the creep rate, $\dot{\varepsilon}_s$, of the particle hardened Mar-M200 is 2-6 orders in magnitude slower than that of pure nickel. Firstly, such a low creep rate may be explained by the high activation energy for creep of two-phase alloys. It has been reported that the activation energies for steady state creep of Mar-M200 and

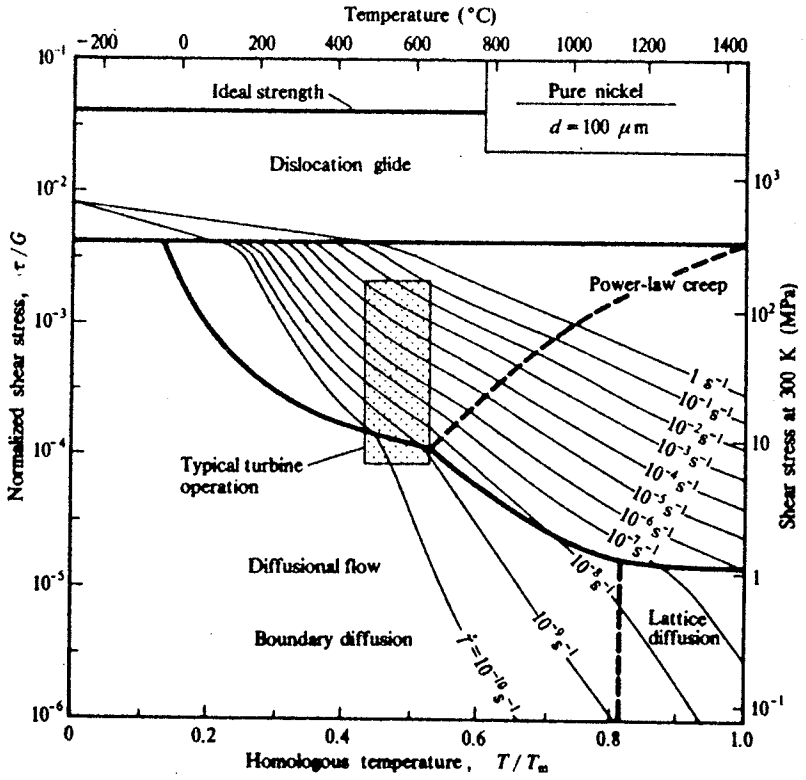

Figure 9a. Creep deformation mechanism map of pure nickel[24].

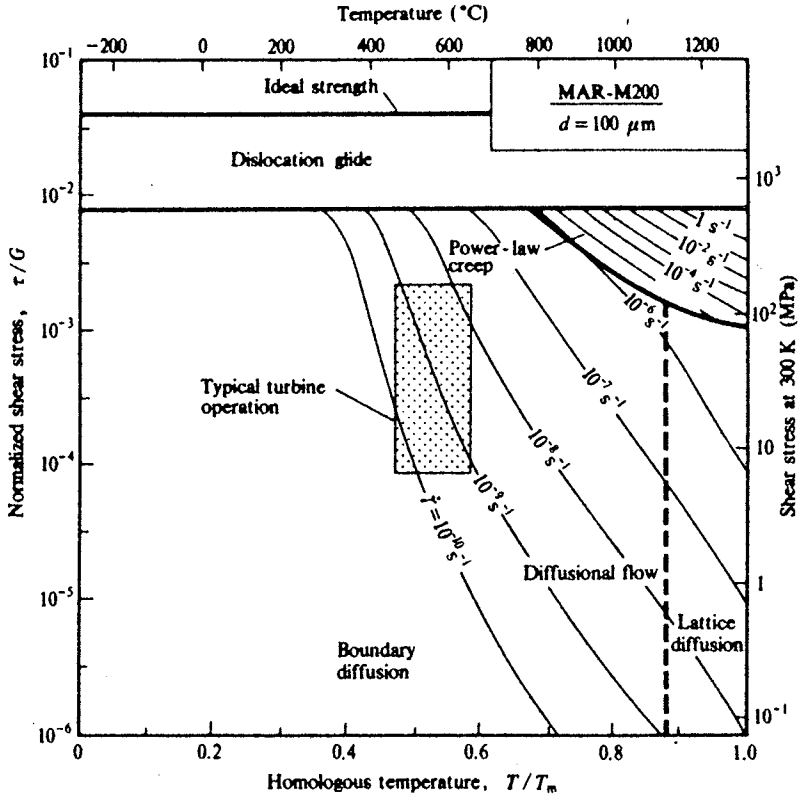

Figure 9b. Creep deformation mechanism map for the superalloy MAR-M200[24].

some other nickel base superalloys is twice as high as that of unalloyed nickel and also considerably higher than that for solid solution hardened nickel base alloys[43-46]. Secondly, on the microscopic scale the increment of the creep resistance can be attributed to the dispersed second phase particles which act as obstacles to dislocation motion and retard the recovery process[22].

1. Particles acting as obstacles

When a dislocation moving through a matrix containing particles encounters particles it may do one of four things. It may bow out between two particles, climb over, cut through or push the particles in front of it. Which process occurs depends on the particle size, the testing temperature and applied stress. All these processes will hinder dislocation movement, increase the yield strength and thereby increase creep resistance.

2. Particles retarding the thermal recovery process.

Another factor increasing creep resistance by introducing second phase particles is the retention of strain-hardening or resistance to recovery. As shown in Figure 10, the dispersed particles will be joined by a network of dislocations which effectively increase the dislocation density and thus hinders the movement of all dislocations. Therefore, dispersion-hardened structures will increase the strain-hardening rate. However, it is believed that although rapid strain-hardening, via an increase in dislocation density should reduce the elongation in instantaneous

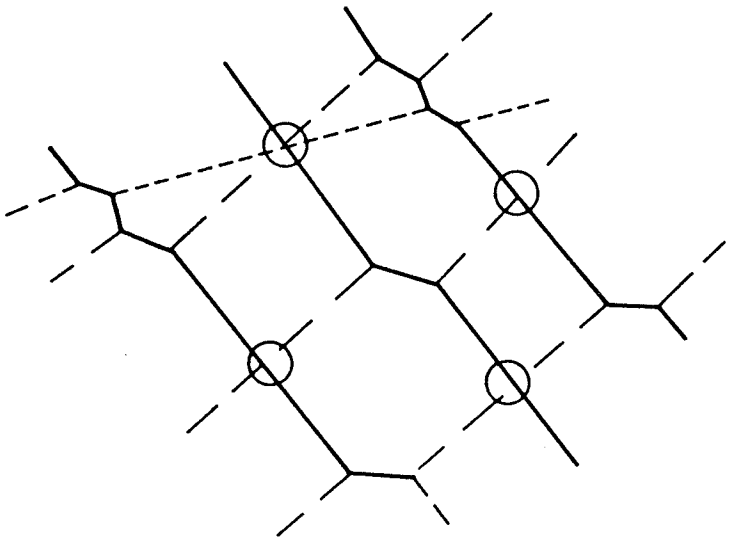

Figure 10. Anticipated dislocation network anchored by dispersed particles. (———) dislocations moving into the plane of paper, (— — —) dislocations moving out of the plane, (----) dislocations on a third plane which might form junctions with both other sets[22].

instantaneous and primary creep, a low steady state creep rate might not be obtained. The reason is as follows. At the normal creep service stress level, which is usually less than the yield stress, the strain-hardening coefficient, $\partial\sigma_i/\partial\varepsilon$, is very high. A large strain-hardening coefficient is realized only by some hardening process such as back-stress-hardening in which there is a relatively large flow-stress increment for a small increase in dislocation length. This high strain-hardening rate will result in a high rate of recovery, i.e., high rate of elimination of dislocations due to relatively large flow-stress increment. It seems that the retention of this rapid strain-hardening, or resistance to recovery, may be the more vital factor in reducing the steady state creep rate. Figure 10 suggests that a dispersed phase can act as anchoring points for a dislocation network and hinder not only slip but also climb and thus retard recovery.

Therefore a stable dispersed phase increases not only the flow stress but also the resistance to recovery. Indeed, it seems that the influence of second phase particles on recovery is the more important effect. The strength level of good-creep-resistant metal is not difficult to raise by such methods as a modest increase in dislocation density or by the addition of solute atoms, but these are not nearly as effective as dispersed particles in hindering thermal recovery and softening at elevated temperatures.

2.3.2 Theoretical models of secondary creep in two phase alloys.

2.3.2.1. Dislocation creep models

Ansell and Weertman[47] were the first to develop a quantitative model to describe the creep behaviour of dispersion-hardened alloys. They assumed that the rate-controlling process is the climb of dislocations over the second phase particles. A three-dimentional dislocation network which provide F-R sources is assumed to be present in the matrix. The second assumption may not be true since in particle-hardening alloys short dislocation lines may start at one particle and terminate at a neighbouring particle. At high stresses these short segments could act as F-R sources while in the case of low stresses, they may not be sources. In developing the equations they considered the case where dislocations originate at F-R sources whose lengths were much greater than the distance between particles.

1. Creep rate at low stress level

In the low stress range, i.e., from a stress which would be just sufficient to activate a F-R source if no particles were present, to a stress which is large enough to force a dislocation past the particles by pinching off loops around the particles, no plastic deformation takes place at low temperature. However, at high temperature plastic flow can occur by dislocation climb around the particles with no

pile-up or bowing of dislocations at the particles, as shown in Figure 11. The steady state creep rate, $\dot{\varepsilon}_s$, calculated from this model varies with applied stress, σ, and particle size, d, and is given by

$$\dot{\varepsilon}_s = \pi\sigma b^3 D/2KTd^2 = (A\sigma/d^2) \exp(-Q_m/RT) \qquad (2.15)$$

This is valid in the stress range $Gb/L_F < \sigma < Gb/\lambda$. In this expression d is particle diameter, Q_m is the activation energy for self diffusion of matrix, L_F is the length of F-R sources λ is the mean interparticle spacing, A is a constant and the rest of the parameters are as defined earlier.

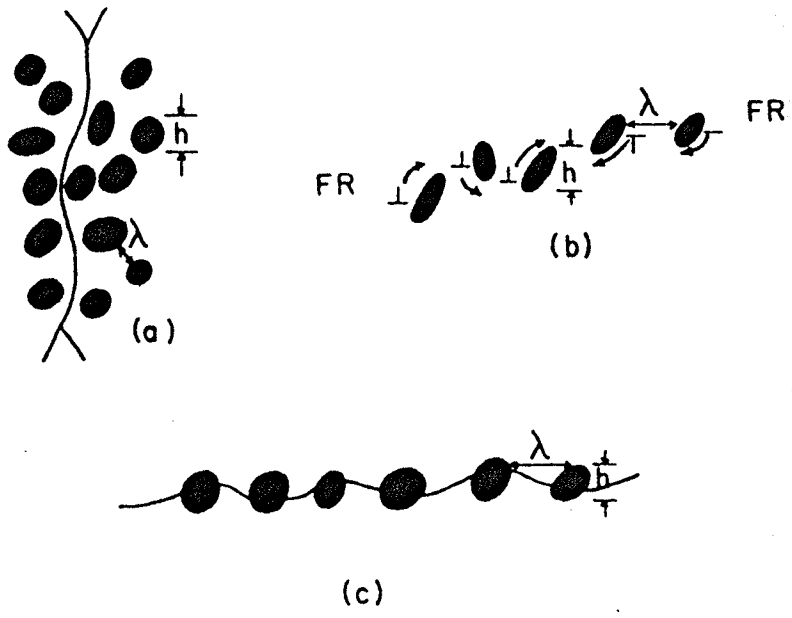

Figure 11. Dispersion-hardening model at low stress level[46]
(a) F-R source with slip plane in plane of paper.
(b) dislocation loops under stress with slip plane horizontal and perpendicular to paper, the arrows indicate direction of slimb.
(c) view of dislocation line from the direction of motion.

2. Creep rate in the high stress range

At a stress greater than the Orowan stress, Gb/λ, the dislocation will bow out and pinch off loops around the particles. This occurs until the back stress exerted by the loops around the particles prevents new dislocations from bowing to a position between the particles. The creep rate is governed by the rate of the following process. The inner most loop climbs off the particle and annihilates itself, allowing a further dislocation to bow between particles in order to pinch off and replace the lost dislocation loop. This model is schematically illustrated in Figure 12. The

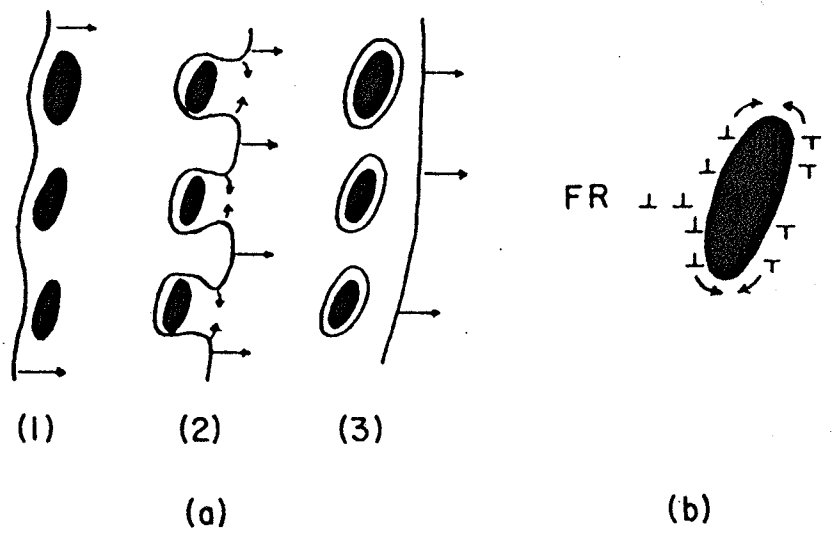

Figure 12. Creep processes at a high stress level
(a) pinching off of dislocation loops
(b) climb of dislocation around a particle.(46)

steady state creep rate can be expressed as

$$\dot{\varepsilon}_s = 2\pi\ \sigma^4 \lambda^2 D/KT\ G^3 d \qquad (2.16a)$$

or $$\dot{\varepsilon}_s = A'd\ D\sigma^4 = A\ d\sigma^4 \exp(-Q_m/RT) \qquad (2.16b)$$

where A, A' are constants and the rest of the parameters are as defined earlier.

However this fourth power law is not in agreement with experimental results. In general, the stress exponent is larger than 4 and the activation energy for creep of particle hardened alloys is usually greater than that for matrix diffusion. This disagreement may be due to the fact that the precipitate particles exert a back-stress on the moving dislocations.

McLean[22], Clauer and Wilcox[48] and Grant[49] developed theoretical models to describe the creep behaviour of dispersion hardened alloys qualitatively, as will be discussed later.

2.3.2.2 Diffusional creep theories of two-phase alloys.

It has been found[24, 40-53] that the diffusional creep rate can be significantly inhibited by the presence of certain second phase particles. The effect of particle distribution on diffusional creep in a two-phase alloy is

schematically shown in Figure 13. During diffusional creep, the grain boundaries, which are normal to the stress, emit vacancies while the parallel boundaries absorb vacancies and thereby collect precipitates. This results in grain boundary collapse permitting the grains on either side to move towards each other.

Since the presence of particles should not affect the diffusion rate the inhibition of diffusional creep by second phase particles has been interpreted in terms of some limitation of grain boundaries as vacancy sources and sinks[50-53]. Two suggestions made by Harris[50] are that either the precipitates inhibit grain boundary sliding (which is a necessary component of diffusion creep deformation) or

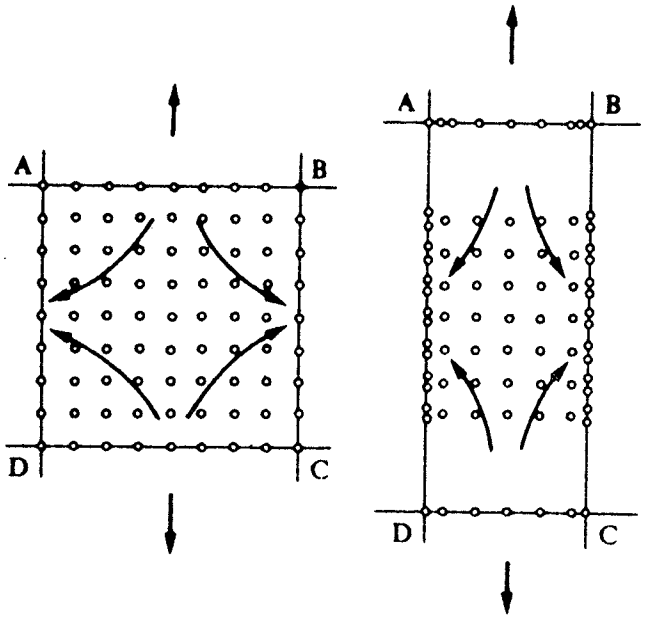

Figure 13. Schematic representation of the effect of diffusional creep on particle distribution in a two-phase alloy.[24]

that the precipitates restrict the ability of the parallel grain boundaries to collapse. The latter proposal has been considered in great detail by Harris[51], and Burton[52]. According to their model the metal vacancies cannot condense at, or diffuse along precipitate/matrix interfaces without the co-operative movement of the atoms which comprise the precipitates. (This is possible for pure metals where vacancy condensation occurs at high angle grain boundaries). Therefore the sliding which requires diffusional accommodation will be more difficult at the precipitate/matrix interface than at high-angle grain boundaries, i.e. the shear concentration cannot be easily relaxed by shear strain at the interface. Thus, the grains on either side of the boundary cannot move towards each other unless the matrix deforms plastically around particles. It is believed that such a stress relaxation can be achieved by the punching of prismatic intersititial dislocation loops into the matrix due to the stress concentration at the precipitate/matrix interface, as shown in Figure 14. A second prismatic loop is

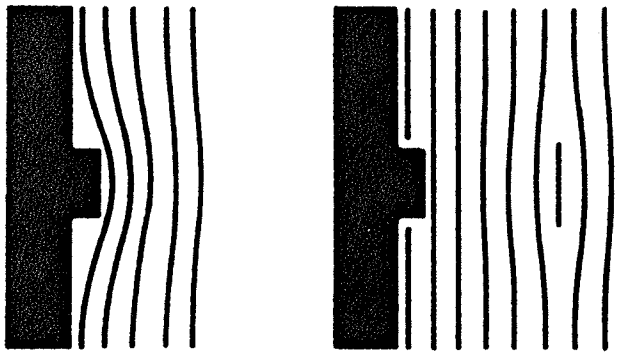

Figure 14. 'Punching' of prismatic intersititial loop into matrix by a particle.(24)

subsequently formed and moves away from the interface due to the stress concentration. The loops decrease in size with increasing distance from precipitates. This is due to the

fact that the loops will shrink by absorption of vacancies, thus compensating for the fact that condensation on the interface is not possible. This process is shown in Figure 15.

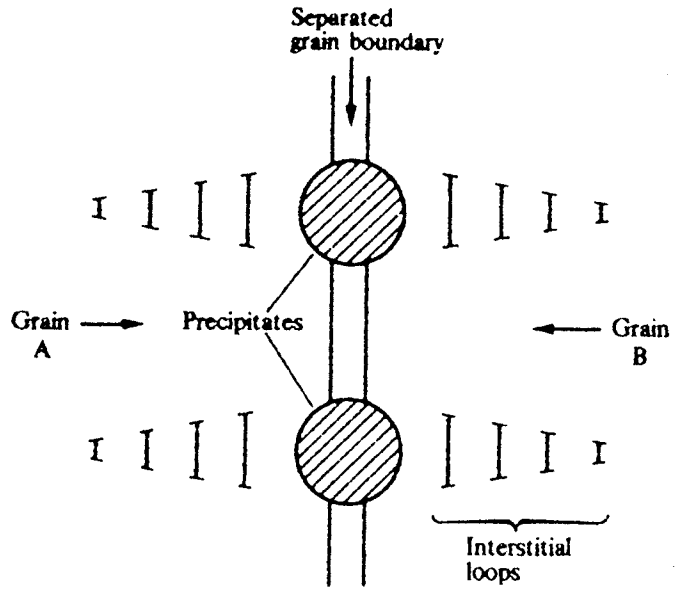

Figure 15. The grain boundary between grains A and B has been allowed to separate as a result of the condensation of vacancies. In order that the two grains may move towards each other, thereby closing the gap, intersititial loops are generated in the matrix adjacent to the precipitates.(24)

This model predicts a threshold stress, $\sigma_o = (2\Gamma/br_p)V$ (where r_p is the radius and V is the volume fraction of precipitate particles) for diffusional creep, which corresponds to the stress required to nucleate these interstitial prismatic loops. It is observed that the critical shear stress for nucleation of these loops, τ_N, is significantly higher for coherent, strongly bonded precipitates than that for incoherent, weakly bonded precipitate (τ_N = G/10 and G/100 respectively for the two

cases)[51]. Therefore, the linear relationship between $\dot{\varepsilon}_s$ and σ_a is lost and is replaced by the following expression

$$\dot{\varepsilon}_s = BDb^3(\sigma_a - \sigma_o)/d^2KT \qquad (2.17)$$

where B is a constant and the rest of the terms are as defined earlier. It is also observed that in many cases the creep rate progressively decreases with strain, i.e., the inhibiting effect of the particles increases with increasing strain[24,52]. This is due to the vacancy-absorbing capabilities of parallel boundaries being impaired by the progressive collection of precipitates.

2.3.3 The effect of particle size on creep rate of two-phase alloys.

2.3.3.1 Prediction of steady state creep rate by different creep models

The effect of particle size and spacing on creep rate in two-phase alloy has been investigated by Ansell and Weertman[47], McLean[22], Clauer and Wilcox[48] and Grant[49]. Applying the theories of Ansell and Weertman, which are expressed by equations (2.16) and (2.17), it has been suggested that for a given volume fraction of particles, in the small particle size range the steady-state creep rate decreases with increasing particle size, i.e., $\dot{\varepsilon}_s \alpha d^{-2}$, until a minumum value of $\dot{\varepsilon}_s$ is reached. The creep rate then increases linearly with further increase in particle size, i.e., $\dot{\varepsilon}_s \alpha d$. This is shown in Figures 16 and 17.

Similar to the suggestion of Ansell and Weertman, McLean[22] postulated that for large particle sizes,

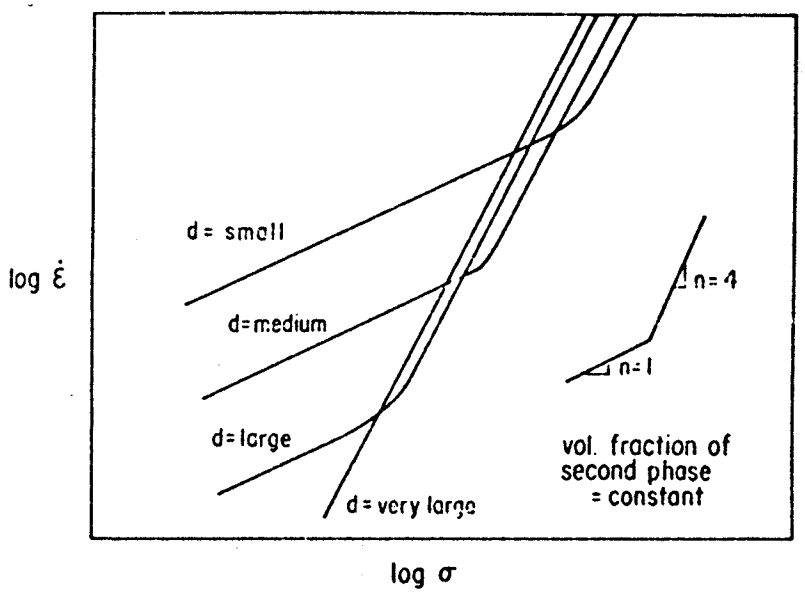

Figure 16. Influence of particle size, d, of the second hard phase on the creep rate-stress relation for a given matrix material according to Weertman-Ansell theory.[6]

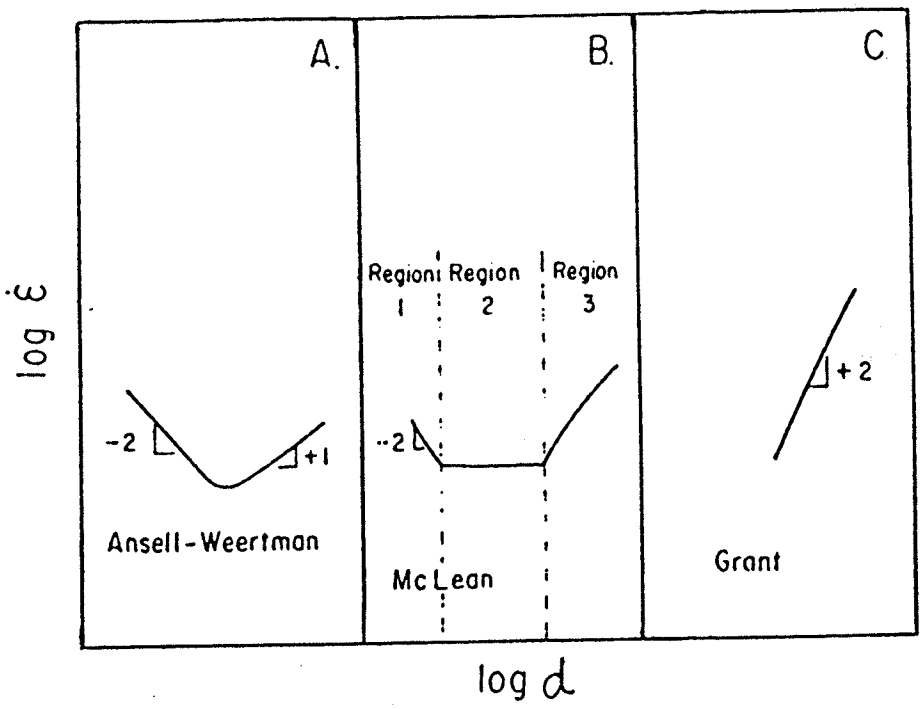

Figure 17. Influence of particle size, d, of the second hard phase on the creep rate of a given matrix material at a constant stress according to Ansell and Weertman, McLean and Grant.[6]

dislocations bow around particles so that the creep rate should increase with increasing particle size. When the particle size is very small, dislocations are considered to move by pushing the particles ahead of them, and in this case the rate-controlling process is that of vacancy migration from the tension side to the compression side of the coherent particles. This also leads to a creep rate varying as d^{-2}. At intermediate particle sizes, McLean[22] assumed that dislocations alternately climb a distance proportional to the particle diameter, d, and then glide a distance λ before their progress is impeded by another particle. This model leads to a creep rate varying with λ/d, i.e., the creep rate would be independent of particle size since $\lambda \alpha d$ for a constant volume fraction of particles.

Clauer and Wilcox[48] have also suggested that when the applied stress is lower than the Orowan stress, the climb of edge dislocations over particles is important during creep of two-phase alloys. According to them, $\dot{\varepsilon}_s$ should be proportional to λ^2/d or $\dot{\varepsilon}_s \alpha d$. Grant[49] has developed a qualitative discussion of particle size effect on creep by consideration of stored energy. He assumed that each particle acts as a pinning centre for dislocations. For a given volume fraction of second phase, the finer the particle size the greater the dislocation density. The high dislocation density means a high degree of stored energy which results in a low creep rate. He also assumed that

dislocations are in the form of tangles or subgrains whose size is equal to the mean free path, λ, between particles. These subgrains are believed to be the barriers to dislocation motion. McLean[40] put forward a similar model earlier in which he considered the tangles to act as barriers to dislocation movement. Both models predict that the creep rate should increase with the square of the particle size, $\dot{\varepsilon}_s \alpha d^2$, as shown in Figure 16.

2.3.3.2 Experimental observation of particle size effect on creep rate

Singhal and Martin[54] have studied the effect of γ' (Ni_3Ti) particle size upon the creep rate, $\dot{\varepsilon}_s$, of a Fe-Ni-Cr-Ti alloy. Their results are in agreement with the predictions of Ansell and Weertman[47] and McLean[22] although there are not enough data available to confirm the existence of McLean's constant creep rate region. The diffusion coefficient, D, calculated from the slope of the $\dot{\varepsilon}_s$ vs d^{-2} graph, $b^3 D\sigma/KT$, was found to be much smaller than the matrix diffusion coefficient. This suggests that the activation energy for creep of these alloys is much greater than that of self-diffusion.

Recently Treadgill and Wilshire[55] have investigated the effect of particle size and spacing on the creep rate of two-phase Cu-Co alloys. The stress and interparticle dependences of the steady state creep rate are shown in Figures 18 and 19. It has been observed that in a Cu -

0.88% Co alloy, the stress exponent, n, changes from ~ 4.5 to 12 when the stress level is changed from a stres less than yield strength to a stress greater than the yield strength. It is also seen that at a high stress level the creep rate decreases with increasing particle size until a minimum creep rate is reached and then increases with further increase in particle diameter, as shown in Figure 19. This is in agreement with the predictions of both Ansell and Weertman[47] and McLean[9,22].

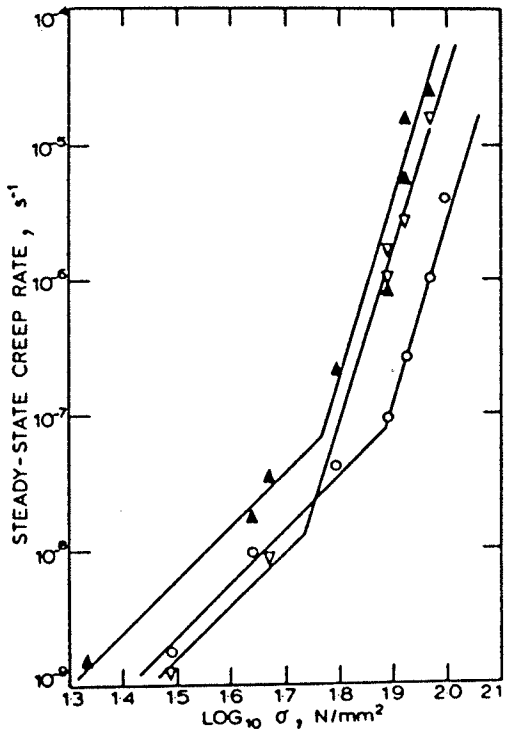

Fig. 18. The stress-dependence of the steady state creep rate at 712K for Cu-0.88% Co alloy having particle diameters of 3.3 nm (▲), 8.3 nm (o), and 17.2 nm (▽).[55]

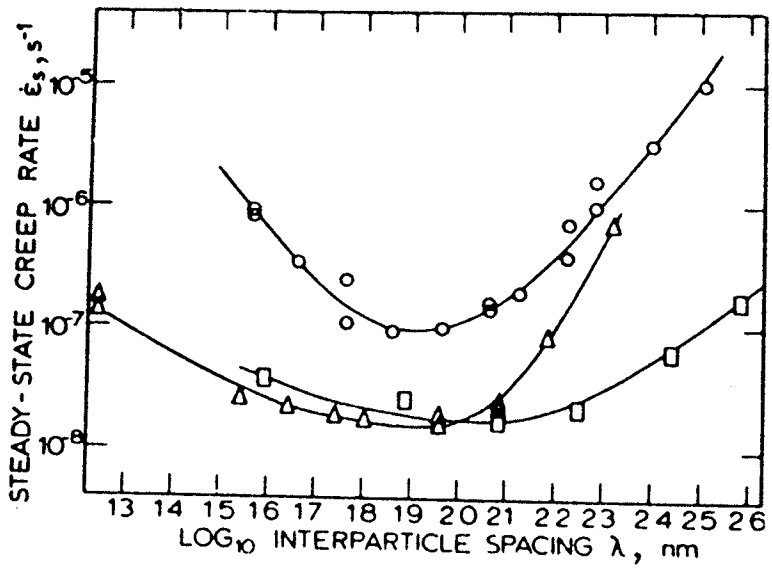

Figure 19. Variation of the steady state creep rate with particle interspaciung for Cu - Co alloys containing 0.88% (o), 2.48% (Δ), and 4.04% (□) tested at 77.2 N/mm^2 and 712K.(55)

The effect of volume fraction and particle size of ThO_2 on the creep rate in dispersion-strengthened TD nickel has been studied by Clauer and Wilcox[48]. Their results are in good agreement with the expression $\dot{\varepsilon}_s \propto \lambda^2/d$, which suggests that the rate-controlling process of creep is the climb of edge dislocations over ThO_2 particles.

It has been reported that for Ni-Cr-Al-Ti alloys[43] containing 10 - 20% γ' precipitates, the smallest γ' particle size give optimum creep resistance at 970K and that the particle size was more important than volume fraction in determining creep life. It seems that in this alloy system the optimum interparticle spacing for creep resistance is of the order of 50 nm.

2.4 Threshold stress and back stress in elevated temperature creep.

As mentioned earlier, the creep behaviour of metals and alloys is normally described in terms of the dependence of secondary creep rate, $\dot{\varepsilon}_s$, on applied stress, σ_a, and temperature, T,

$$\dot{\varepsilon}_s = A \sigma_a^{n_a} \exp(- Q_c/RT) \qquad (2.5)$$

where $n_a \simeq 1$ for diffusional creep, $n_a \simeq 3 \sim 6$ for dislocation creep and Q_c is equal to the activation energy for self diffusion for most pure metals and single phase alloys. However for most commercial creep resistant materials containing dispersed second phase particles, the values of n_a and Q_c have been generally found to be considerably greater than those for pure metals and solid

solution alloys.[45,56-66] The values of n_a for precipitation hardened alloys usually are in the range of 5 to 10, while for dispersion hardened alloys $n_a \simeq 10 - 40$[45,59], and for Ni-20 Cr-2ThO_2 single crystal $n_a = 9-75$[60]. Furthermore, in many particle-strengthed alloys, the values of n_a and Q_c vary with applied stress[62]. For example, values of $n_a \simeq 5$ and $Q_c = 140$ KJ/mol at low stresses, and values of $n_a \simeq 12$ and $Q_c = 210$ KJ/mol at high stresses have been observed in a series of two-phase Cu-Co alloys[55]. This suggests that a different rate controlling process operates in the high and low stress regions.

These observed variations can be rationalized using the equation:

$$\dot{\varepsilon}_s = A^* \left(\frac{\sigma_a - \sigma_o}{G}\right)^{n_e} \exp\left(- Q_e/KT\right) \qquad (2.18)$$

where the effective stress exponent $n_e \simeq 1$ for diffusional creep and $n_e \simeq 3-6$ for dislocation power law creep in pure metals, single phase and two phase alloys. The effective activation energy Q_e for two phase alloys is equal to the activation energy for creep of the single phase matrix, and σ_o is termed the back stress, internal stress, friction stress or threshold stress. This concept has been discussed extensively[67] by Gibeling and Nix.

2.4.1 Threshold stress in diffusional creep

The existence of a threshold stress means that the value of applied stress must exceed a certain minimum value

before deformation can occur and it is limited to situations where the resistance to flow is independent of the imposed stress or strain rate. For example, surface tension effects and Orowan bowing can produce thresholds. Threshold stresses have been found during fluid flow, superplastic deformation and diffusional creep process.

In most of the theoretical models of threshold stress for diffusional creep, the source of threshold is considered to be the imperfect nature of grain boundaries as sources and sinks for vacancies[51,52, 68-71]. Ashby[68] considered edge dislocations at grain boundaries to be these kinds of sources and sinks, i.e., vacancies can be created or destroyed by the climb of dislocations whose Burgers vectors are normal to the boundary. This model predicts a threshold stress of

$$\sigma_{oA} = 2\Gamma/b\lambda = (2\Gamma/br_p)V^{1/2} \qquad (2.19)$$

where Γ is the dislocation line tension, λ is the interparticle spacing, r_p is the particle radius and V is the volume fraction of precipitates. However, according to Harris[51] and Burton[52] the threshold stress, σ_o, for diffusional creep of second phase strengthened alloys corresponds to the stress required to nucleate interstitial prismatic dislocation loops around the second phase particles. Their model predicts that σ_o varies linearly with volume fraction, i.e.

$$\sigma_{oH} = (2\Gamma/br_p)\ V \qquad (2.20)$$

There are some experimental results that agree with equation

(2.20). It has been found[51,70,72] that the critical shear stress, τ_N, for nucleation is significantly higher for coherent, strongly bonded precipitates than that for incoherent, weakly bonded precipitates ($\tau_N \sim G/10$ and $G/100$ respectively).

2.4.2 Back stress in elevated temperature dislocation creep.

The back stress, σ_o, is the stress opposing deformation during creep. The term "back stress" is used where the forces opposing deformation are dependent on the deformation history and current stress or strain conditions, i.e., $\sigma_o = f(\sigma,T,s)$ where s is a structure term[64].

A number of authors[73-76] have proposed that high temperature creep deformation can be characterized in terms of back stress (or internal stress) and effective stress. The mean internal stress, σ_o (or σ_i), provides the driving force for recovery and the mean effective stress, $\sigma_e = \sigma_a - \sigma_o$, provides the driving force for glide. According to Ahlquist and Nix[80], in the primary creep stage, as the strain hardening proceeds, the internal stress increases and the effective stress which drives the glide process diminishes accordingly, as shown in Figure 20. The internal

back stress during steady creep is established by the balance between strain hardening, which tends to raise σ_o (or σ_i) and recovery, which lowers it by dislocation annihilation and rearrangement which are controlled by dislocation climb. According to modern theories of elevated temperature dislocation power law creep, it is considered that dislocation motion is opposed by back stresses which result from the interaction between moving dislocations and the substructure. There are two slightly different models to describe the back stress, viz., the recovery model which describes network back stress and the combined glide-recovery model which describes the dislocation back stress.

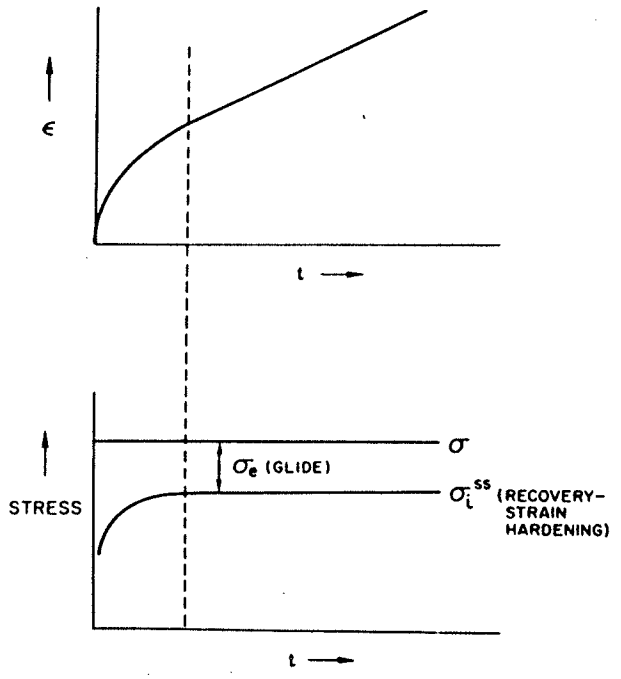

Figure 20. Variation of average internal stress during transient creep of a typical pure metal[79].

2.4.2.1 Recovery model and network back stress.

The recovery-creep model has been discussed earlier in this chapter. This model is based on the concept that creep is controlled by the recovery (growth) of a three-dimensional network of dislocation to provide links of sufficient length to act as dislocation sources.

The experimental works of Mitra and McLean[75], Wilshire and his coworkers[62-64,77] and Evans and Harrison[78,79] have confirmed the network growth models. They observed delay times or incubation periods, Δt, after small stress reductions, $\Delta\sigma$, during secondary creep. The delay time is taken as the time required for the network to grow to its new steady state size at which point the reduced stress is again able to break dislocation segments free from their pinning points, i.e., to activate F-R sources.

The results of these experiments have been interpreted in terms of the existance of a back stress, σ_o, opposing deformation. The presence of a back stress leads to a net stress, $\sigma_e = \sigma_a - \sigma_o$, which is the driving force for the dislocation recovery process and determines the creep rate by defining the average dislocation mesh size[62-65]. The back stress, σ_o, is characteristic of the substructure, i.e., it depends on the subgrain size and total dislocation density. However it does not depend on the local dislocation segment length in the network[63]. Therefore, the network back stress, σ_o, is taken to be a measure of the long-range back stresses associated with the dislocation substructure. The

network back stress is normally measured by successive load reductions during steady state creep. Typically, 5% of the applied stress is removed and after a delay time a further stress decrement is made as soon as forward creep is detected as illustrated in Figure 21a. Eventually the incubation period becomes very long. In order to determine σ_o, the data are usually plotted as cumulative incubation time, $\Sigma\Delta t$, versus cumulative stress reduction, $\Sigma\Delta\sigma$. The network back stress, σ_o, is taken as the asymptotic value of the remaining stress when the cumulative incubation period appears to be infinite, as shown in Figure 21b.

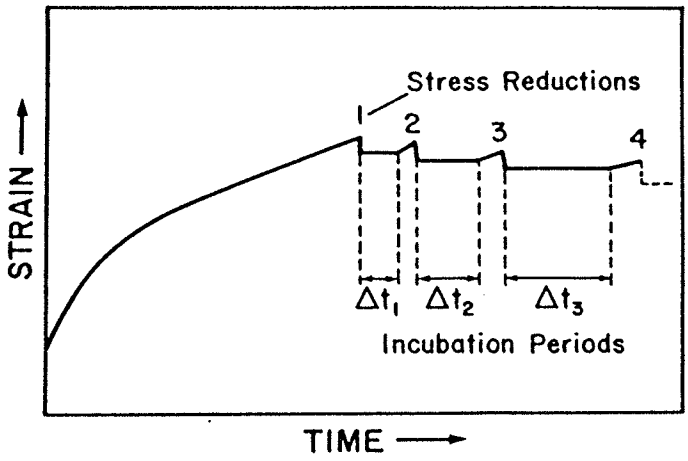

Figure 21a. Schematic strain-time behaviour after successive stress reductions during a $\Delta\sigma$ - Δt test[67].

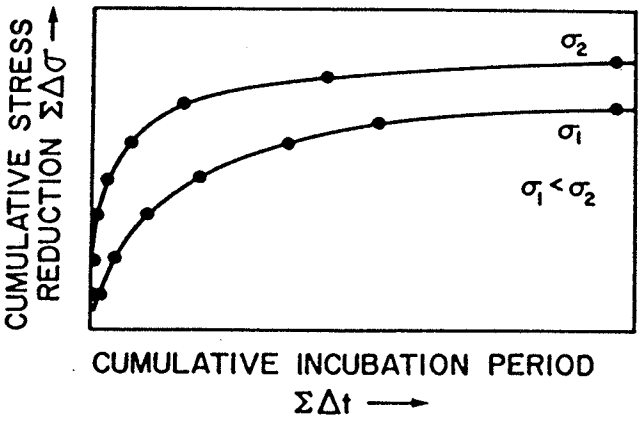

Figure 21b. Schematic plot of cumulative incubation time against cumulative stress reduction used to determine a network back stress[67].

2.4.2.2 Combined glide-recovery model and dislocation back stress or internal stress

In the combined glide-recovery model, glide is a thermally activated process driven by the effective stress, $\sigma_a - \sigma_o$, which is the difference between the applied stress and the dislocation back stress or internal stress resulting from strain hardening. The glide process may be either jerky or viscous and the time of flight of the dislocations is comparable with or greater than the time spent waiting at obstacles. In general, a moving dislocation experiences a local back stress which is position dependent. The dislocation back stress, σ_o, can be measured by the strain transient dip test[73,80] or stress transient dip test[81,82] as shown in Figure 22. This measured mean internal stress (the critical reduced stress for zero creep rate) is the average value of back stress since the positional dependence of the internal back stress is actually periodic in nature.

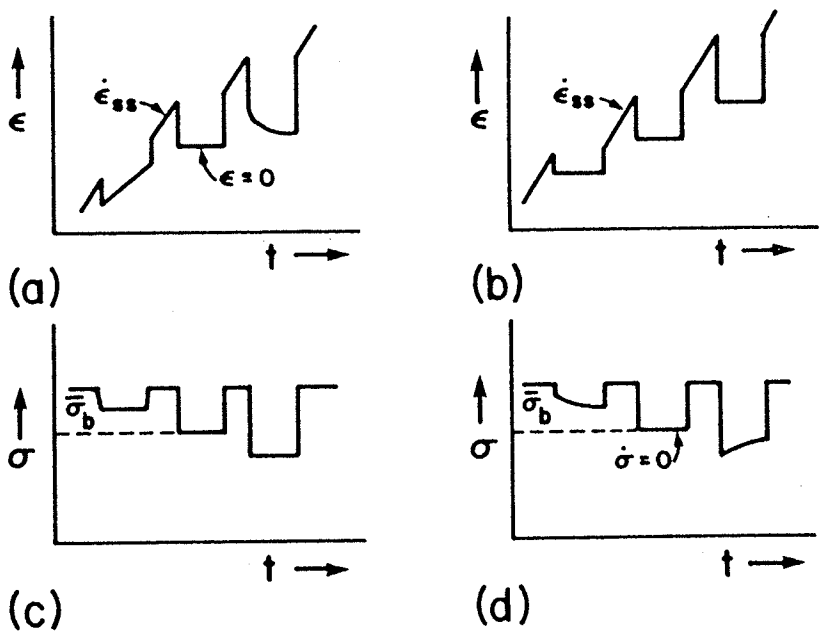

Figure 22. Schematic stress change experiments illustrating the operational definition of the dislocation back stress. (a), (c) strain transient test, (b)(d) stress transient test[67].

2.4.3 Back stress in two-phase alloys

There are two theoretical models to describe the back stress in two-phase alloys, i.e. the dislocation bowing or Orowan bowing model and the dislocation climb model.

2.4.3.1 Orowan bowing model

According to this model there exists a threshold stress which must be overcome in order for a dislocation to bypass particles. It has been suggested that the back stress in two-phase alloys consists of two parts, resistance arising from the second phase particles, i.e., Orowan bowing stress and resistance due to the matrix substructure[60,83]. The

former is independent of the applied stress and the latter is usually considered to be a function of the dislocation substructure, i.e., applied stress and deformation history. However it has been observed[48,49,60,84] that in some dispersion strengthened alloys, no pronounced dislocation substructure is developed during creep and hence its contribution can be expected to be much smaller than that due to inert dispersoids. In the case of γ' strengthened superalloys with dislocation substructures developed by prior creep[83], the contribution due to a fairly dense dislocation substructure was no more than 10% of the total flow stress. Lund and Nix[60] found that for single crystals of Ni-20Cr-2ThO_2, when the applied stress exceeds the Orowan stress, the crystal creeps in response to the difference between the applied stress and the Orowan stress, i.e., the effective stress $\sigma_e = \sigma_a - \sigma_o$, following the creep law for the Ni-20 Cr matrix. Purushothaman and Tien[83] observed that in oxide dispersion strengthened (O.D.S.) solid solution alloy the back stress, σ_o, calculated from the equation $\dot{\varepsilon}_s = A (\sigma_a - \sigma_o)^{n_e} \exp(-Q_c/RT)$ by assuming $n_e = 4$, is of the order of the stress needed for the Orowan bypassing of the inert dispersoids by the mobile dislocations. Similar results have also been found in ODS superalloy containing γ' phase as well as in a γ' strengthened wrought superalloy crept at elevated temperature of 1253K[83].

However, recent investigations[82-88] have shown that

creep occurs below the Orowan stress. Therefore the dislocation climb model has been proposed.

2.4.3.2 Dislocation climb models

Brown and Ham[86] and Shewfelt and Brown[87] proposed a theory based on the localized climb of edge dislocation over particles. They assumed that the part of the dislocation in front of the obstacle climbs while the adjacent part remains in the slip plane. Thus the back stress arises from the energy required to increase the dislocation line length. Later Hausselt and Nix[84] assumed that the localized edge dislocation climbs over particles and the dislocation arms can also climb out of the slip plane. However, the back stress calculated using these assumption is too low compared to observed values. Therefore it was further suggested that the back stress consist of the back stresses resulting from the interaction of a moving dislocation with other dislocations, subgrain boundaries and the fine twins which they observed and the back stress calculated from the localized climb model. With this treatment a good correlation with the experimental data was observed[67].

2.5 Scope of the present investigation

The above review of the literature suggests that the creep behaviour of two phase alloys is an extremely complex process. The creep mechanisms and the relatively new concept of back stress are a function of precipitate morphology, the nature of the matrix and the temperature and stress at which

creep deformation occurs. It is also evident that no single theoretical model can explain all aspects of the creep behaviour of all metals and alloys. The present investigation is therefore confined to study the effect of precipitate particle size on the steady state creep behaviour and the deformation mechanism during steady state creep of Inconel alloy 718 in the stress range of 620-865 MN/m^2 and in the temperature range of 853 - 943K.

CHAPTER 3 EXPERIMENTAL TECHNIQUES

3.1 Materials

The material used in this investigation was commercial Inconel 718 superalloy provided by International Nickel Company of Canada. The starting material was 4.74 mm, 3.4 mm and 2.50 mm thick sheet with a nominal chemical composition (wt%) of 19 Fe - 18 Cr - 5 (Nb + Ta) - 0.5 Al - 1 Ti - 3 Mo - 0.03 C-Ni balance. The actual chemical composition is given in Table 1. This alloy is strengthened by coherent, ordered, disc shaped BCT γ'' phase and sperical, ordered FCC γ' phase particles. In the peak aged condition the total volume fraction of the precipitates was 17% and the ratio of the volume fraction of γ'' to γ' was between 2.5 - 4.0[4,5,92].

Table 1
Chemical Composition of Inconel 718 (wt%)

C	Fe	Ni	Cr	Al	Ti	Mo	Nb+Ta
0.03	19.24	52.37	18.24	0.52	0.97	3.07	4.94

Mn	S	Si	Cu
0.007	0.007	0.30	0.04

3.2 Preparation of tensile and creep specimens

The 3.4 mm thick sheets of commercial alloy Inconel 718 were cold rolled to 1.3 mm thickness. The tensile and creep specimens with a cross-section of ~ 1.3 x 5.5 mm^2, as shown in Figure 23, were machined from these 1.3 mm thick strips. A numerically controlled universal milling machine

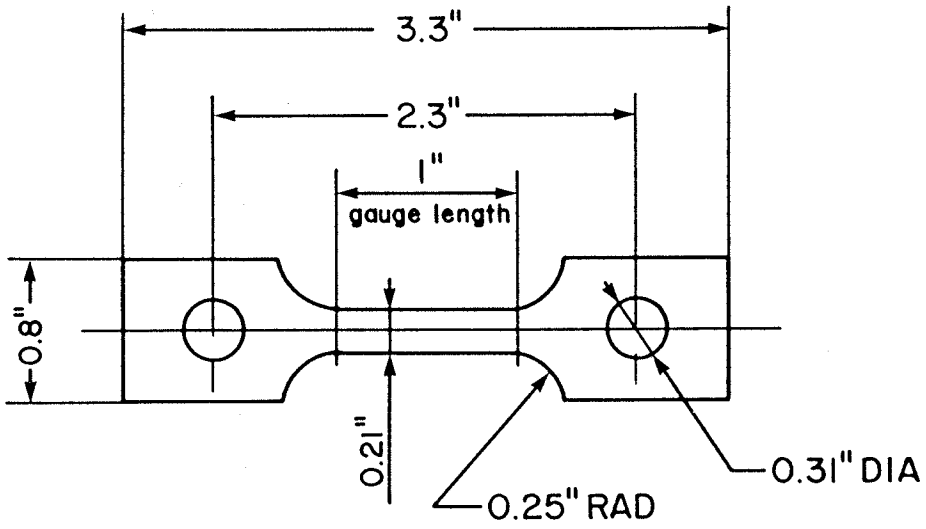

Figure 23. Dimention of creep and tensile specimens.

was used to machine the specimens. These specimens were given a solution heat treatment of 1.0 hours at 1323K in argon quenched in cold water. They were then aged at 998K for various periods of time and quenched in cold water to obtain various particle sizes of γ" and γ' phases. the specimens were wrapped in stainless steel sheets during the aging treatment to minimize oxidation. The final grain size

after the solution treatment was found to be in the range of 0.09 ~ 0.15 mm. Before creep testing the speciman surfaces were cleaned by sanding with 600 grade wet sandpaper.

3.3 Tensile tests

In order to select appropriate creep stress levels, tensile tests of peak aged specimens were carried out at 873K and 923K in an Instron testing machine. The strain rates used in tensile tests were 3.3×10^{-2} to 3.3×10^{-9} sec^{-1}. The testing temperature was controlled within ± 5K by a three-zone furnace filled with argon and monitored by a thermocouple attached to the upper part of the speciman grip.

3.4 Creep tests

The tensile creep tests were carried out in two T48 Avery-Denison constant stress creep machines, shown in Figures 24 and 25. The creep strain was monitored during the test recording on a strip chart recorder, the displacement of an LVDT extensometer attached to the speciman grips inside the argon-filled chamber. The accuracy of the LVDT was within 1% and the temperature of the region near the LVDT was ~ 310K which is less than operating temperature limit of the LVDT. The strain rate was calculated by assuming that all of the measured displacement was due to homogeneous deformation of the gauge length of the sample. The testing temperature was controlled within ± 2 K by a three-zone furnace and was monitored by two thermocouples attached to the upper and lower gauge length sections of the specimen.

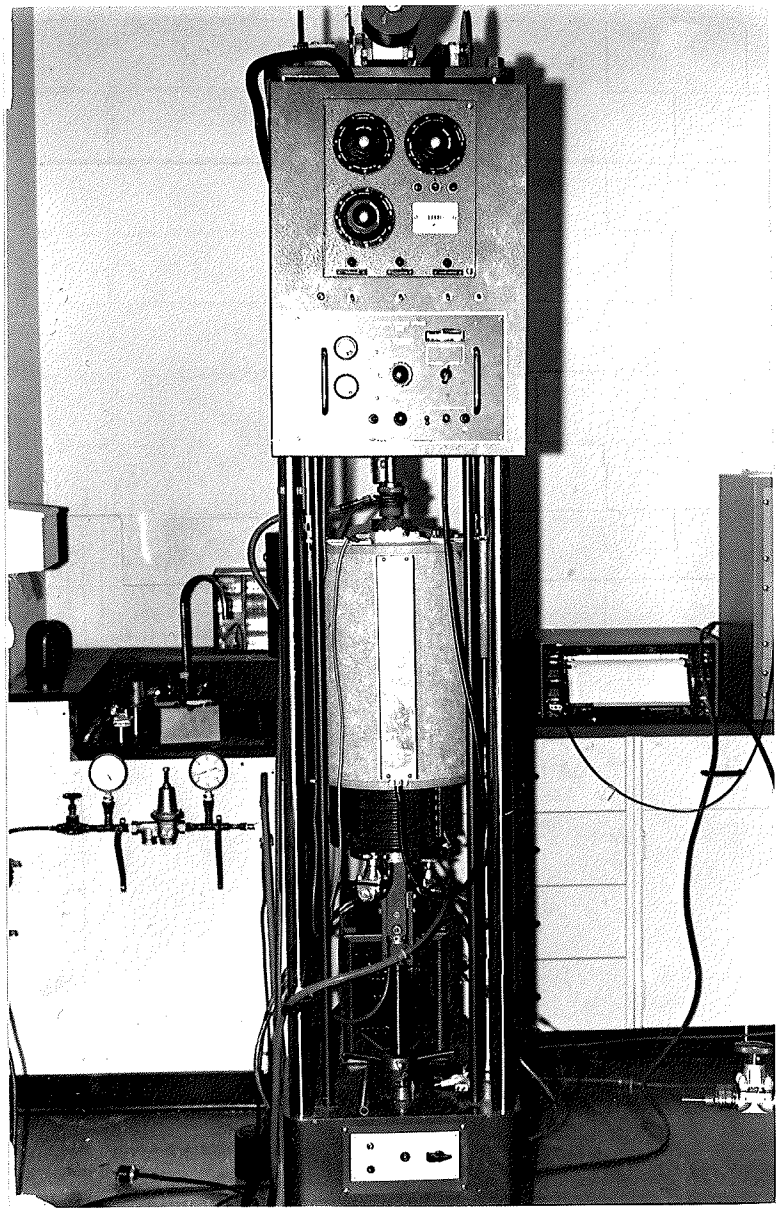

Figure 24. T48 Avery-Denison constant stress creep machine.

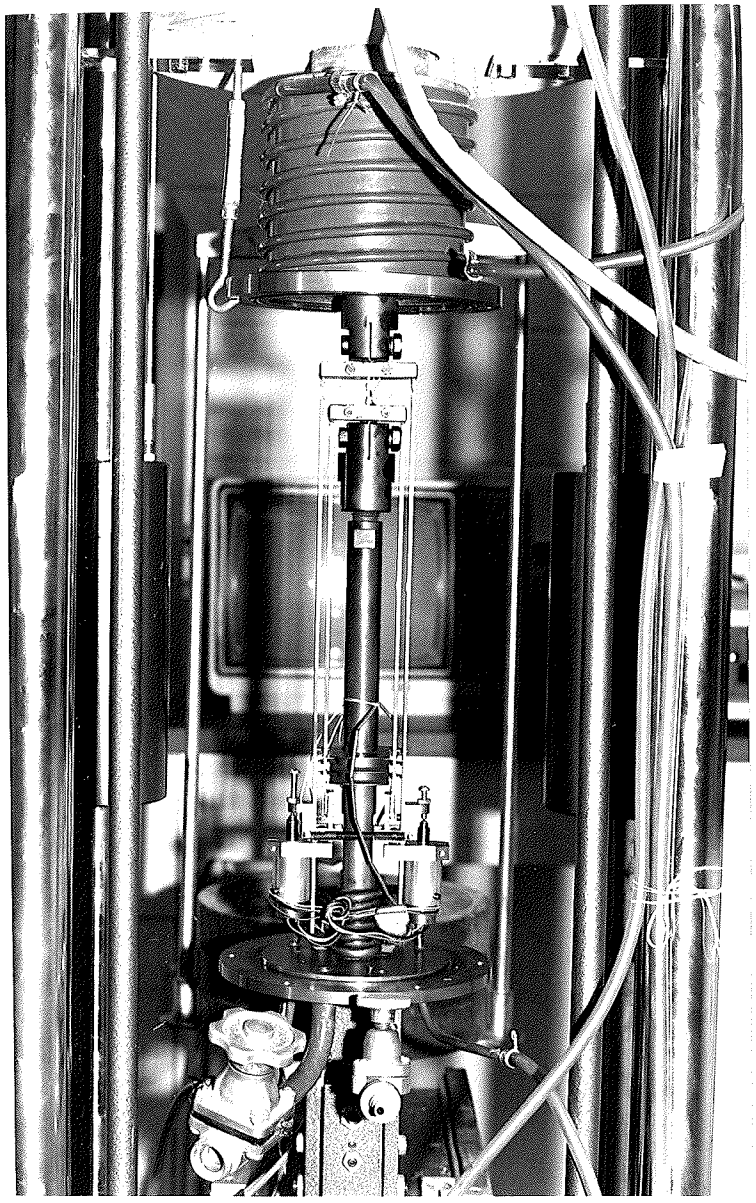

Figure 25. Inside of the testing specimen chamber of T48 Avery-Denison constant stress creep machine.

The back stress or threshold stress was determined by the Wilshire technique or the consecutive stress reduction method[63-65,93]. When the creep test reached the secondary creep stage the applied stress was reduced by a small amount, $\Delta\sigma_1$, typically ~ 0.05 σ_a. This stress reduction resulted in an elastic contraction of the specimen, which was followed by an incubation period of zero creep rate. Creep then recommenced with a slower creep rate at the reduced stress level. As soon as a new steady state creep rate was reached a second small stress reduction, $\Delta\sigma_2$, was made and so on. The duration of successive incubation periods (Δt_1, Δt_2...) was recorded for each consecutive small stress reduction ($\Delta\sigma_1$, $\Delta\sigma_2$,.....). Eventually, the incubation period became very long. In order to determine σ_o, the data were plotted as cumulative incubation time, $\Sigma\Delta t$, against the remaining stress on a linear scale. The back stress or threshold stress, σ_o, was taken as the asymptotic value of the remaining stress when the cumulative incubation time approached infinity.

3.5 Preparation of thin foils and electron microscopy

3.5.1 Measurement of γ" and γ' particle sizes

The 4.74 mm thick sheets were cold rolled to ~ 0.2 mm thick strips with intermediate annealing at 1473K. The final solution treatment of these strips was carried out in a 1473K furnace for 1 hour in sealed vycor capsules, partially filled with pure argon. The specimens were then quenched in cold water with the capsules always being broken in the cold water

to ensure a homogeneous supersatuated solid solution. The quenched specimens were aged in sealed, evacuated vycor capsules at a temperature of 998 K for various periods of time, then quenched in cold water.

The aged strips were cleaned using 600 grade sandpaper and discs of 3 mm diameter were punched from the strips. These 3 mm discs were thinned with a jet electropolishing unit using 15% perchloric acid, 85% methanol electrolyte at 223-233K and a current of 85 to 100 MA. This procedure produced good quality thin foils which were then examined in a Philips EM-300 electron microscope. Due to the presence of large coherent strains around the γ'' and γ' particles, individual particles could only be observed in the dark field using their superlattice reflections. Furthermore, the γ'' phase in Inconel 718 grows coherently into discs on {100} planes of the FCC matrix with the c axis of the γ'' phase being perpendicular to the discs. The γ' phase also forms coherently on the {100} FCC matrix planes[3,5]. Therefore in order to determine the true sizes of γ'' and γ' particles their dimensions were measured only in dark field micrographs taken in the {100} thin field orientation. About 300 particles in each specimen were measured to assure the statistical accuracy of the measurement.

3.5.2 Microstructural examination of creep specimens.

In order to relate the creep behaviour to the microstructure, some of the crept specimens were examined by electron microscopy. The gauge length part of the crept

specimen was hand-ground into ~ 0.2 mm thick strips using 240-600 grit abrasive paper. The method and equipment used to prepare thin foils were the same as mentioned previously. The dislocation structure of these specimens was examined using the bright field technique usually taking the {111} thin foil orientation.

3.6 Optical microscopy

The grain sizes of creep specimens were measured in a optical microscope. The specimens were polished mechanically and the etchant used to reveal the grain size of the polished specimens was HCl: H_2O_2 = 1:1 solution. The method for determining grain size was the ASTM comparative method[94].

The optical microstructures of creep specimens before and after creep tests were also examined in the optical microscope. The etchant used for this purpose was 10% Cr_2O_3 in H_2O: HCl = 1:3.

CHAPTER 4 RESULTS

4.1 Grain size

In order to produce specimens of similar grain size from 3.4 mm and 2.5 mm thick starting material, the effect of the amount of deformation and annealing time on grain size was studied. It was found, as illustrated in Figures 26a and b, that the grain sizes of materials deformed 60% and 45%, followed by annealing for 1 hr at 1323 K were nearly the same, i.e. the grain size of 60% deformation material was 0.12 mm, and that of 45% deformed material was 0.11 mm. The similarity in the grain size of 60% and 45% deformed material may be due to the presence of impurities since the material used is a commercial alloy. Therefore, 3.4 mm thick strips were deformed 60% and 2.5 mm thick strips were deformed 45% to produce 1.4 mm thick strips. These strips were used to produce tensile and creep specimens. They were then solution heat treated for 1 hour at 1323 K and water quenched. The grain size of these specimens was generally about 0.11 0.12 mm.

The temperature of solution treatment was observed to affect the creep behaviour. The results of the preliminary tests showed that the specimens solution treated at 1473 K had a lower creep rate but the creep life results had too great a scatter when compared with the specimens solution treated at 1323 K for 1 hour which is similar to the commercial practice. Therefore the temperature of 1323 K was used for solution treatment in this investigation.

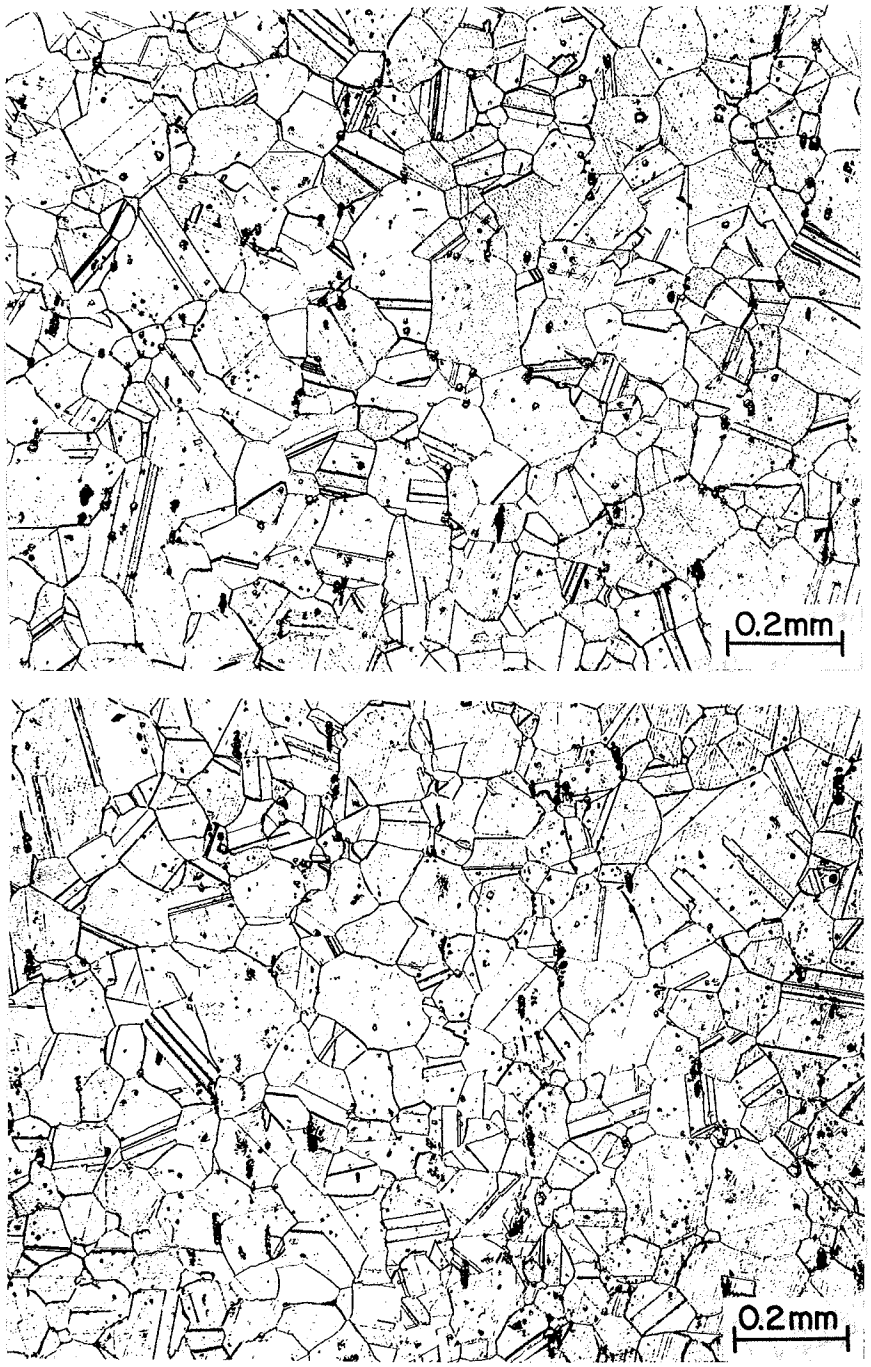

(a)

(b)

Figure 26: Grain size. Etchant. Hcl: H_2O_2 = 1:1,
a. 1323 K/1 hour, 60% deformation
b. 1323 K/1 hour, 45% deformation

4.2 Precipitation and Coarsening Behaviour of γ" and γ' phases.

In an earlier study the microstructural analysis of this alloy, aged under various conditions, was carried out[4,5]. It was found that when the deformed Inconel 718 alloy was annealed for 1 hour at 1473 K or 1323 K a supersaturated, FCC solid solution is obtained. Upon subsequent aging in the temperature range of 973 to 1023 K both γ" and γ' phases precipitate simultaneously in the FCC γ matrix. Figures 27 and 28 shown typical bright field structures and dark field structures by using (100) reflection for specimens aged at 998 K for 15 hrs and 200 hrs respectively. In these micrographs the dark, spherical particles are γ' precipipates and the disc shaped particles are γ" precipitates. The γ' precipitates have an ordered FCC LI_2 structure and precipitate coherently with an orientation relationship of {100} γ' || {100} γ, < 001 > γ' || < 001 > γ. The γ" precipitates have an ordered BCT DO_{22} structure and precipitate coherently with an orientation relationship of {100} γ" || {100} γ and < 001 > γ" || < 001 > γ. The c axis of the γ" phase was normal to the disc plane and the ratio of diameter to thickness, or the aspect ratio dγ"/hγ" is in the range of 3.60 to 4.03. The lattice misfit between γ' and γ matrix was about 0.407% and the tetragonal distortion between

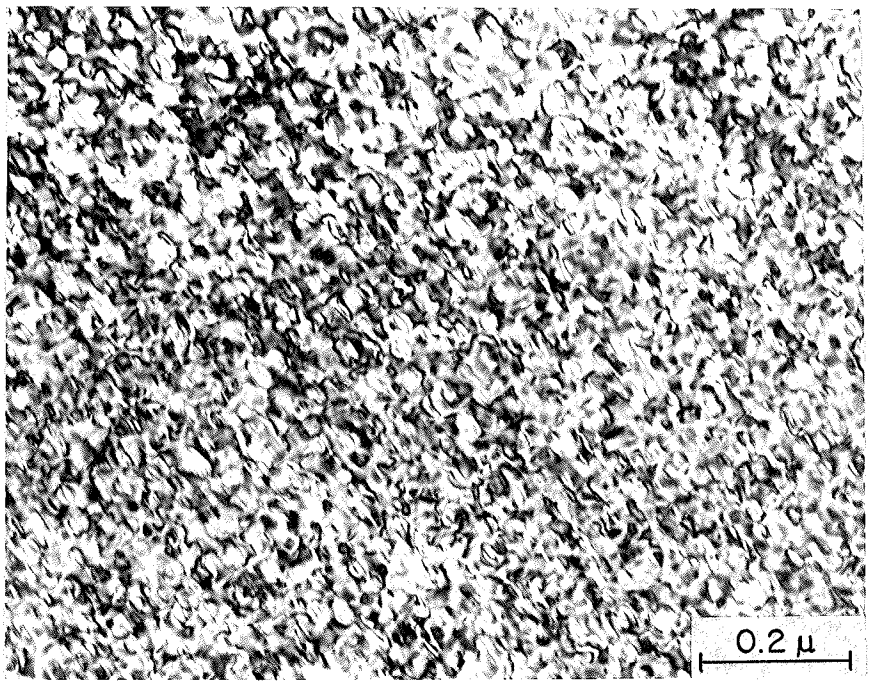

(a)

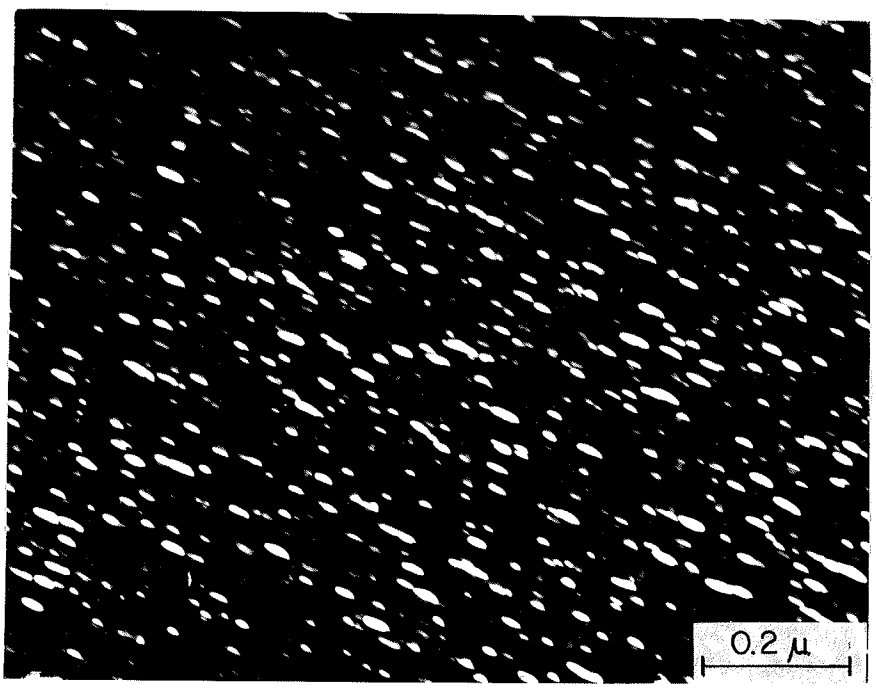

(b)

Figure 27: Microstructure of a specimen aged for 15 hrs at 998K
(a) Bright field
(b) Dark field taken with (001) reflection spot.

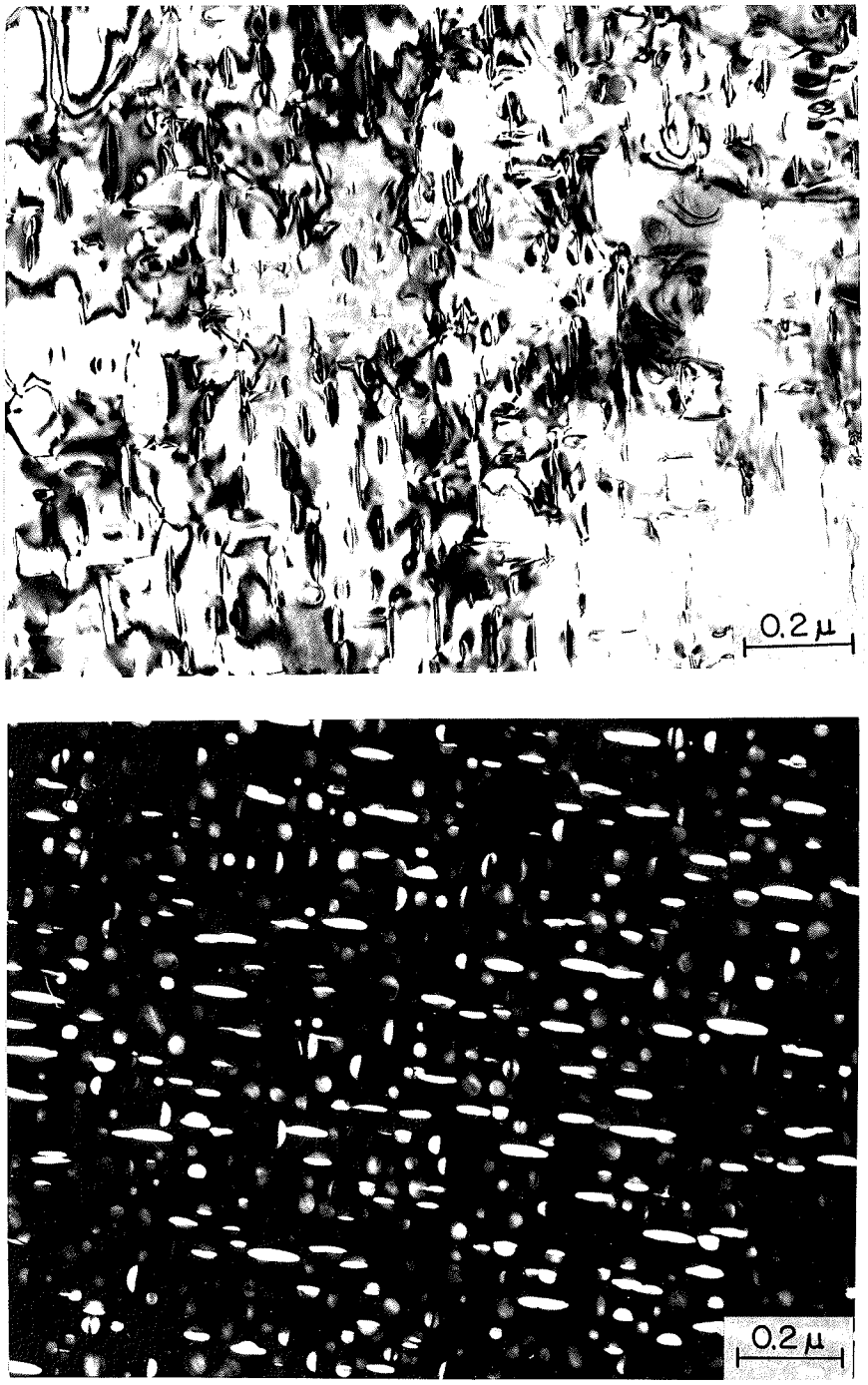

(a)

(b)

Figure 28: Microstructure of a specimen aged for 200 hrs at 998 K.
(a) Bright field
(b) Dark field taken with (001) reflection spot.

γ'' phase and γ matrix was ~ 2.86%. The total volume fraction of γ'' and γ' phases for specimens aged at 998 K for more than 4 hours was about 16.6% and the ratio of volume fraction of γ'' and γ' precipitates, $f\gamma''/f\gamma'$, was in the range of 2.50 to 3.67 with an average ratio of 3.0. The coarsening behaviour of both γ'' and γ' precipitates in this alloy has been found to follow the diffusion controlled LSW (Lifshitz-Wagner) theory, i.e., $\bar{d}^3 - \bar{d}_o^3 = Kt$, where $\bar{d}_o$ is the average particle size at the onset of the coarsening process[5]. Therefore, whenever the precipitate particles in creep specimens were too small to be measured by micrographs, their size was estimated by extrapolating the plot of log d vs. log t in the larger particle size region as shown in Figure 29.

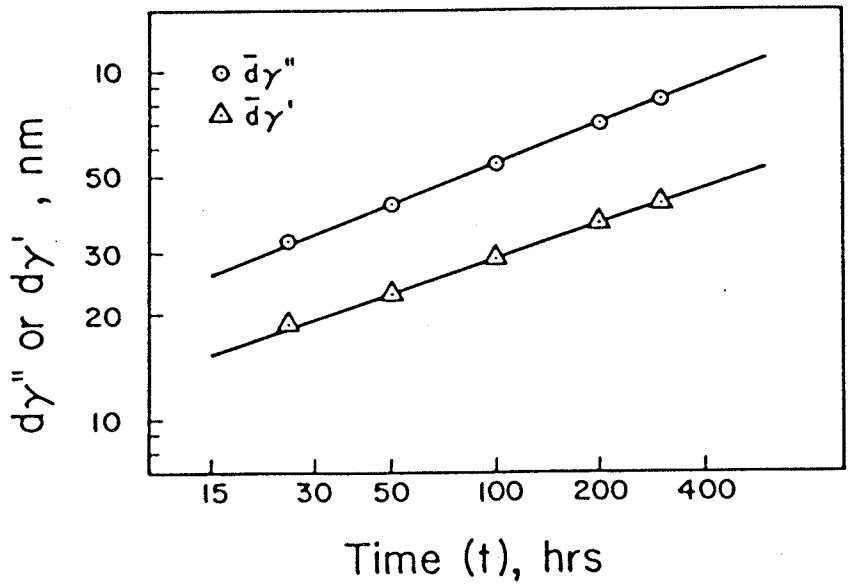

Figure 29: Log plots of mean particle diameter of γ'' and γ' particles v. aging time at the temperature of 998K.

4.3 Results of tensile tests

In order to select the stress level of creep tests some tensile tests were carried out in an Instron machine at temperatures of 873 K and 923 K. The yield stresses of specimens solution treated at 1323 K for 1 hr and aged at 998 K for 3, 7, 15 hrs are listed in Table 2. The strain rates of these tensile tests were in the range of $3.3 \times 10^{-2} \sim 3.3 \times 10^{-9}$ sec^{-1}. The results show that the effect of aging time on yield stress at high temperature is similar to that at room temperature[4], i.e. the optimum yield strength is obtained when specimens are aged at 998 K for about 15 hrs. The results in Table 2 also show that the yield stress is not very sensitive to the strain rate in the strain rate range of 3.3×10^{-2} to 3.3×10^{-9}; i.e. the difference in yield stresses at various strain rates is less than 10%. It seems the maximum yield stress is obtained when the strain rate is of the order of $10^{-7} sec^{-1}$.

Table 2 Experimental results of tensile tests

Aging time at 998K	Testing Temp	Strain rate $\dot{\varepsilon}(sec^{-1})$	$\sigma_{0.2}$ (MN/m^2)	$\sigma_{0.05}$ (MN/m^2)
15 hrs	873 K	3.3×10^{-2}	817	
		3.3×10^{-3}	830	
		3.3×10^{-4}	819	
		3.3×10^{-5}	872	844
		1.3×10^{-6}	850	815
		3.3×10^{-7}	896	845
		3.3×10^{-8}	874	847
		3.3×10^{-9}	800	800
3 hrs	923 K	3.3×10^{-4}	620	
7 hrs		3.3×10^{-4}	714	
15 hrs		3.3×10^{-4}	758	
25 hrs		3.3×10^{-4}	745	

4.4 Determination of steady state creep rates, $\dot{\varepsilon}_s$

As discussed in Chapter 2, the steady creep rate can be expressed as

$$\dot{\varepsilon}_s = A_1 \sigma_a^{n_a} \exp(-Q_c/RT) \quad (2.5)$$

and $$\dot{\varepsilon}_s = A^* \left(\frac{\sigma_a - \sigma_o}{G}\right)^{n_e} \exp(-Q_e/RT) \quad (2.18)$$

or $$\dot{\varepsilon}_s = \pi \sigma_a b^3 D/2KTd^2 \quad (2.15)$$

and $$\dot{\varepsilon}_s = A' d D\sigma_a^4 \quad (2.16)$$

Therefore in order to study the creep deformation mechanism and the effect of particle size on creep rate, the steady state creep rate, $\dot{\varepsilon}_s$, and the value of back stress, σ_o, were determined.

Creep tests were carried out in the temperature range of 853 K - 943 K and the stress range of 620 to 840 MN/m^2. The normal creep behaviour was observed during the creep tests, i.e., decelerating creep in primary stage followed by an extended steady state creep, and then an accelerating creep rate in the tertiary stage. This is illustrated in Figure 30, which is the creep curve of a specimen aged for 15 hrs at 998 K and tested at a temperature of 898 K and a stress of 738 MN/m^2. Since only secondary creep was of interest in this study the creep tests were usually terminated before the tertiary creep stage. The steady state creep rates were measured from creep curves of specimens heat treated and tested under various stress and temperature

conditions. The results are listed in Tables 3, 4, 5 and 6. Table 3 shows the steady creep rate, $\dot{\varepsilon}_s$, of specimens aged for 15 hours at 998 K (where the peak yield strength of this alloy at room temperature is obtained) crept at temperatures in the range of 853 K - 943 K and at stresses in the range of 620 - 746 MN/m^2. The above data are also plotted in Figure 31. It is seen that a linear relationship exists between log $\dot{\varepsilon}_s$ and

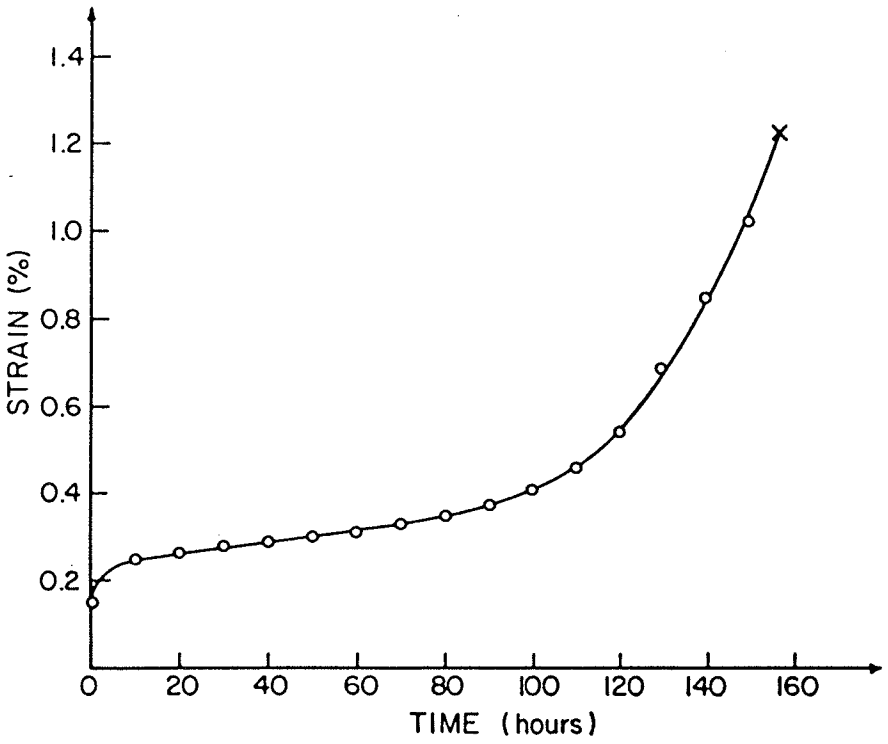

Figure 30: Creep curve of Inconel 718 alloy aged for 15 hrs at 998 K and tested at 873 K and a stress of 738 MN/m^2.

Table 3 Steady state creep rate, $\dot{\varepsilon}_s$, of the specimens aged for 15 hrs at 998 K ($d\gamma'' = 26.9$ nm) and tested in the low stress range.

$\dot{\varepsilon}_s$ / σ_a / T.T.	620	643	670	695	720	746
853 K			0.38×10^{-9}		0.70×10^{-9}	1.03×10^{-9}
873 K	0.59×10^{-9}		1.60×10^{-9}		2.78×10^{-9}	
			1.73×10^{-9}	2.08×10^{-9}	3.10×10^{-9}	3.95×10^{-9}
898 K	2.50×10^{-9}		4.65×10^{-9}	7.08×10^{-9}	9.65×10^{-9}	
923 K	8.97×10^{-9}		19.75×10^{-9}			
			16.30×10^{-9}	28.50×10^{-9}	38.61×10^{-9}	
943 K	18.50×10^{-9}	27.7×10^{-9}	35.40×10^{-9}	64.80×10^{-9}		

σ_a MN/m^2

$\dot{\varepsilon}_s$ sec^{-1}

T.T. Testing Temperature

Table 4 Steady state creep rate, $\dot{\varepsilon}_s$, of the specimens aged for 15 hrs at 998 K ($d\gamma'' = 26.9$ nm) and tested in the high stress range.

	765 MN/m^2	790 MN/m^2	815 MN/m^2	840 MN/m^2
873 K	8.1×10^{-9}			
873 K	8.9×10^{-9}	13.8×10^{-9}	17.8×10^{-9}	31.8×10^{-9}
898 K	16.7×10^{-9}	29.9×10^{-9}	40.6×10^{-9}	79.0×10^{-9}

Table 5 Steady state creep rate, $\dot{\varepsilon}_s$, of the specimens aged for 3,7,15 and 100 hrs at 998 K and tested at 873 K.

$\dot{\varepsilon}_s$ / σ_a / T.T.	σ_a = 620	σ_a = 643	σ_a = 670	σ_a = 695	σ_a = 720	σ_a = 746
3 hrs ($d\gamma''$ = 14.8 nm)	1.06×10^{-9}	1.39×10^{-9}	2.16×10^{-9}	2.68×10^{-9}	3.83×10^{-9}	
7 hrs		0.81×10^{-9}	1.14×10^{-9}		2.08×10^{-9}	
($d\gamma''$ = 20.3 nm)		0.75×10^{-9}	1.21×10^{-9}	1.39×10^{-9}	2.36×10^{-9}	3.11×10^{-9}
15 hrs			1.60×10^{-9}		2.78×10^{-9}	
($d\gamma''$ = 26.9 nm)	0.59×10^{-9}		1.74×10^{-9}	2.08×10^{-9}	3.10×10^{-9}	3.95×10^{-9}
100 hrs						
($d\gamma''$ = 53.8 nm)		4.63×10^{-9}	7.6×10^{-9}	10.60×10^{-9}	14.70×10^{-9}	

σ_a MN/m^2 T.T. Testing Temperature

$\dot{\varepsilon}_s$ sec^{-1}

Table 6. Dependence of creep rate on particle size in the stress range of 670 ~ 815 MN/m^2 at 873 K.

Aging time(hrs) at 998 K	$d\gamma''$ (nm)	$d\gamma'$ (nm)	$\dot{\varepsilon}_s$ (10^{-9} sec^{-1})				
			σ^* = 670	σ = 695	σ = 720	σ = 765	σ = 815
1	9.9	6.5			9.55		
3	14.8	9.2	2.16	2.68	3.83	8.90	22.7
5	17.2	11.0	1.62	2.05	2.52	5.80	13.9
7	20.3	12.3	1.21	1.39	2.08	3.56	7.07
10	23.2	13.7	0.90	1.05	1.77	2.95	5.10
15	26.9	15.7	1.736	2.08	2.94	4.63	7.12
25	32.6	18.4	2.78	4.17	5.20	7.67	13.0
50	42.4	23.0	4.86	5.56	9.14	14.67	21.4
100	53.8	29.2	10.00	12.50	15.0		

* σ = 670 MN/m^2

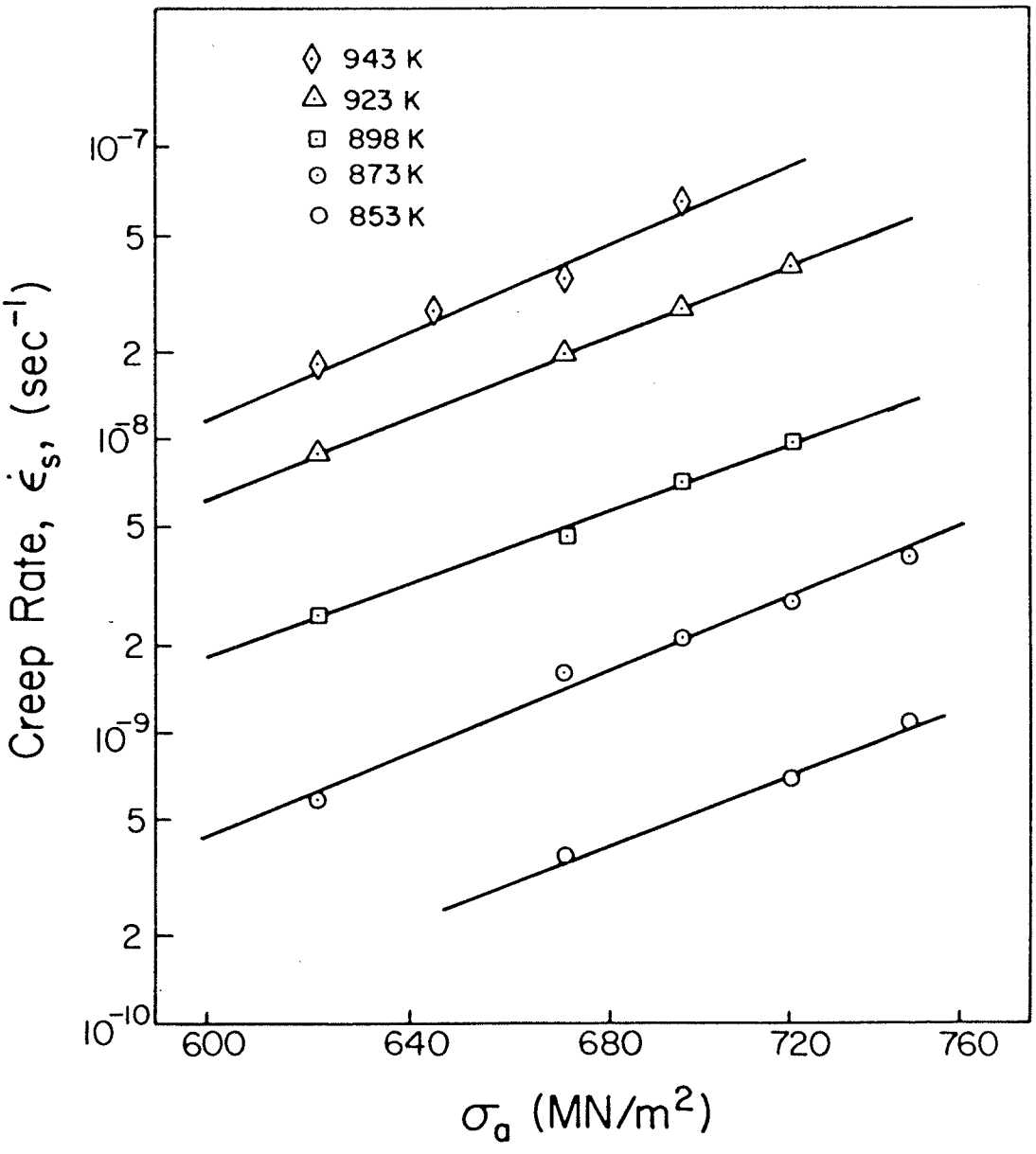

Figure 31: Dependence of steady state creep rate on applied stress at various temperatures of specimens aged at 998 K for 15 hrs, for determining the values of apparent stress exponent, n_a.

log σ_a at each testing temperature. It is also found that, as expected, the steady state creep rates increase with the testing temperature. The creep rates, $\dot{\varepsilon}_s$, of peak strengthened specimens tested at 873 K and 898 K at a stress in the high stress region of 765 - 840 MN/m^2 are listed in Table 4. For comparison, the dependence of $\dot{\varepsilon}_s$ on σ_a at 873 K and 898 K in both the low stress range of 620 - 746 MN/m^2 and the high stress region of 765 - 840 MN/m^2 are shown in Figure 32. It is seen that the slopes of the log $\dot{\varepsilon}_s$ vs. log σ_a plots are greater in the high stress range than in the low stress range. This suggests that the creep rate, $\dot{\varepsilon}_s$, is more sensitive to the applied stress in the high stress region than in the low stress region. Table 5 as well as Figure 33 shows the dependence of steady state creep rate, $\dot{\varepsilon}_s$, on the applied stress, σ_a, for specimens with different sizes of γ'' and γ' phases, tested at a temperature of 873 K and at stresses in the range of 620 - 746 MN/m^2. For each particle size a linear relationship between log $\dot{\varepsilon}_s$ and log σ_a is obtained; i.e., a $\dot{\varepsilon}_s \propto \sigma_a^{n_a}$ relationship exists. It is also seen that at all the stress levels, specimens with a particle size of $d\gamma''$ = 20.3 nm, i.e., specimens aged at 998 K for 7 hours, have the lowest creep rate.

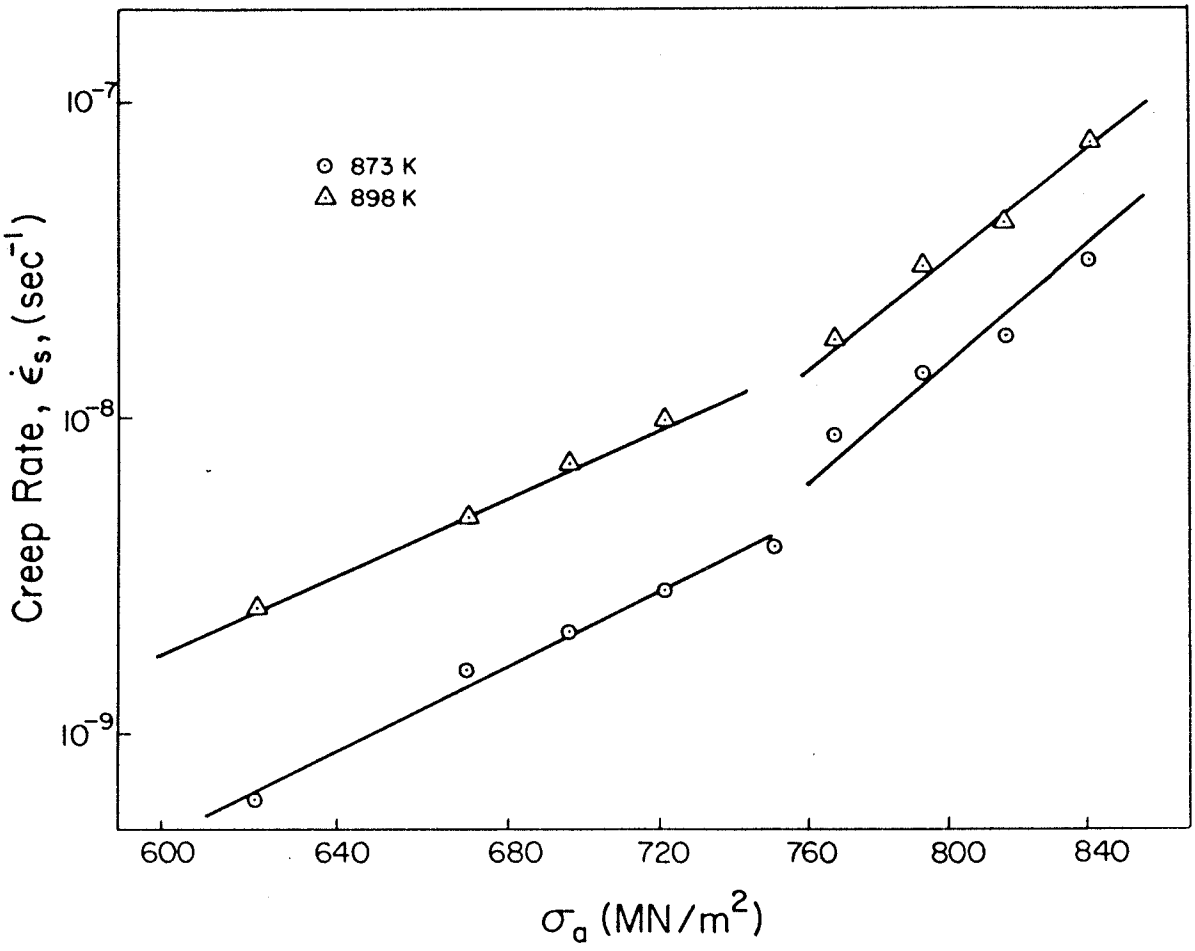

Figure 32: Dependence of $\dot{\epsilon}_s$ on applied stress in different stress ranges of the specimens aged for 15 hrs at 998 K and tested at 873 and 898 K, for determining the values of apparent stress exponent, n_a.

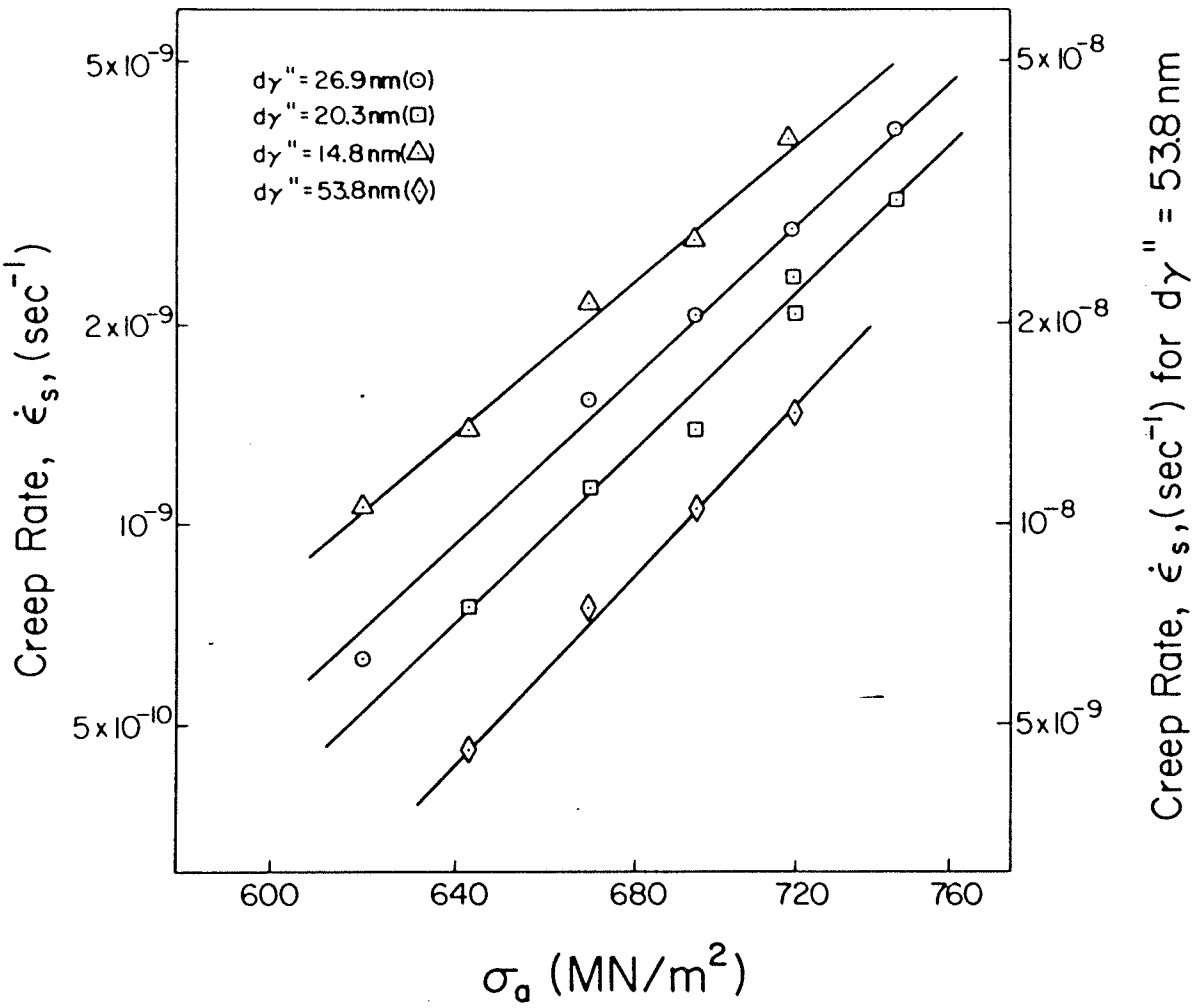

Figure 33: Dependence of $\dot{\varepsilon}_s$ on applied stress of specimens with different particle sizes tested at 873 K and in the stress range of 620 - 746 MN/m^2, for determining the values of apparent stress exponent, n_a.

4.5 Determination of back stress, σ_o, and threshold stress, $\sigma_o(th)$.

The back stress, σ_o, or threshold stress, $\sigma_o(th)$, of underaged and overaged Inconel 718 in the applied stress range of 620 - 865 MN/m^2 and the temperature range of 853 - 943 K has been measured by the consecutive stress reduction method. The strain vs. time curves showed the presence of incubation periods after small stress reductions, the length of which depended on the testing condition, i.e., the remaining stress, the testing temperature and the aging time of the specimens. A typical example is illustrated in Figure 34, which is the creep curve of a specimen aged at 998 K for 15 hrs tested at 873 K with a starting applied stress of 790 MN/m^2. The amount of the stress reduction was 5% of the starting applied stress. In order to determine the back stress, the curves of the remaining stress vs. cumulative incubation period ($\Sigma\Delta t$) were plotted. A few typical examples shown in Figure 35. The back stress or threshold stress, σ_o is taken as the asymptotic value of remaining stress when the cumulative incubation time appears to be infinite.

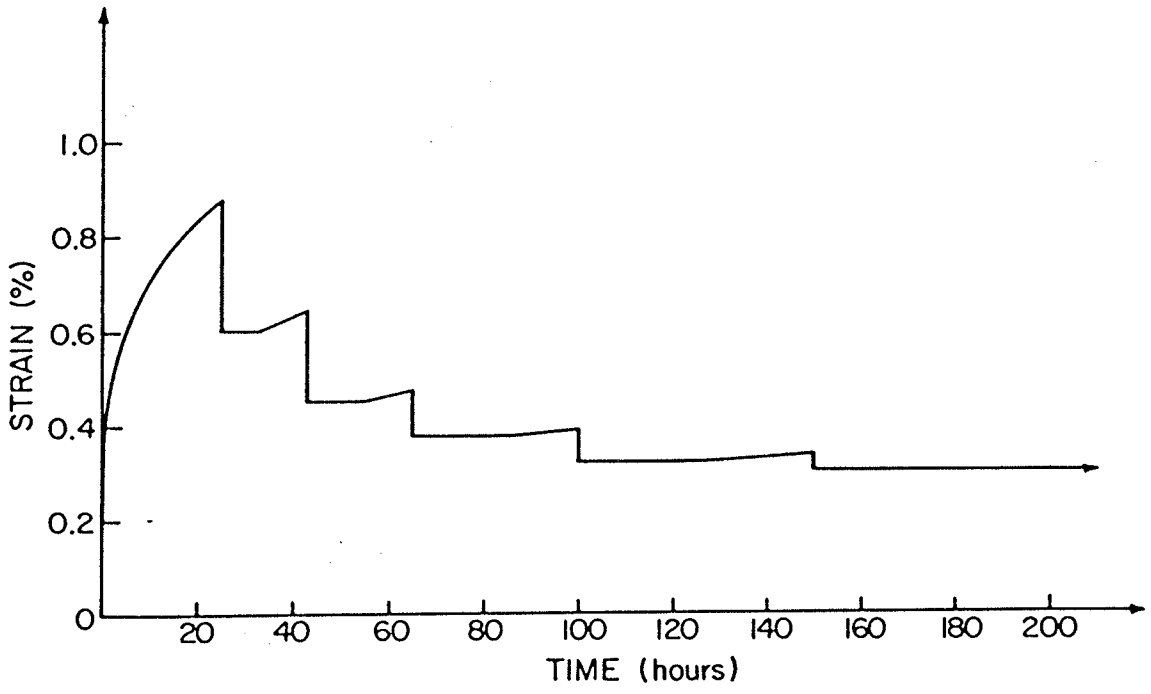

Figure 34: Strain vs. time curve during consectuive stress reduction tests. The specimen was aged at 998 K for 15 hrs and tested at 873 K and stress from 790 MN/m^2 to 622 MN/m^2.

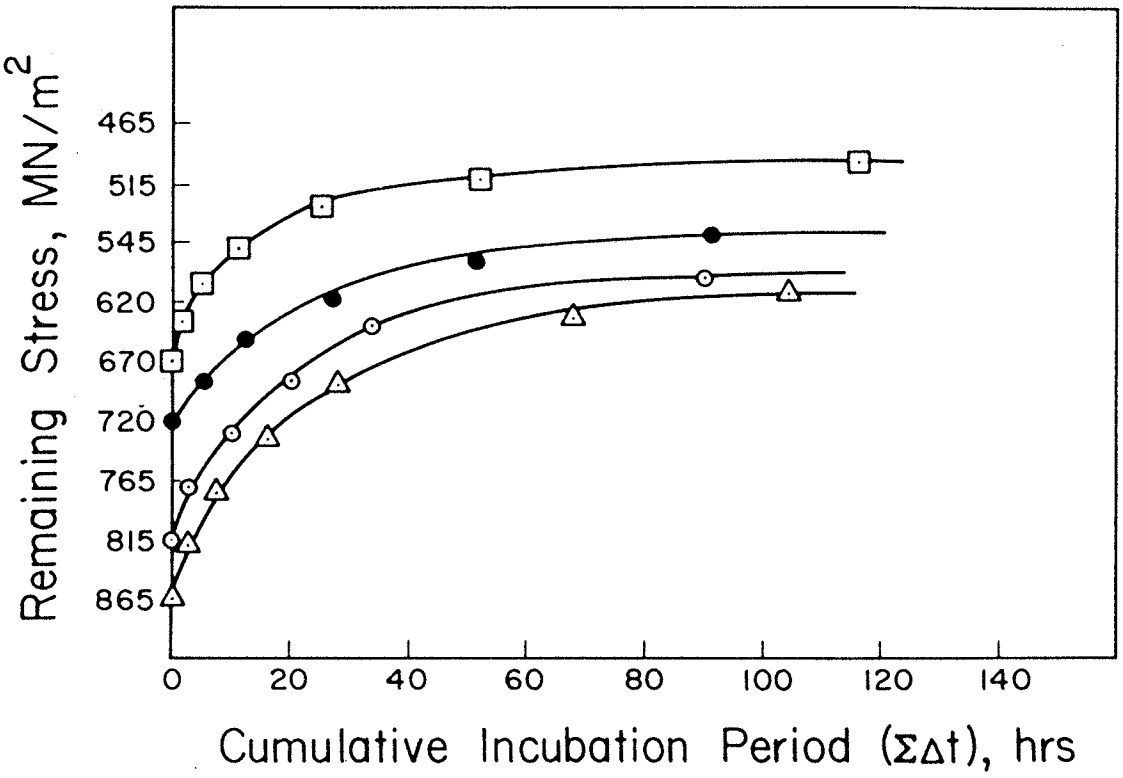

Figure 35: The curves of remaining stress vs. cumulative incubation time ($\Sigma\Delta t$) for specimens aged at 998 K for 15 hrs, and tested at the temperatures of 873 K at initial stress of 865 MN/m^2 (△) and 815 MN/m^2 (⊙), 898 K at initial stress of 720 MN/m^2 (●), 923 K at initial stress of 670 MN/m^2 (⊡).

The measured values of σ_o for various specimens are given in Table 7. The results in Table 7 show that when specimens aged for 15 hrs at 998 K were tested in the temperature range of 853 K - 923 K the value of σ_o remained constant, i.e., there existed a threshold stress, $\sigma_o(th)$, as long as the applied stresses were below a critical value. These critical values are seen to depend on test temperatures. For example, the value of σ_c at 853 and 873 K was 746 MN/m^2, while at 898 K and 923 K the value of σ_c was 720 and 695 MN/m^2, respectively. However, when the applied stress exceeded these critical stresses the back stress, σ_o, increased with increasing applied stress. The rate of increase in σ_o with applied stress, $d\sigma_o/d\sigma_a$, was found to be 0.27 and 0.24 at temperatures of 873 and 898 K, respectively. Table 7 also shows that the threshold stress, $\sigma_o(th)$, and back stress, σ_o, decrease with increasing testing temperature. In the lower stress range of 620 - 720 MN/m^2, the threshold stress, $\sigma_o(th)$, has values of 617,576, 540 and 510 MN/m^2 for testing temperatures of 853, 873, 898 and 923 K, respectively, which is also shown in Figure 36. In the high applied stress range, i.e., $\sigma_a > 765$ MN/m^2, only two data points were obtained. However they seem to follow a similar trend as well. For example, when $\sigma_a = 765$ MN/m^2 the value of σ_o decreases from 588 MN/m^2 to 571 MN/m^2 as the testing temperature increases from 873 K to 898 K. When $\sigma_a = 815$ MN/m^2 the value of σ_o decreases from 604 MN/m^2 to 583 MN/m^2 as the temperature increases from 873 K to 898 K.

Table. 7 Experimentally determined backstress of Inconal 718 alloy

Aging time at 998K(hrs)	dγ"(nm)	Testing temp. (K)	σ_a(MN/m^2)	σ_o(MN/m^2)	σ_o/σ_a
		853	643 - 746	617	0.83 - 0.95
		873	620 - 720	576	0.80 - 0.93
		873	765	588	0.77
		873	815	604	0.74
		873	865	615	0.71
15 hrs	26.9	898	620 - 720	540	0.75 - 0.87
		898	765	571	0.74
		898	815	583	0.71
		898	840	589	0.70
		923	620 - 695	510	0.73 - 0.82
		943	620 - 695	437 - 473	0.68 - 0.70
1	9.9			467	0.65 - 0.75
3	14.8			564	0.78 - 0.91
5	17.2			590	0.82 - 0.95
7	20.3			600	0.83 - 0.97
10	23.2	873	620 - 720	600	0.83 - 0.97
15	26.9			576	0.80 - 0.93
25	32.6			564	0.78 - 0.93
50	42.4			538	0.75 - 0.87
100	53.8			522	0.73 - 0.84
200	70.2			472	0.66 - 0.76
400	90.8			416	0.58 - 0.67

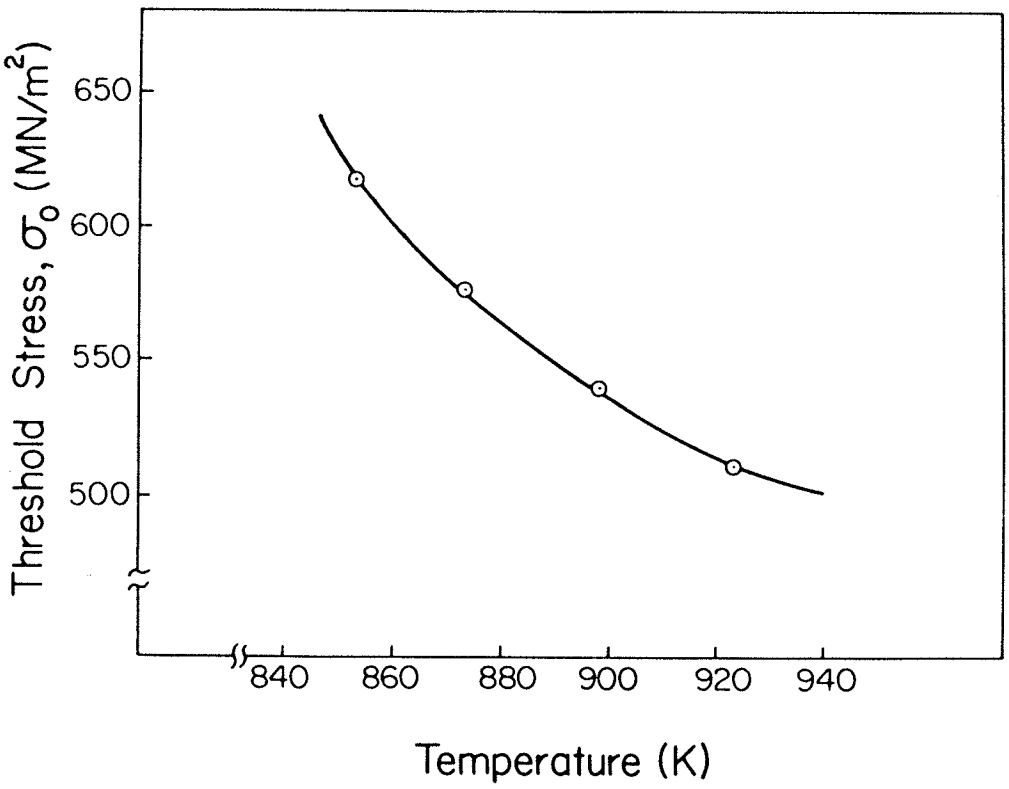

Figure 36: The variation of threshold stress on testing temperature for specimens aged at 998 K for 15 hrs and tested in the stress range of 620 - 720 MN/m^2.

The dependence of the threshold stress, $\sigma_o(th)$, on particle size for specimens tested at 873 K at stresses in the range of 620 - 720 MN/m^2, is also listed in Table 7 and further shown in Figure 37. These results show that when the particle size is small, i.e., in the under-peak aged region, the threshold stress, $\sigma_{o(th)}$, increases with particle size until a maximum $\sigma_{o(th)}$ is reached (when the diameter of γ'' is 23.2 nm). With further increase in γ'' particle size, i.e., in the overaged region, $\sigma_{o(th)}$ decreases with increasing particle size.

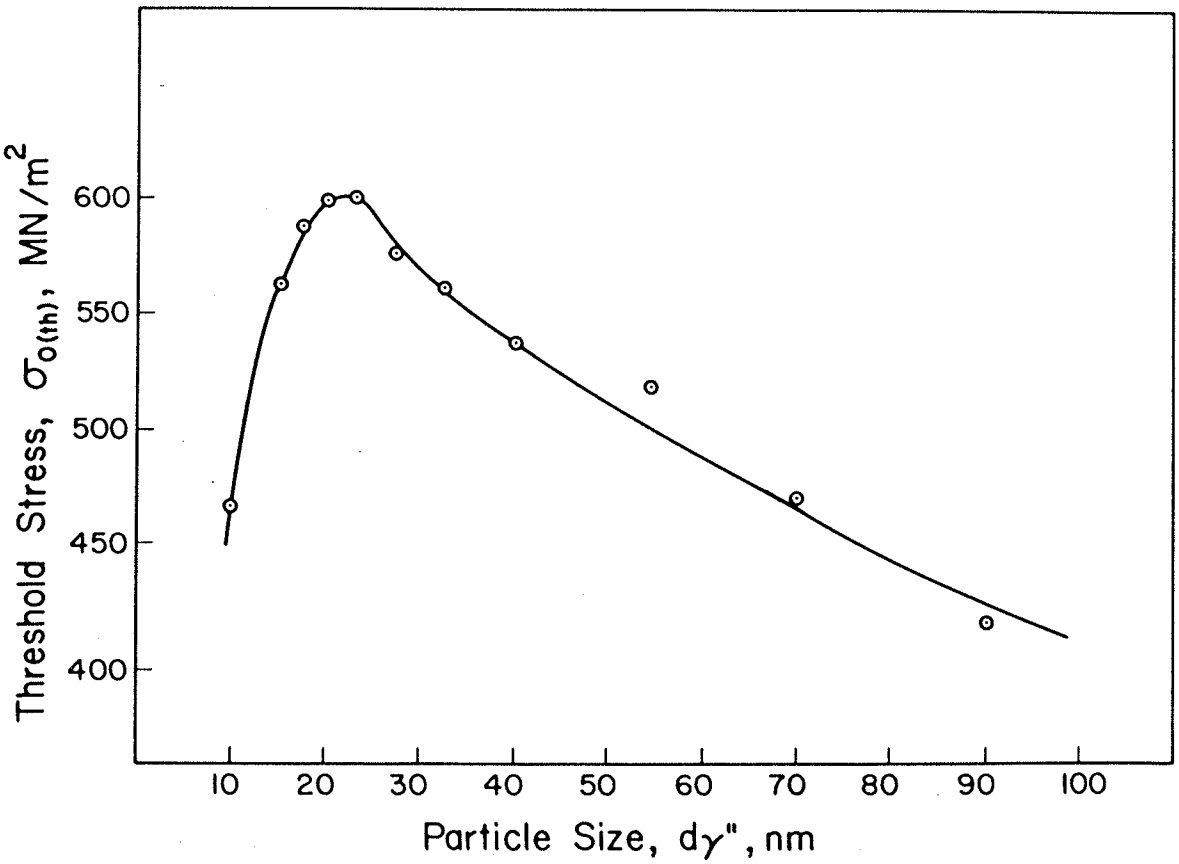

Figure 37: The dependence of threshold stress on particle size for specimens were aged at 998 K for 15 hrs and tested at 873 K and in the stress range of 620 MN/m^2 - 720 MN/m^2.

4.6 Apparent and effective parameters of creep rate equations.

As discussed in Chapter 2, the creep deformation mechanism of secondary creep can be determined from the values of effective stress exponent and activation energy for the creep rate equation (2.18). Therefore, in order to study the creep mechanism of Inconel 718 alloy, the apparent and effective stress exponents, n_a and n_e, and activation energies, Q_c and Q_e for the secondary creep rate equations (2.5) and (2.18) were determined by experimentally measuring the steady state creep rate, $\dot{\varepsilon}_s$, and the back stress, σ_o.

4.6.1 Apparent and effective stress exponents, n_a and n_e.

Based on the experimental data shown in Tables 3, 4, 5 and 7 and Figures 31, 32 and 33, the apparent stress exponent values, n_a for the creep rate equation

$$\dot{\varepsilon}_s = A_1 \sigma_a^{n_a} \exp(-Q_c/RT) \qquad (2.5)$$

calculated from the slopes of the log $\dot{\varepsilon}_s$ vs. log σ_a plots are listed in Tables 8 and 9 for various conditions and particle sizes. Similar to most alloys containing second phase particles the values of stress exponents are between 8.57 and 15.93. These values are greater than the value of unity, which is the value for diffusional creep and values of 3-6, which are values for dislocation power law creep.

Table 8 Experimentally determined values of n_a, n_e and σ_o
(specimens aged for 15 hrs at 998 K with $d\gamma'' = 26.9$ nm, $d\gamma' = 15.7$ nm)

Testing Temp. (K)	σ_a (MN/m^2)	σ_o (MN/m^2)	n_a	n_e
853	670 - 746	617	9.77 ± 0.10 E-01	1.12 ± 0.36 E-02
873	620 - 746	576	10.12 ± 0.43 E-02	1.37 ± 0.56 E-02
898	620 - 720	540	9.10 ± 0.13 E-02	1.68 ± 0.72 E-02
923	620 - 695	510	10.31 ± 0.53 E-02	2.36 ± 0.92 E-02
943	620 - 695	437 - 473	10.40 ± 0.72 E-02	5.12 ± 0.83 E-02
873	765 - 840	588 - 613	13.49 ± 0.48 E-02	5.10 ± 0.51 E-02
898	765 - 840	571 - 587	15.93 ± 0.58 E-02	5.65 ± 0.53 E-02

Table 9 Experimentally determined values of n_a, n_e and σ_o at a testing temperature of 873 K.

aging condition	$d\gamma''$(nm)	$d\gamma'$(nm)	σ_a (MN/m^2)	σ_o (MN/m^2)	n_a	n_e
998 k/3 hrs	14.8	9.1	620 - 720	564	8.57 ± 0.12 E-02	1.25 ± 0.44 E-03
998 K/7 hrs	20.3	12.3	643 - 746	590	9.14 ± 0.42 E-02	1.21 ± 0.90 E-03
998 K/15 hrs	26.9	15.7	620 - 746	576	10.12 ± 0.40 E-02	1.37 ± 0.57 E-02
998 K/100 hrs	53.8	29.2	643 - 720	518	10.13 ± 0.95 E-03	2.37 ± 0.15 E-03

The experimentally measured values of back stress, σ_o, are also listed in Tables 8 and 9. Upon knowing the values of back stress, σ_o, the effective stress exponents, n_e, of the creep rate equation

$$\dot{\varepsilon}_s = A^* \left(\frac{\sigma_a - \sigma_o}{G}\right)^{n_e} \exp\left(-Q_e/KT\right) \qquad (2.18)$$

can be obtained from the slope of the logarithmic plot of steady state creep rate, $\dot{\varepsilon}_s$, vs. shear modulus compensated effective stress, $(\sigma_a - \sigma_o)/G$. The plots of log $\dot{\varepsilon}_s$ vs log $\left(\frac{\sigma_a - \sigma_o}{G}\right)$ are shown in Figures 38 and 39. Figure 38 shows the log $\dot{\varepsilon}_s$ vs. log $\left(\frac{\sigma_a - \sigma_o}{G}\right)$ plots for materials aged at 998k K for 15 hours and crept at temperature in the range of 853 - 943 K at stresses in the ranges of 620 - 746 MN/m^2 and 765 - 840 MN/m^2. Figure 39 shows the log $\dot{\varepsilon}_s$ vs. log $\left(\frac{\sigma_a - \sigma_o}{G}\right)$ plots of specimens of this alloy with different particle size, (i.e., dγ" = 14.8 nm, 20.3 nm, 26.9 nm and 53.8 nm for specimens aged at 998 K for 3, 7, 15 and 100 hrs respectively) crept at 873 K and in the stress range of 620 - 746 MN/m^2.

The values of the effective stress exponent, n_e, are between 1.12 and 5.65 and are given in Tables 8 and 9. It is observed that the effective stress exponents, n_e, increase with an increase in either the test temperature or applied

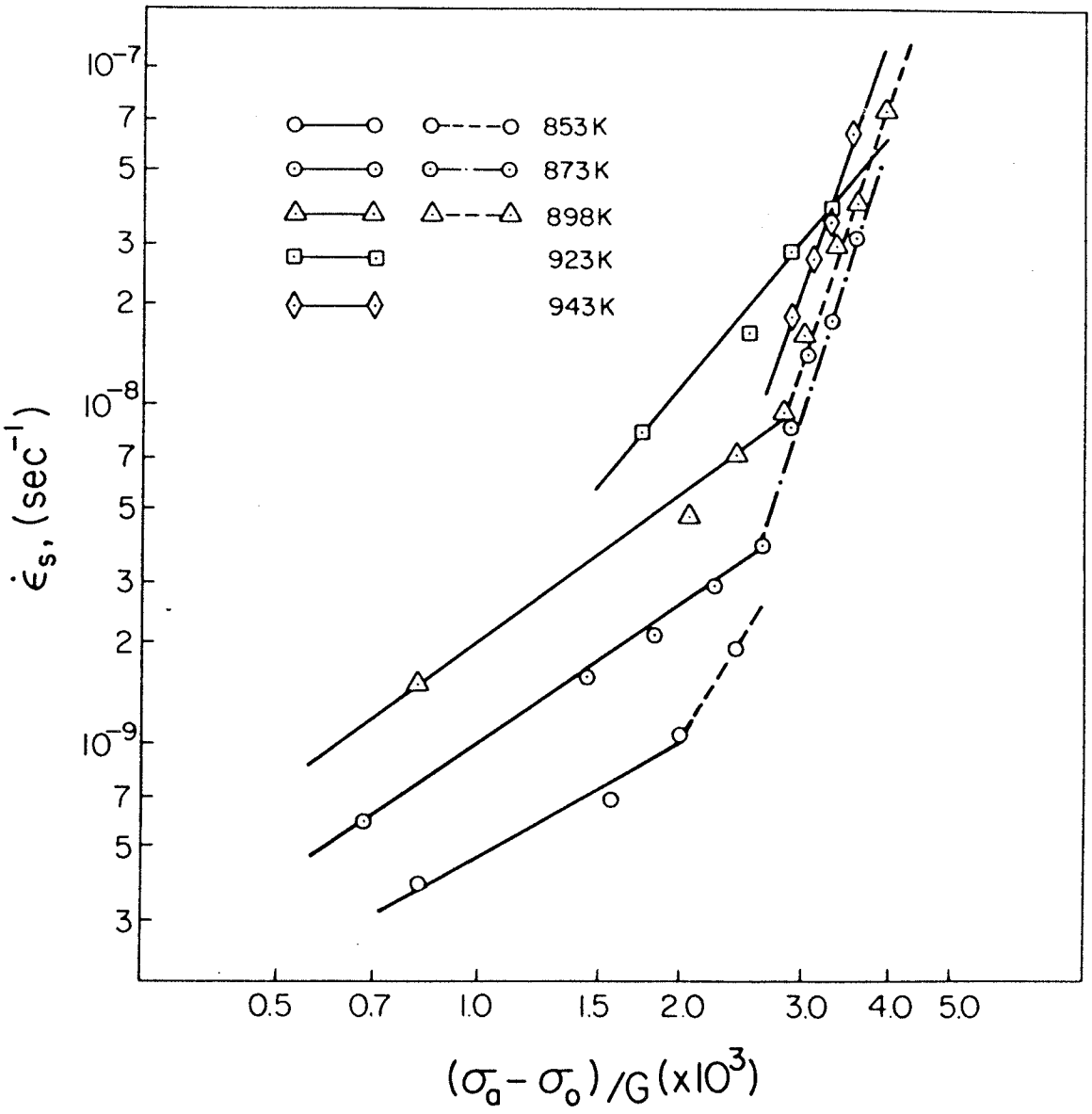

Figure 38: Dependence of steady state creep rate, $\dot{\varepsilon}_s$, on shear modulus compensated effective stress of the specimens aged at 998 K for 15 hrs and tested at 853K - 943K and in the stress ranges of σ_a = 620 - 720 MN/m^2 (——) and σ_a = 765 - 840 MN/m^2 (——·——), for determining the values of effective stress exponent, n_e.

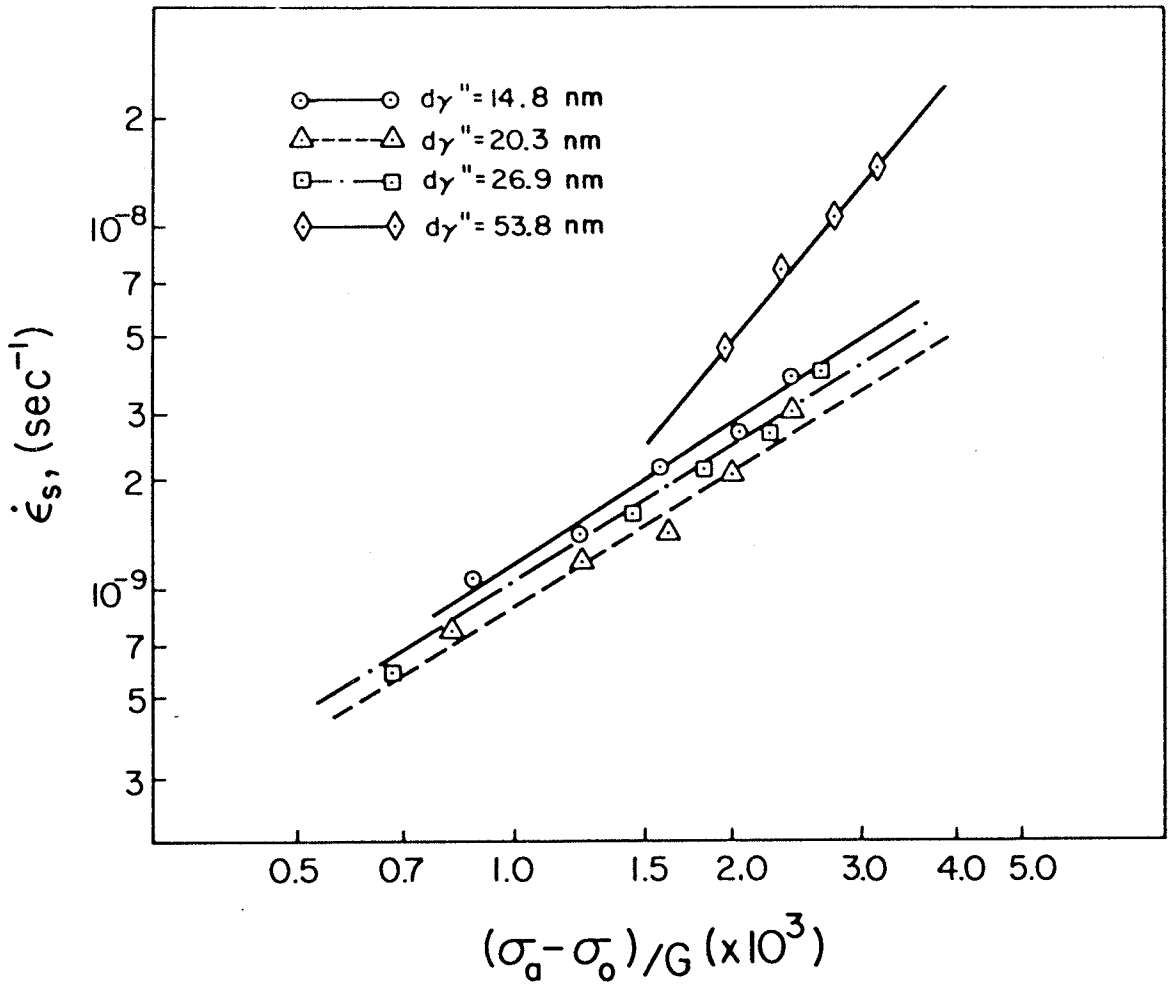

Figure 39: Dependence of $\dot{\varepsilon}_s$ on shear modulus compensated effective stress of specimens with different particle sizes and tested at 873 K and in the stress range of 620 - 720 MN/m^2, for determining the values of effective stress exponent, n_e.

stress, i.e., in the stress range of 620 - 746 MN/m^2 the values of n_e increase from n_e = 1.12 at the testing temperature of 853 K to n_e = 5.12 at 943 K. On the other hand, at the temperatures of 873 K and 898 K the values of n_e increase from 1.37 and 1.68 in the low stress range of 620 - 746 MN/m^2 to 5.10 and 5.65 in the high stress range of 765 - 840 MN/m^2.

The results in Table 9 show that the particle size affects the effective stress exponent, i.e., n_e increases from n_e = 1.21 - 1.37 when the particle size, $d\gamma''$ is less than 27.0 nm to n_e = 2.37 when the particle size is equal to 53.8 nm.

4.6.2 Apparent and effective activation energies, Q_c and Q_e.

To determine the apparent activation energies for the creep processes in this alloy the dependence of steady state creep rates, $\dot{\varepsilon}_s$, on inverse testing temperature, 1/T, at various applied stresses have been plotted in Figure 40. The original data for the plots are also listed in Table 10. A linear relationship between log $\dot{\varepsilon}_s$ and 1/T is seen to exist at all the four applied stress levels. The apparent activation energies of creep, Q_c, from the creep rate equation

$$\dot{\varepsilon}_s = A_1 \sigma_a^{n_a} \exp(-Q_c/RT) \qquad (2.5)$$

obtained from the slopes of $\ell n\ \dot{\varepsilon}_s$ vs. 1/T plots are in the range of 349.5 KJ/mol to 370.9 KJ/mol. These are also included in Tables 10 and 11.

As discussed in Chapter 2, after considering the dimensions of equation (2.5) and taking the temperature effect into account, the creep rate equation can be modified to

$$\dot{\varepsilon}_s = A' (\sigma_a/G)^{n_a} (Gb/KT) \exp (- Q_c^*/KT) \qquad (2.8a)$$

Further, the shear modulus G usually changes with temperature, therefore the activation energy, Q_c^*, can be

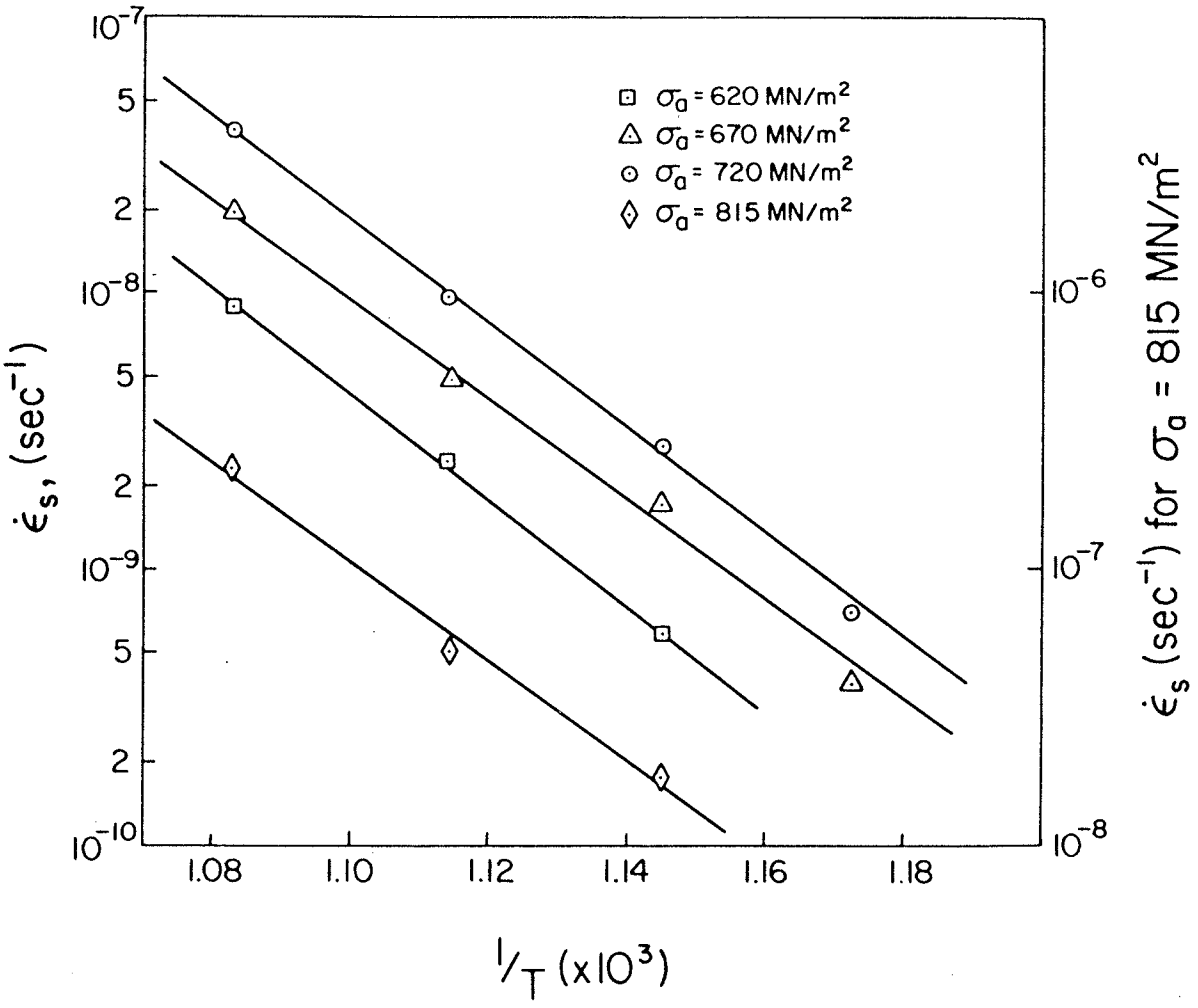

Figure 40: Dependence of $\dot{\varepsilon}_s$ on testing temperature, 1/T, of specimens aged at 998 K for 15 hrs and tested at various stress levels, for determining the values of apparent activation energy, Q_c.

Table 10 Data for determining activation energy, Q_c, not including the dependence of G on T. (i.e. data for ploting $\ell n\ \dot{\varepsilon}_s \sim 1/T$ at various stress levels).

T.T. (K)	$\dot{\varepsilon}_s$ sec^{-1} / σ_a (MN/m^2) / 1/T (K^{-1})	620	670	720	815
923	1.08×10^{-3}	8.97×10^{-9}	19.75×10^{-9}	38.61×10^{-9}	238.00×10^{-9}
898	1.11×10^{-3}	2.50×10^{-9}	4.85×10^{-9}	9.65×10^{-9}	50.40×10^{-9}
873	1.14×10^{-3}	0.59×10^{-9}	1.73×10^{-9}	2.78×10^{-9}	17.80×10^{-9}
853	1.17×10^{-3}		0.38×10^{-9}	0.70×10^{-9}	
Slope of $\ell n\ \dot{\varepsilon}_s \sim 1/T$		- 44.27	- 43.24	- 44.61	- 42.04
$Q_c = - R\ d\ \ell n\ \dot{\varepsilon}_s\ d(\frac{1}{T})$		368.3	359.5	370.9	349.5

Table 11 Data for determining activation energy, Q_c^*, with inclusion of change in G with T (i.e., data for plotting $\ell n \left(\frac{\dot{\varepsilon}_s T}{G}\right)\left(\frac{G^*}{\sigma_a}\right)^{n_a} \sim 1/T$ at various stress levels).

T.T. (K) \ σ_a (MN/m^2)	$\left(\frac{\dot{\varepsilon}_s T}{G}\right)\left(\frac{G}{\sigma_a}\right)^{n_a}$	620	670	720	815
923	1.08×10^{-3}	16.60×10^{-9}	16.80×10^{-9}	16.00×10^{-9}	28.5×10^{-9}
898	1.11×10^{-3}	4.89×10^{-9}	4.37×10^{-9}	4.23×10^{-9}	6.40×10^{-9}
873	1.14×10^{-3}	1.19×10^{-9}	1.63×10^{-9}	1.27×10^{-9}	2.35×10^{-9}
853	1.17×10^{-3}		0.38×10^{-9}	0.34×10^{-9}	
Slope of $\ell n\left(\frac{\dot{\varepsilon}_s T}{G}\right)\left(\frac{G}{\sigma}\right)^{n_a} \sim 1/T$		- 42.79	- 41.65	- 43.02	- 40.46
$Q_c = -R \, d \, \ell n\left(\frac{\dot{\varepsilon}_s T}{G}\right)\left(\frac{G}{\sigma}\right)^{n_a} d\left(\frac{1}{T}\right)$		356.0	346.3	357.7	336.4

* E(538°C)= 25.5×10^6 psi (175.8×10^3 MN/m^2) E(649°C)= 24.5×10^6 psi (168.9×10^3 MN/m^2)[43] $G = E/2(1+\mu)$ and $\mu = 0.33$

Temp.	943 K	923 K	898 K	853 K
G(MN/m^2)	63.0×10^3	63.5×10^3	64.6×10^3	65.1×10^3

** $n_a = 10$

obtained from the slope of the plot of $\ln (\dot{\varepsilon}_s T/G)(G/\sigma_a)^{n_a}$ vs. 1/T. These plots for various applied stress levels are shown in Figure 41 and the original data for these plots are listed in Table 11. The slopes of the plots and the values of Q_c^* have been also listed in Table 11, which show that the apparent activation energies after consideration of the shear modulus variation with temperature are in the range of 336.4 KJ/mol to 357.7 KJ/mol.

These apparent activation energies, either Q_c or Q_c^*, obtained from both methods are considerably higher than the activation energies for self diffusion or for the creep process of pure nickel and Ni-Cr solid solution. For example, the values of the activation energy for self diffusion and creep of Ni have been reported to be 265 - 280[60] and 276 KJ/mol[95], while the activation energy for creep of Ni - Cr alloy was found to be 295 KJ/mol[65].

However, by considering the back stress, σ_o, the creep rate equation is modified to[96]

$$\dot{\varepsilon}_s = A' \left(\frac{\sigma_a - \sigma_o}{G}\right)^{n_e} \left(\frac{Gb}{KT}\right) \exp\left(-Q_e/RT\right) \qquad (4.1)$$

Therefore the effective activation energies, Q_e can be determined by the slopes of $\ln \left(\frac{\dot{\varepsilon}_s T}{G}\right)\left(\frac{G}{\sigma_a - \sigma_o}\right)^{n_e}$ vs. 1/T plots. Figure 42 shows the plots of $\ln \left(\frac{\varepsilon_s T}{G}\right)\left(\frac{G}{\sigma_a - \sigma_o}\right)^{n_e}$ vs. 1/T for four different applied stress levels. The data

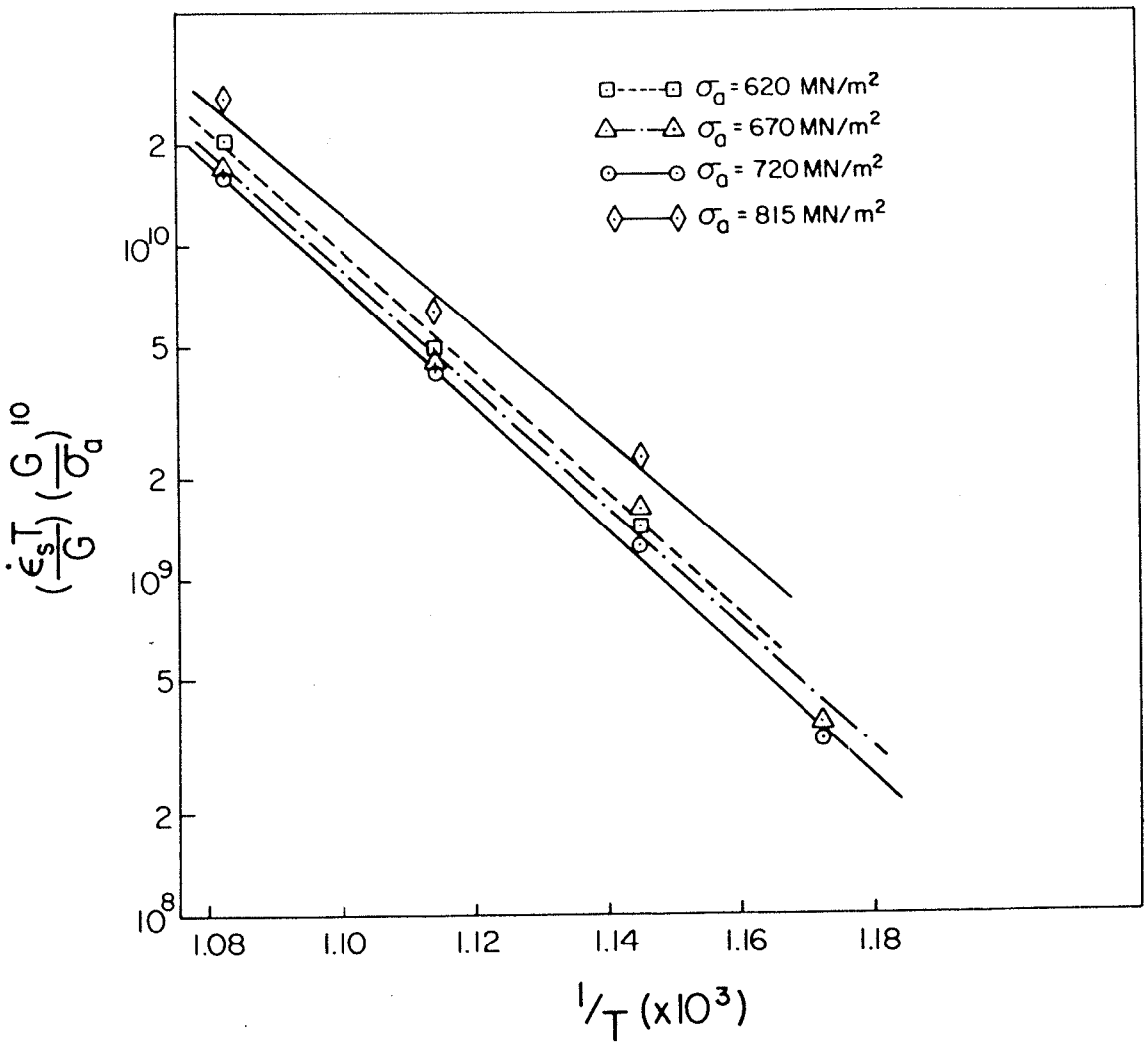

Figure 41: Determination of the values of apparent activation energy, Q_c, with consideration of variation of shear modulus with temperature.

for the plots are listed in table 12. The larger values of the terms $(\frac{\dot{\varepsilon}_s T}{G})(\frac{G}{\sigma - \sigma_o})^{n_e}$ at the high stress level of 815 MN/m^2 are due to the larger value of n_e, i.e. n_e is equal to ~ 4.0 at a stress level of 815 MN/m^2, while at lower stress levels, n_e is equal to ~ 1.0. The results in Table 12 show that the effective activation energies are in the range of 249.4 KJ/mol to 296.8 KJ/mol, which are in a reasonable agreement with the activation energies of self-diffusion or creep process of pure nickel and Ni-Cr solid solution alloy, as quoted earlier. For comparison all the activation energies, Q_c, Q_c^*, Q_e and Q_d are listed in Table 13.

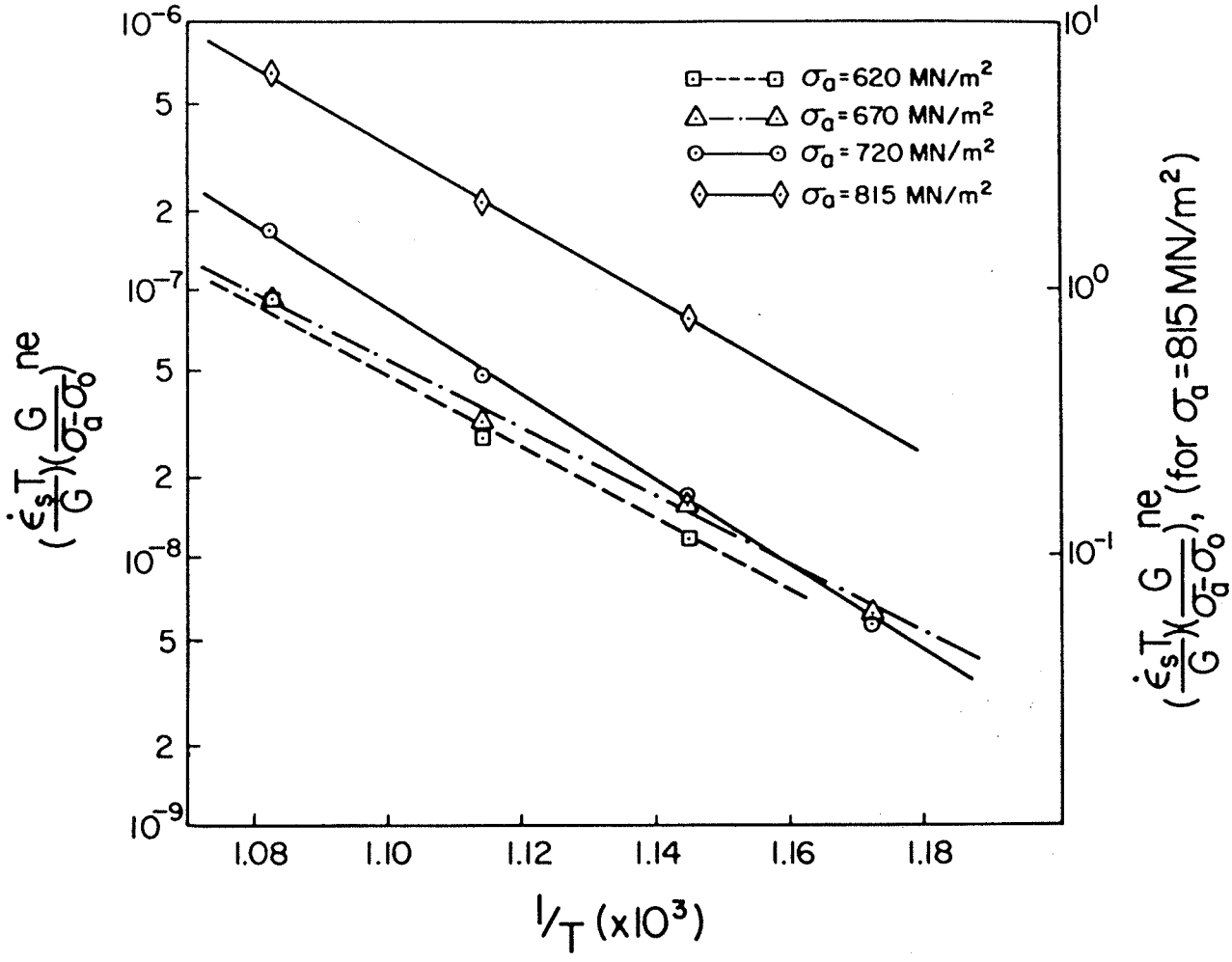

Figure 42: Determination of the values of effective activation energy, Q_e, with inclusions of the variation of shear modulus with temperature and back stress.

Table 12 Data for determining activation energy, Q_e, at various stress levels (i.e., data for plotting $\ell n \left(\frac{\dot{\varepsilon}_s T}{G}\right)\left(\frac{G}{\sigma-\sigma_o}\right)^{n_e} \sim 1/T$)

T.T. (K)	$\frac{\dot{\varepsilon}_s T}{G}\left(\frac{G}{\sigma-\sigma_o}\right)^{n_e}$ vs $1/T$ (K^{-1})	σ_a (MN/m^2) 620 ($n_e = 1$)	670 ($n_e = 1$)	720 ($n_e = 1$)	815 ($n_e = 4$)
923	1.083×10^{-3}	75.30×10^{-9}	94.00×10^{-9}	169.70×10^{-9}	6.50
898	1.114×10^{-3}	28.10×10^{-9}	32.10×10^{-9}	48.10×10^{-9}	2.08
873	1.145×10^{-3}	11.58×10^{-9}	15.50×10^{-9}	16.80×10^{-9}	0.78
853	1.172×10^{-3}		6.15×10^{-9}	5.83×10^{-9}	
Slope of $\ell n\left(\frac{\dot{\varepsilon}_s T}{G}\right)\left(\frac{G}{\sigma-\sigma_o}\right)^{n_e} \sim 1/T$		- 30.30	- 30.0	- 35.71	- 34.37
$Q_e = -R\, d\, \ell n\left(\frac{\dot{\varepsilon}_s T}{G}\right)\left(\frac{G}{\sigma-\sigma_o}\right)^{n_e} / d\left(\frac{1}{T}\right)$		352.1	249.4	296.8	285.7

Table 13 Experimentally determined apparent and effective activation energies Q_c and Q_e ($d\gamma''$ = 26.9 nm, $d\gamma'$ = 15.7 nm)

σ_a (MN/m^2)	Q_c (KJ/mol)	Q_c^* (KJ/mol)	Q_e (KJ/mol)	$Q_a^{N_i}$ (KJ/mol)
620	368.3	356.0	252.1	265 ~ 295 [62]
670	359.5	346.3	249.4	
720	370.9	357.7	296.8	
815	349.5	336.4	285.7	

Q_c Apparent activation energy from equation $\dot{\varepsilon}_s = Af(\sigma) \exp(-Q_c/RT)$

Q_c^* Apparent activation energy from equation $\dot{\varepsilon}_s = A' (\frac{\sigma}{G})^{n-1} (\frac{\sigma\Omega}{KT}) \exp(-Q_c/RT)$

$$Q_c = -R\, d\ell n\, \dot{\varepsilon}_s / d(\frac{1}{T})$$

$$Q_c^* = -R\, d\ell n (\frac{\dot{\varepsilon}_s T}{G})(\frac{G}{\sigma})^n / d(\frac{1}{T})$$

$$Q_e = -R\, d\ell n\, (\frac{\dot{\varepsilon}_s T}{G})(\frac{G}{\sigma - \sigma_o})^{n_e} / d(\frac{1}{T})$$

4.7 Effect of particle size on creep rate

The influence of particle size on steady state creep rate was established by using the specimens aged at 998 K for various lengths of time from one to 100 hrs. These specimens were creep tested in the stress range of 670 - 815 MN/m^2 at a temperature of 873 K. The steady state creep rates of specimens with different particle sizes tested at stresses of 670, 695, 720, 765 and 815 MN/m^2 at 873 K are listed in table 6 and shown graphically in Figure 43. It is observed that at all the applied stress levels the steady state creep rate, $\dot{\varepsilon}_s$, decreases with increasing particle size until a critical size is reached and then the creep rate starts to increase with any further increase in particle size. The minimum steady state creep rate is obtained when the aging time is 10 hrs at 998 K and where the particle sizes are $d\gamma''$ = 23.2 nm and $d\gamma'$ = 13.7 nm. These particle sizes are slightly smaller than those observed in the specimen that exhibited maximum room temperature yield strength, i.e., the specimen aged for 15 hrs at 998 K, where the γ'' particle size was 26.9 nm and γ' was 15.7 nm.

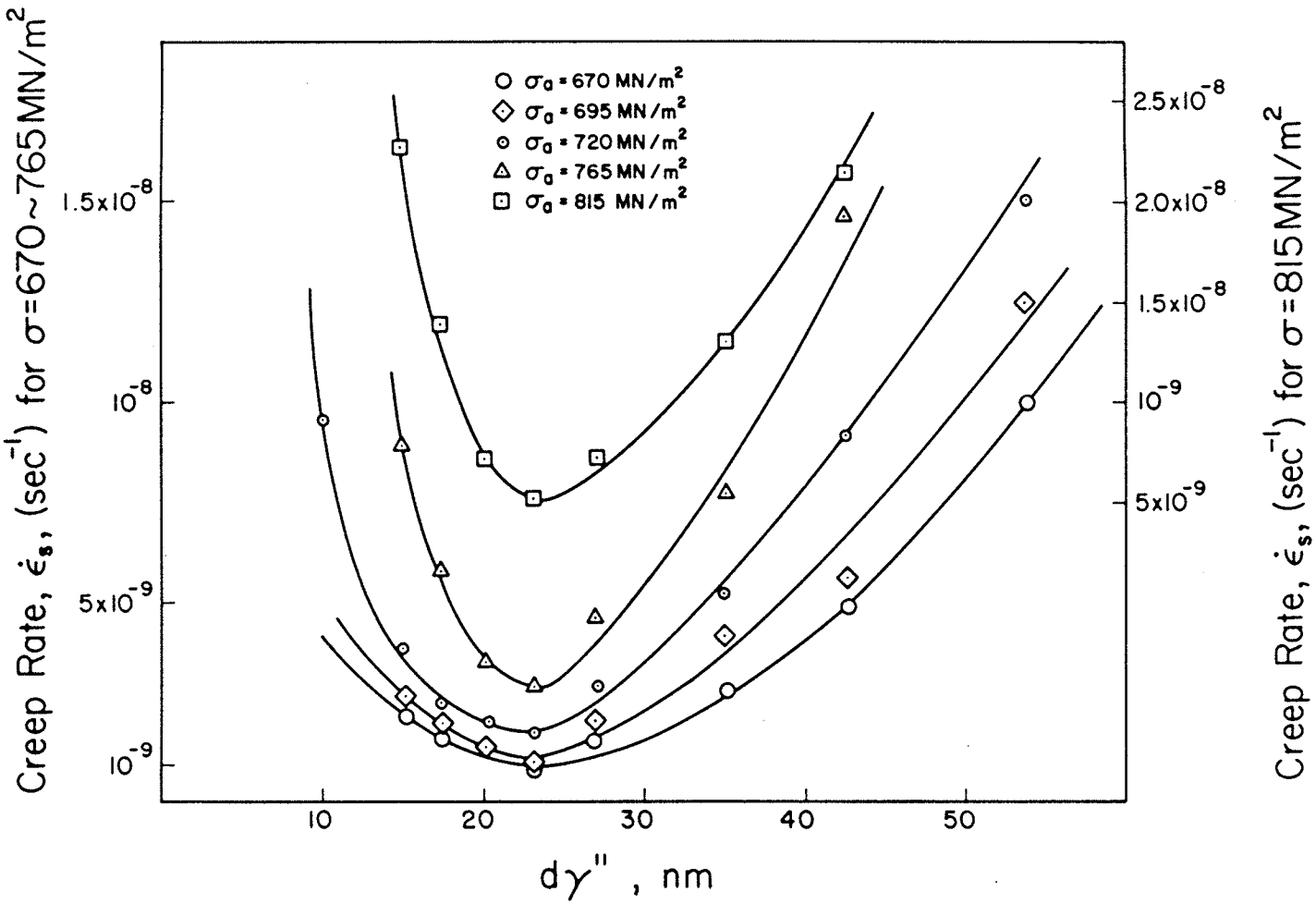

Figure 43. Dependence of $\dot{\epsilon}_s$ on particle size, dγ", at various stress levels, the specimens were aged for various periods of time at 998K and tested at 873K.

The relationship between the steady state creep rate, $\dot{\varepsilon}_s$, and particle size, d, can be established by calculating the power exponent value, n, of the equation $\dot{\varepsilon}_s \alpha d^n$. It is observed that in the underaged condition, where the volume fraction of precipitates is constant, the value of n is in the range of n = - 1.91 to - 2.51 as shown in Table 14. This is in a reasonable agreement with Ansell and Weertman's[47], as well as, McLean's[22] theoretical models, i.e., $\dot{\varepsilon}_s \alpha d^{-2}$. On the other hand, in the case of the overaged condition, where $d\gamma'' > 26.9$ nm and the applied stress is likely to be greater than the Orowan stress, Gb/λ, the value of n is between 2.40 to 2.51, which seems to agree with Grant[49] and McLean's[40] stored energy model.

According to Ansell and Weertman[47] at low stress levels, i.e., when the applied stress is less than the Orowan stress, Gb/λ, but greater than the stress required to activate Frank-Read sources, Gb/L_F, the creep rate can be expressed as

$$\dot{\varepsilon}_s = \pi \sigma_a b^3 D/2 \, KT \, d^2 \qquad (2.15)$$

Table 14 Experimentally determined exponent value, n, of equation $\dot{\varepsilon}_s \alpha d^n$ for specimens tested at 873 K.

	Underaged condition ($d\gamma'' < 23$nm)						Overaged condition ($d\gamma'' > 23$ nm)				
σ(MN/m^2)	670	695	720	746	765	815	670	695	720	765	815
n	-1.91	-2.11	-2.03	-2.22	-2.52	-3.42	2.48	2.40	2.42	2.51	2.43

Table 15 Diffusion Coefficient, D, and activation energy, $Q_c(A)$* from $\dot{\varepsilon}_s = \pi b^3 D\sigma/2KTd^2$, and activation energy, $Q_c(B)$ from $\dot{\varepsilon}_s = A\sigma^n \exp(-Q_c/RT)$

σ (MN/m^2)	670	695	720	746	765
σ (dyne/cm^2)	6.70×10^9	6.95×10^9	7.20×10^9	7.46×10^9	7.65×10^9
$\pi b^3 D\sigma/2KT$	4.24×10^{-21}	6.05×10^{-21}	9.84×10^{-21}	12.67×10^{-21}	22.47×10^{-21}
D (cm^2/sec)	3.27×10^{-21}	4.48×10^{-21}	7.04×10^{-21}	8.74×10^{-21}	15.00×10^{-21}
Q_c(A)(KJ/mol)	354.3		348.7		
Q_c(B)(KJ/mol)	359.5		370.9		

* $b = 2.50 \times 10^{-8}$ cm
$D_o = 5.0$ cm^2/sec [60]

Therefore the diffusion coefficient, D, can be obtained from the slope of the $\dot{\varepsilon}_s$ vs. d^{-2} plot since the rest of the terms in this expression are constant. For this purpose the slopes of $\dot{\varepsilon}_s$ vs. d^{-2} plots of the underaged specimens at various stress levels have been calculated and are listed in Table 15. Furthermore, by using the value of $D_o^{Ni} = 5 \times 10^{-4} m^2/sec$ [60] the activation energies, Q_c, were estimated to be 354.3 KJ/mol and 348.7 KJ/mol for applied stresses of 670 MN/m^2 and 720 MN/m^2, respectively. These values are nearly the same as the apparent activation energies obtained from the dependence of creep rate on testing temperature, $Q_c = - R d\ell n \dot{\varepsilon}_s / d(1/T)$, i.e., 359.5 and 370.9 KJ/mol for applied stresses of 670 MN/m^2 and 720 MN/m^2 respectively.

4.8 Observation of microstructure

In order to relate the creep behaviour of this alloy to its microstructure, transmission electron microscopic (TEM) studies were carried out. Microstructures of specimens crept under various testing temperatures and applied stresses were examined and a few typical examples are shown in Figures 44 to 47. Figures 44a and 44b are the TEM photomicrographs of specimens aged at 998 K for 15 hrs (peak aged condition) and crept at 923 K at a stress of 720 MN/m^2 for 60 hrs and at 815 MN/m^2 for 9 hrs, respectively. Dislocation loops are observed in both cases, and many short dislocation segments have been observed especially in the specimen that was crept at the higher stress level (Figure 44b). Figure 45 shows the dislocation structure of a specimen aged at 998 K for 7 hrs (underaged condition) and crept for 68 hrs at 873 K and a stress of 670 MN/m^2. Dislocation loops are observed in this specimen also even though the stress level is low and the creep rate is also low, i.e., $\dot{\varepsilon}_s = 1.14 \times 10^{-9}$/sec. Figure 46a is the photomicrograph of a specimen aged for 25 hrs at 998 K (slightly overaged condition) and crept for 222 hrs at 873 K and 720 MN/m^2. More and relatively well defined dislocation loops were observed and their sizes are

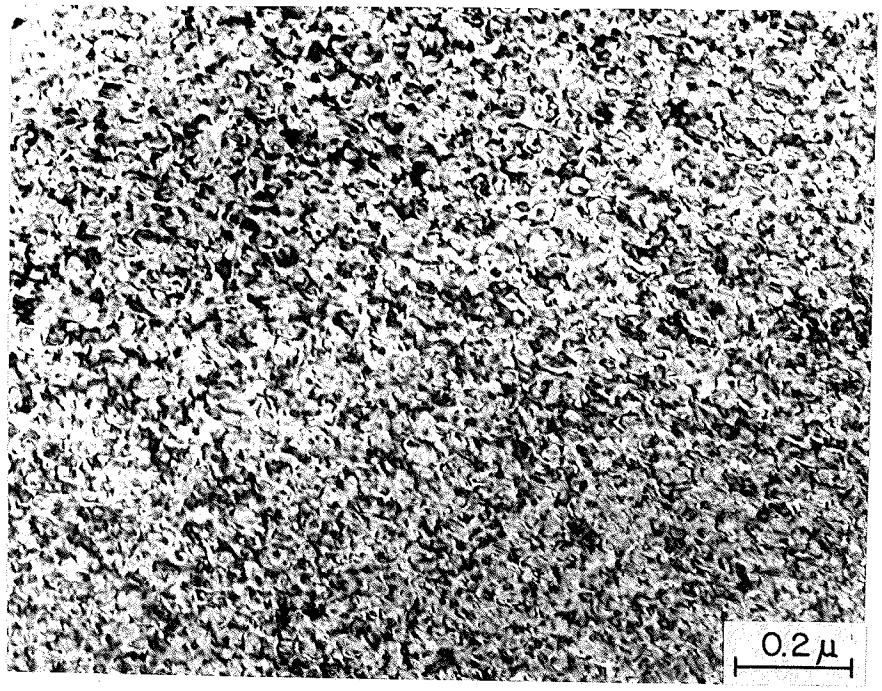

(a)

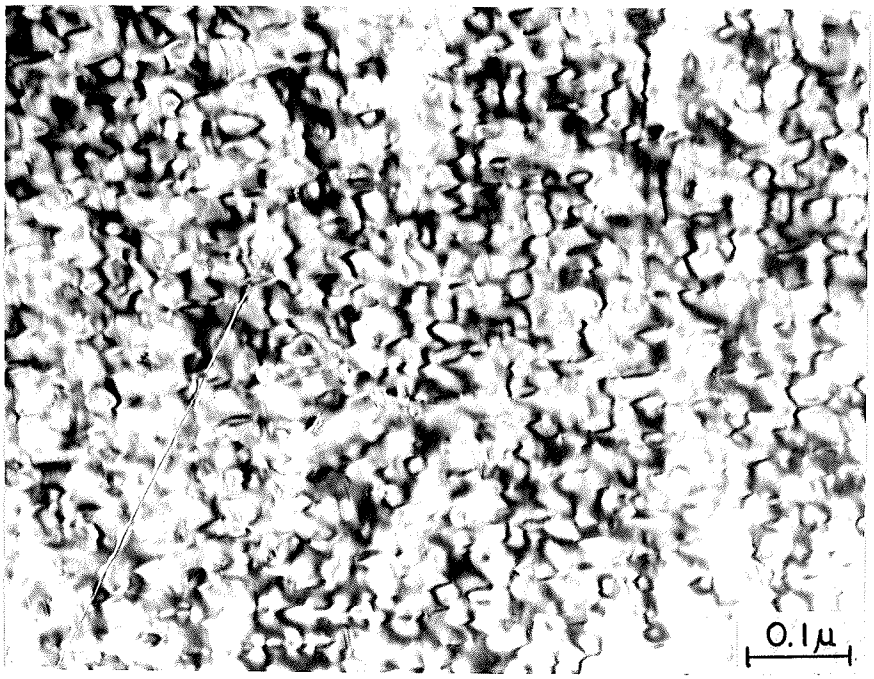

(b)

Figure 44 Dislocation structure of a specimen aged for 15 hrs at 998 K and crept at 923 K and stresses of (a) 720 MN/m^2 (60 hours, total elongation = 1.5%) (b) 815 MN/m^2 (9 hours, total elongation = 0.8%)

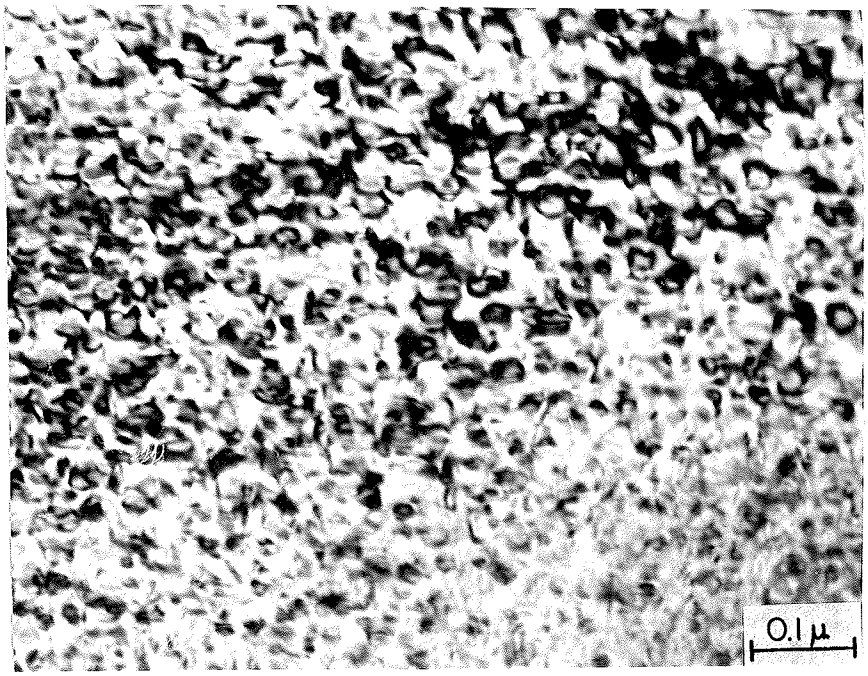

Figure 45: Dislocation structure of a specimen aged at 998K for 7 hrs and crept at 873K under 670 MN/m^2 for 68 hrs.

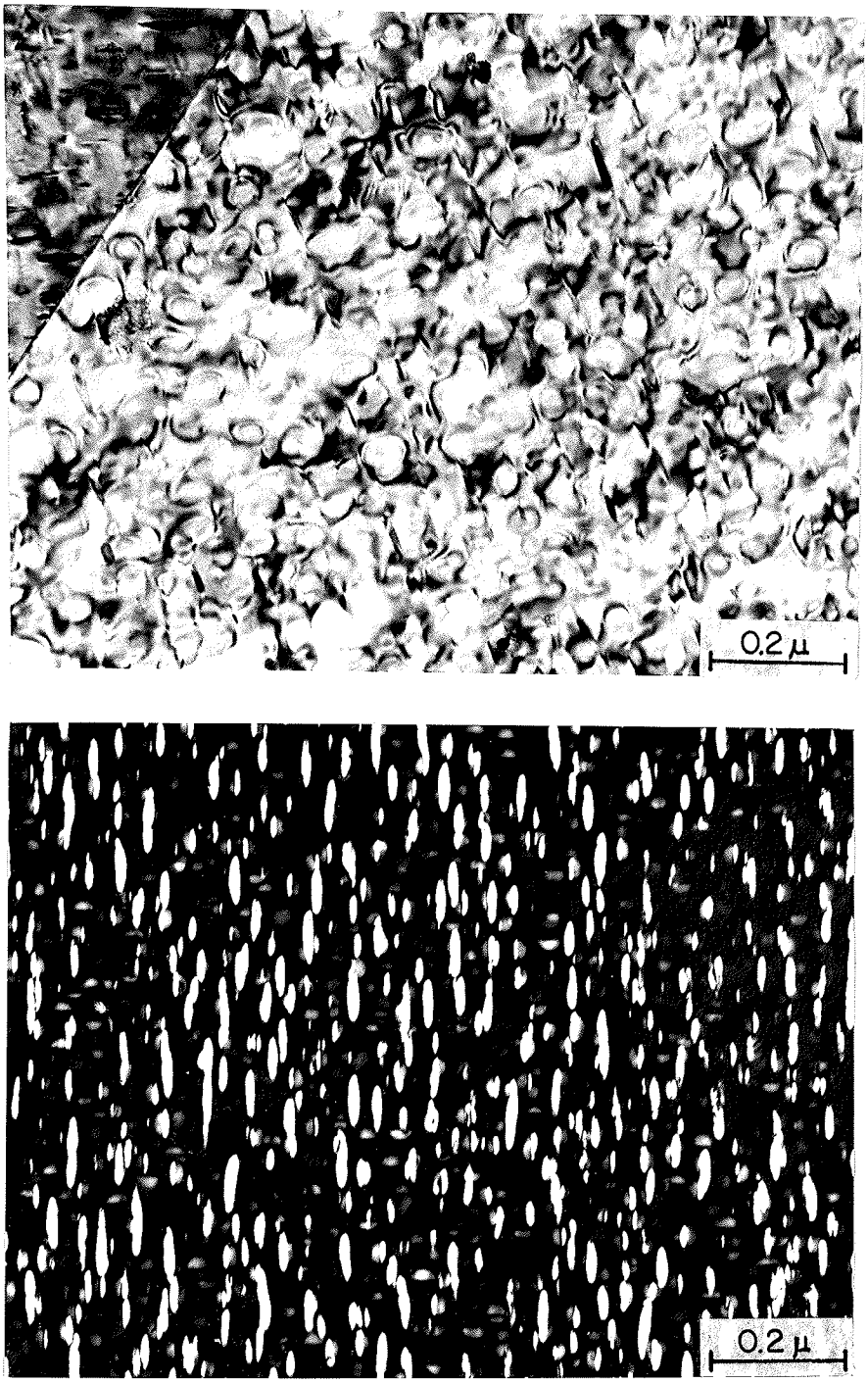

(a)

(b)

Figure 46: Microstructure of a specimen aged for 25 hrs at 998K and crept at 873K under 720MN/m^2 for 222 hrs.
(a) Bright field;
(b) Dark field taken with (100) reflection spot.

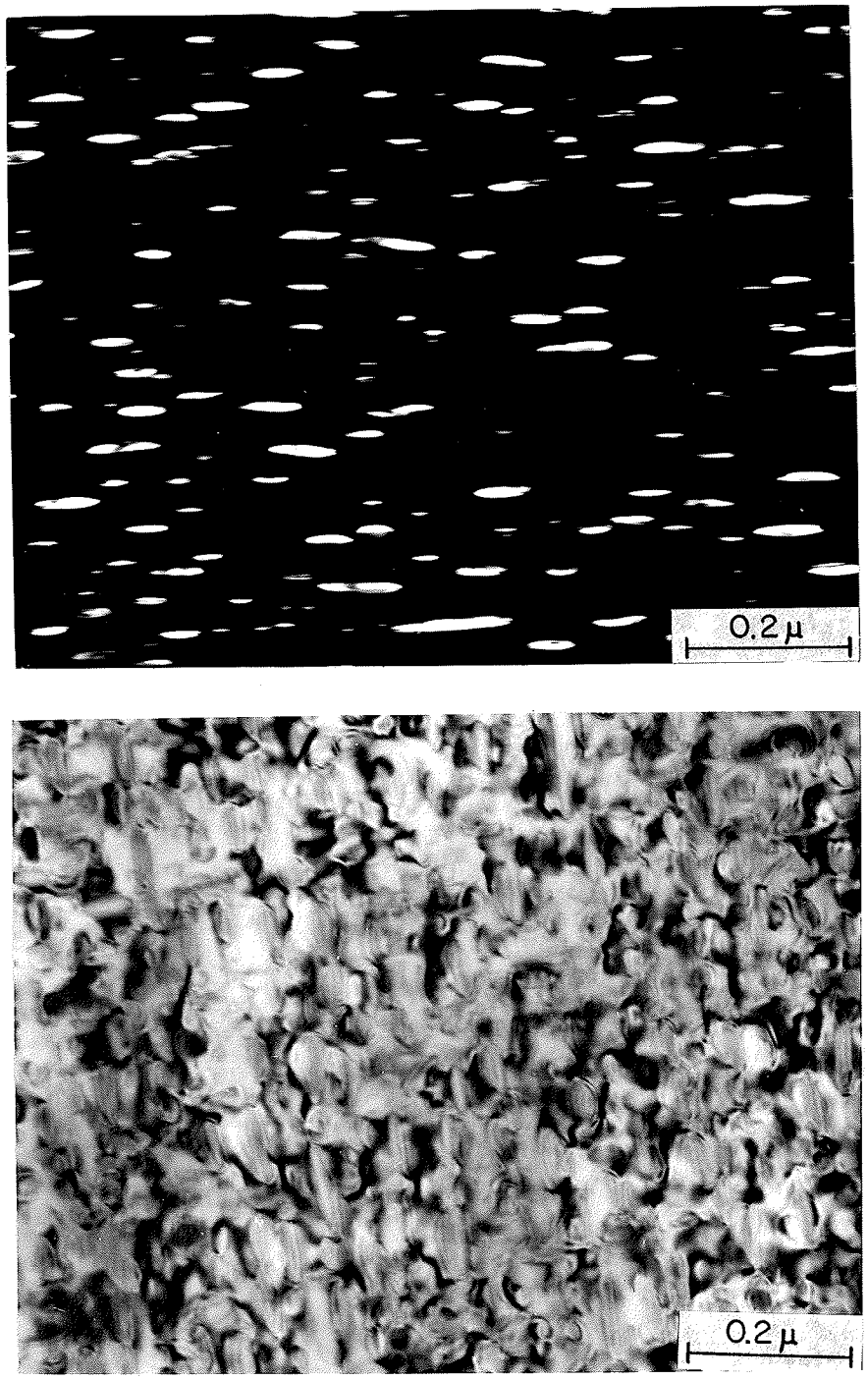

(a)

(b)

Figure 47: Microstructure of a specimen aged for 50 hrs at 998K after consecutive stress reduction test from a stress of 720 MN/m^2 to 590 MN/m^2 at 873K.
(a) Dark field taken with (100) reflection spot;
(b) Bright field.

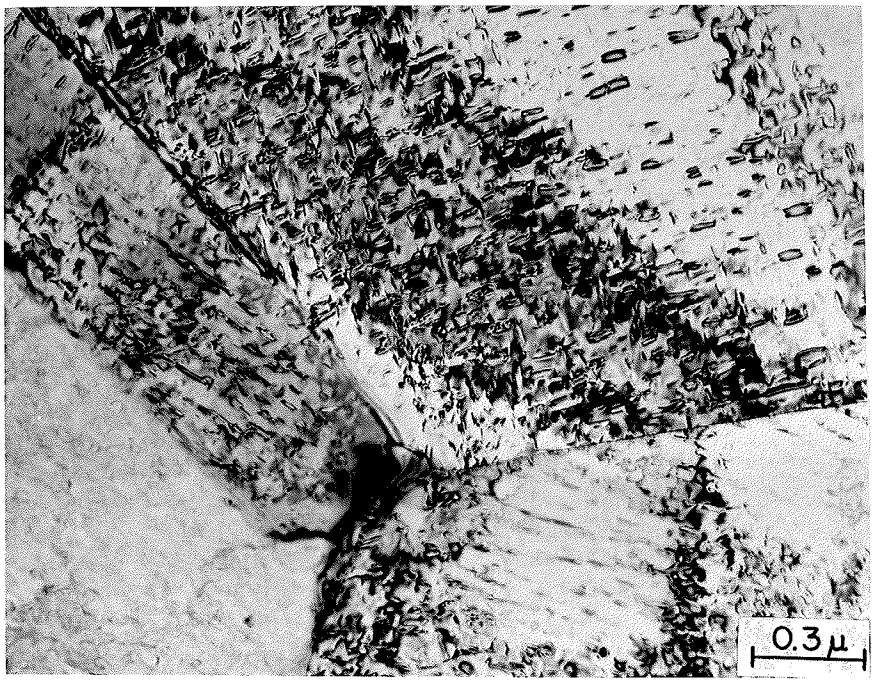

Figure 48: Observation of precipitate-free zone of specimen aged for 25 hrs at 998K and crept at 873K and a stress of 720 MN/m^2 for 222 hrs.

comparable to the precipitate size of $d\gamma''$ = 40 nm. The particle size is slightly larger than the γ'' precipitate size of 32.6 nm observed in a specimen aged for 25 hrs at 998 K. These precipitates are shown in Figure 46b which is the dark field of Figure 46a taken with the (100) reflection spot. Figure 47 shows the microstructures of the specimen aged at 998 K for 50 hrs (averaged condition) and crept at 873 K at stresses of 720 MN/m^2 → 590 MN/m^2; i.e., after a successive stress reduction test with a final stress of 590 MN/m^2. Only a very few dislocation loops are observed and the dislocation density seems to be relatively low. This may be due to the recovery process that occurs during the successive stress reduction test.

Occasionally precipitate free zones of very small width were seen around grain boundaries of crept specimens. An example is shown in Figure 48 which is the structure of a specimen aged for 25 hrs at 998 K and crept for 222 hrs at 873 K and 720 MN/m^2. A precipitate free zone around grain boundaries was not observed in non-creep deformed specimens.

CHAPTER 5 DISCUSSION

5.1 Mechanism of Creep Deformation Process

As discussed earlier in Chapter 2, in two phase alloys the apparent parameters, n_a and Q_c, have no direct physical significance, and the effective parameters, n_e and Q_e, are considered to relate to physically significant processes. Analogous to the analysis of pure metals and solid solution alloys it is considered that in two phase alloys the creep mechanisms can be determined by establishing the values of the effective stress exponent. That is, when the creep process is diffusion controlled the value of n_e is equal to 1.0 and when it is dislocation controlled the value of n_e is found to be between 3 and 6.

The experimental results given in Table 8 show that for the specimens aged for 15 hrs at 998 K the effective stress exponent, n_e, increases as either testing temperature or applied stress increases in the present testing condition. This suggests that both temperature and stress affect the deformation mechanism of creep. In the low stress range of 620 - 720 MN/m^2, the value of n_e increases from n_e = 1.12 at 853 K to n_e = 5.12 at 943 K, suggesting that creep mechanism changes from diffusional or linear creep at 853 - 873 K to dislocation power law creep at temperatures higher than 923 K. On the other hand, in the stress range of 765 - 840 MN/m^2, the power law creep mechanism operates at both 873 K and 898 K temperatures.

The results given in Table 8 also show that at 873 K, the values of n_e change from n_e = 1.37 in the stress range of 620 - 746 MN/m^2 to n_e = 5.10 in the stress range of 765 - 840 MN/m^2. For a testing temperature of 898 K, the effective stress exponent change from n_e = 1.68 at the low stress level of 620 - 720 MN/m^2 to n_e = 5.65 at the high stress level of 765 - 840 MN/m^2. This suggests that the creep mechanism changes from diffusional creep or linear law creep to dislocation power law creep when the applied stress increases from σ_a = 620 - 720 MN/m^2 to σ_a = 765 - 840 MN/m^2 in the temperature range of 873 - 898 K.

An interesting feature of the results in Table 8 is that the value of n_e changes continuously from 1.12 to 5.12 when the testing temperature increases from 853 K to 943 K progressively. Unfortunately, there are not enough data to show whether the values of n_e change continuously from 1.37 to 5.10 at 873 K and from 1.68 to 5.65 at 898 K with an increase in the applied stress. Most of the previous studies on creep mechanisms revealed that the stress exponent, n, changes from n = 1 for diffusional creep to n = 3 - 6 for dislocation power law creep. The question arises: Is there any transition region between these two different creep mechanisms? The results of the present study, which are shown in Tables 8 and 9, suggest that there exists such a transition region. Ashby[17] has pointed out that there exists a transition region between diffusional creep and

homogeneous power law creep. Diffusional flow is regarded as grain boundary sliding with diffusional accommodation. Incompatibility generated by sliding is removed at a steady rate by diffusion of atoms from sources on some grain boundaries to sinks on others. If the strain rate is increased sufficiently, diffusion can no longer accommodate the sliding and a non-uniform, power law creep within grains (called "folds") appears. As the strain rate increases further, flow becomes increasingly uniform and the folds disappear. This process leads to homogeneous power law creep. Furthermore, the results of the present investigation also show that the values of n_e are not exactly equal to 1 but slightly greater than 1 in the low stress range and in the temperature range of 853 K to 873 K, where creep is considered to be diffusion-controlled. The reason for a slightly higher value for n_e may be as follows. Firstly, the mechanism of diffusional creep of two phase alloys is different than that of single phase alloys or pure metals. Diffusional creep in the latter is the result of stress-induced vacancy diffusion or the migration of matter. The accumulation of vacancy diffusion leads to grain boundary sliding and dislocation motion inside the grain is not involved. On the other hand, in two-phase alloys, diffusion will be inhibited at the precipitate/matrix interface. The stress concentration at the interface can only be relaxed by

the punching of prismatic dislocation loops in the matrix [51,52], which annihilate themselves by the absorption of vacancies. Therefore, to accommodate even very limited diffusional strain in two phase alloys, plastic deformation must occur around precipitates either in the grain boundary region or within grains. According to Ansell and Weertman [47], diffusional creep is the process of dislocation climb over the particles. Therefore, diffusional creep in two-phase alloys involves not only vacancy diffusion in the matrix and dislocation motion in the grain boundary region, but also dislocation creation and motion within grains. The rate-controlling process is assumed to be the climb of dislocations over the particles which also depends on the diffusion rate. However if cross-slip is also important in the above process the creep rate will be more sensitive to stress. The microstructures of crept specimens show that dislocation segments and loops do exist within grains even under the testing conditions where diffusional creep is considered to occur. This is shown in Figure 45 which is the microstructure of a specimen aged for 7 hrs at 998 K and tested at 873 K with a stress of 670 MN/m^2.

Secondly, according to Gittus[97] the value of the stress exponent, n, for diffusional creep may be 1 or 2 depending on the deformation mechanism of the diffusional creep. If the creep process is lattice diffusion-controlled the creep rate equation has the form of $\dot{\varepsilon}_s \alpha\sigma$. On the other

hand, in the case where the phenomenon of grain boundary spiral dislocation sink and source operation determines the strain rate the diffusional creep equation can be expressed as $\dot{\varepsilon}_s \alpha\sigma^2$. Which one is the rate-controlling process will depend on the stress level, grain size and temperature. Gittus has also suggested that for materials with small grain size the grain boundary dislocation source-controlled process is most likely to be the rate-controlling process. That is to say, small grain sized materials are more sensitive to the applied stress than large grain sized materials. Therefore the value of n_e can be greater than one.

Diffusional creep in two-phase alloys has three other characteristics besides having a value of n_e equal to 1.

(1) There is a threshold stress below which $\dot{\varepsilon}_s \to 0$, i.e. σ_o = constant;[51-53]

(2) The creep rate decreases with time or total strain. There also exists a limiting total creep strain, ε_ℓ[51,52,69];

(3) There are precipitate free zones around tension grain boundaries.[6]

In the present study, at a stress in the low stress range of 620-720 MN/m^2 and at a temperature below 873 K the values of n_e were observed to be close to 1 and the value of threshold stress, σ_o, constant. To further confirm that

diffusion creep is operative in specimens tested under the above conditions some of the creep tests were conducted for a prolonged time (> 150 hrs) to obtain the dependence of the creep rate, $\dot{\varepsilon}_s$, with time. The results, as shown in Figures 49 and 50, suggest that $\dot{\varepsilon}_s$ decreases with time or total strain and finally the creep rate approaches zero.

Harris[51] and Burton[52] have suggested that the diffusional creep rate depends on the ability of grain boundaries to collect precipitates. When a specimen deforms, the precipitates are progressively collected on compressive grain boundaries and hence their ability to collect precipitates decreases with total strain, i.e., the creep rate decreases with time. According to this model there should be precipitate-free zones around tension grain boundaries when a creep test lasts for a sufficiently long time.

According to Harris[51] and Gittus[97], the total strain, ε_t is equal to $2x/d$, where x is the width of the precipitate free zone and d is the grain size. In the present investigation it was observed that when the specimen with $d\gamma''$ = 27 nm was tested at 720 MN/m^2 and at 873 K the total strain, ε_ℓ, was less than 0.2%. For the specimen in the overaged condition with $d\gamma''$ = 54 nm tested at a stress of 695 MN/m^2 and a temperature of 873 K, the limited total

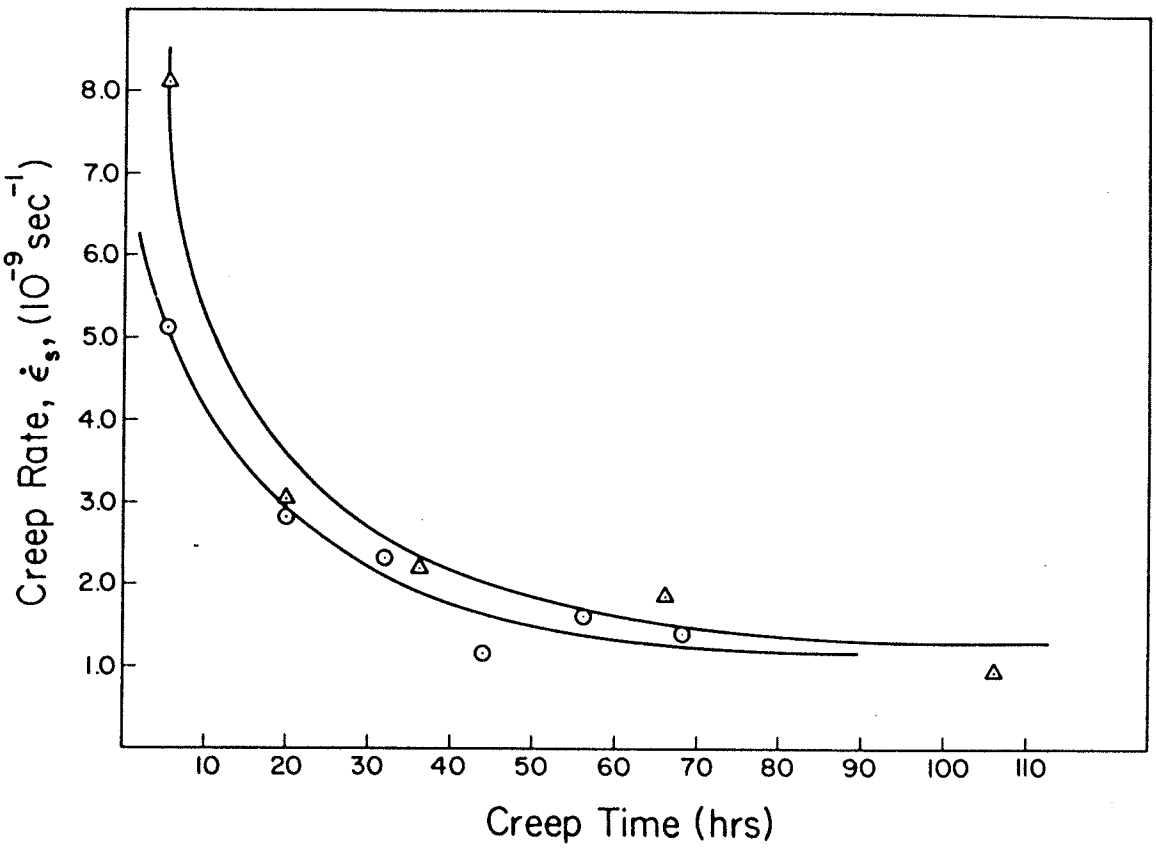

Figure 49: Creep rate vs. time curves of the specimens tested at a stress of 720 MN/m^2 and a temperature of 873 K.

(a) a specimen was aged at 998K for 15 hrs (⊙);
(b) a specimen was aged at 998 K for 25 hrs.(△);

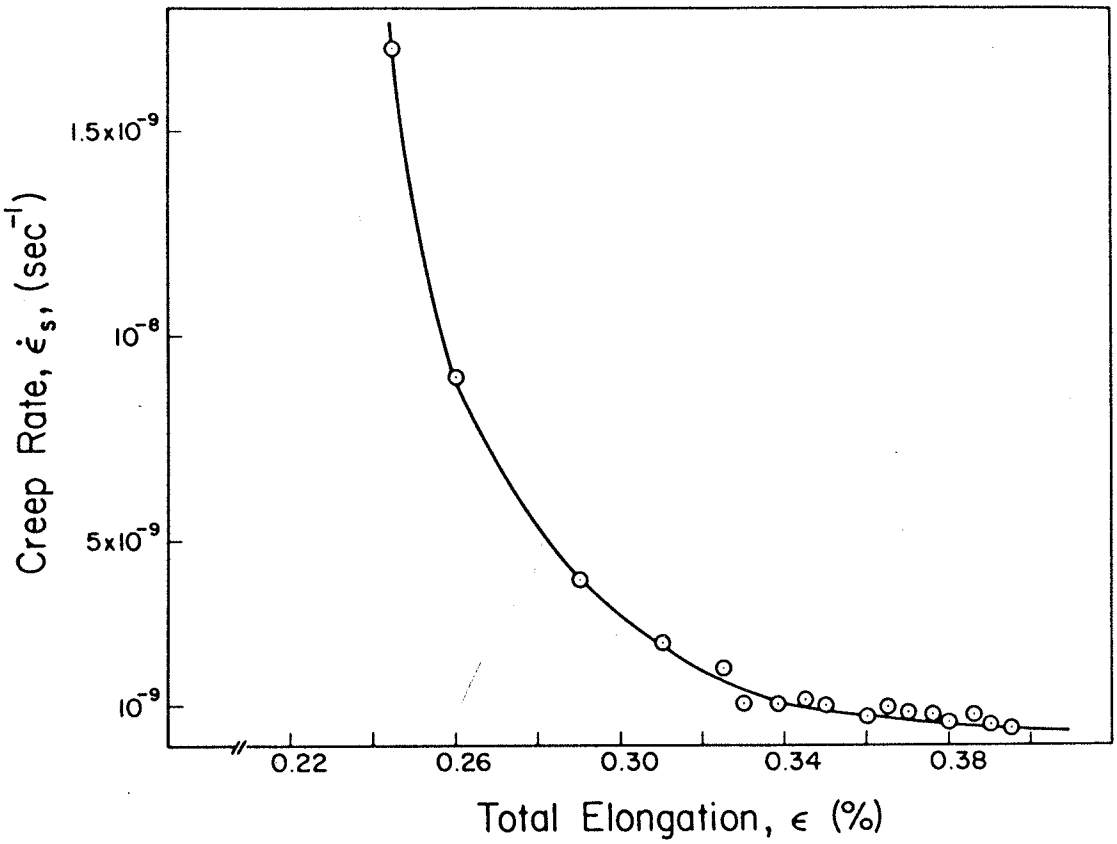

Figure 50: Dependence of creep rate on total elongation of a specimen aged at 998K for 100 hrs and crept at 873K and a stress of 720 MN/m^2 for 320 hrs.

strain, ε_ℓ, was less than 0.5%. In the two cases the calculated widths of precipitate-free zones are no more than 100 nm and 250 nm respectively when grain sizes are ~ 0.1 mm. Such narrow zones cannot be observed with an optical microscope, they should be observed in an electron microscope. Unfortunately, precipitate-free zones (PFZ) have not been observed clearly in the present study. The reason may be as follows. The estimated values of width of PFZ in above two cases are for those grain boundaries that are normal to the applied stress, i.e., around only those grain boundaries that are in tension. There should not be any PFZ around those grain boundaries that are in compression. Therefore, it is believed that the width of PFZ will be proportional to the angle of the orientation between the applied stress and grain boundary, as shown in Figure 51. During electron microscopic observation the examined area is very small, and grain boundaries can take any orientation in a real polycrystal. Therefore, there is a very small probability of finding a grain boundary which is normal to the applied stress. Occasionally, a very narrow PFZ was observed around a triplet point of grain boundaries, as observed in Figure 48.

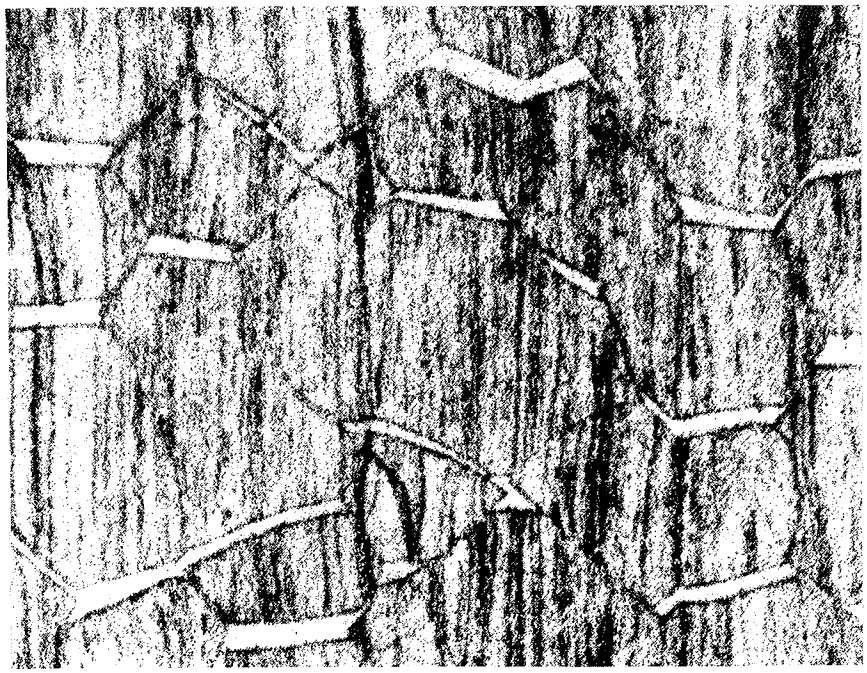

Figure 51: Microstructure of precipitation-hardened magnesium alloy after extensive creep showing the different width of precipitate-free zones at different grainboundary direction[6].

5.2 Back stress and threshold stress.

5.2.1 High creep resistance due to high back stress.

The experimental results given in Table 7 show that Inconel 718 has very high values of threshold stress, $\sigma_{o(th)}$, or back stress, σ_o, under present test conditions, i.e., most of the values of σ_o are between 0.6 σ_a and 0.9 σ_a. This is especially true in the low stress region ($\sigma_a < 720$ MN/m^2) where the creep process seems to be diffusional creep. This is the most probable reason for the high creep resistance of this alloy since a high value of σ_o will result in a low value of effective stress, $\sigma_e = \sigma_a - \sigma_o$ and hence a low creep rate. The high back stress may be due to the following. Firstly, the high antiphase boundary energy[98] (γ_{APB} = 298 MJ/m^2) makes the shearing of particles or the formation of prismatic dislocation loops at the γ''/γ' interface difficult.

Secondly, according to Harris[51] the critical shear stress for nucleation of prismatic dislocation loops is higher for coherent, strongly bonded particles than for incoherent and weakly bonded ones. Since both the strengthening phases in this alloy, γ'' and γ', are coherent and strongly bonded precipitates, a higher value of critical stress to nucleate prismatic loops is required. Therefore, a high value of σ_o in this alloy may be attributed to the nature of the precipitates that are coherent with the matrix.

5.2.2 Applicability of consecutive stress reduction method for determining σ_o during diffusion creep.

According to Wilshire[63-65,93] and Gibeling and Nix[67] the consecutive stress reduction method can usually be used to measure the back stress during dislocation power law creep. In this investigation this method has been used to determine the values of back stresses during dislocation power law creep as well as during diffusional creep. It was found that an incubation time after a small stress reduction appeared in both cases. The reason for this observation may be as follows: According to Harris[51] and Burton[52], for diffusional creep to continue the stress concentration at the precipitate/matrix interface can only be relieved by the formation of prismatic dislocation loops. Ansell and Weertman[47] suggested that diffusional creep in two-phase alloys occurs by the process of dislocation climb over the precipitate particles. Therefore diffusional creep in two-phase alloys involves not only vacancy diffusion in the matrix and dislocation motion in the grain boundary region but also the dislocation creation and motion within grains. The microstructural observation of crept specimens shows that dislocation line segments and networks exist inside the grains, as shown in Figures 44 - 47. Similar to the process of dislocation slip, dislocation climb also requires dislocation networks or line segments to grow to a sufficient length so that they can be activated. These dislocation

segments which become active are known as Bardeen-Herring sources[99]. Therefore the incubation time after a small stress reduction should appear during high temperature diffusional creep. This is confirmed in the present investigation. Therefore, it may be concluded that the consecutive stress reduction method can be used to determine σ_o during diffusion creep as well as during power law creep.

5.2.3 The effect of applied stress and temperature on back stress.

A. Applied stress.

The results of this investigation given in Table 7 show that at certain testing temperatures when σ_a is below a critical level, the value of σ_o is independent of σ_a, i.e., there exists a threshold stress, $\sigma_{o(th)}$. This region is suggested to be the diffusional creep region. On the other hand at higher stress levels, for example, for specimens aged for 15 hrs at 998 K tested at 873 K with $\sigma_a > 765$ MN/m^2, σ_o increases with increasing σ_a. Theoretically, there are two approaches to predict the back stress in two phase alloys. The threshold stress approach proposed by Lund and Nix[60] and Purushothaman and Tien[83] considered that the back stress in two phase alloys is of the order of the Orowan stress. Nix and his co-workers later on suggested a different approach for calculating the back stress[67,84]. They suggested that the back stress in two phase alloys

consists of two parts; the back stress resulting from the interaction of moving dislocations with other dislocations, subgrain boundaries and fine twins, and the back stress arising from the presence of second phase particles. They assumed localized dislocation climb over the particles in estimating the back stress. The back stress arising from the presence of other dislocations, subgrain boundaries and fine twins depend on the deformation history and the applied stress, σ_a. Therefore, the fact that σ_o increases with increasing σ_a in the high stress region in the present alloy implies that the presence of dislocation, subgrain and twin boundaries also contributes to the back stress. Because of the high contrast between γ'' precipitates and γ matrix due to a high coherency strain field and the limitation imposed by the inability to examine large areas in the TEM, and due also to the probability that subgrains may indeed not form during creep of two phase alloys, subgrain boundaries were not observed during TEM examination. However dislocation networks and deformation twins have been observed in crept specimens from microstructural examination as shown in Figures 52 and 53. Therefore, as suggested by Nix et al[67,84], the dependence of σ_o on σ_a at higher values of σ_a may be attributed to the interaction of a moving dislocation with other dislocations and twin boundaries.

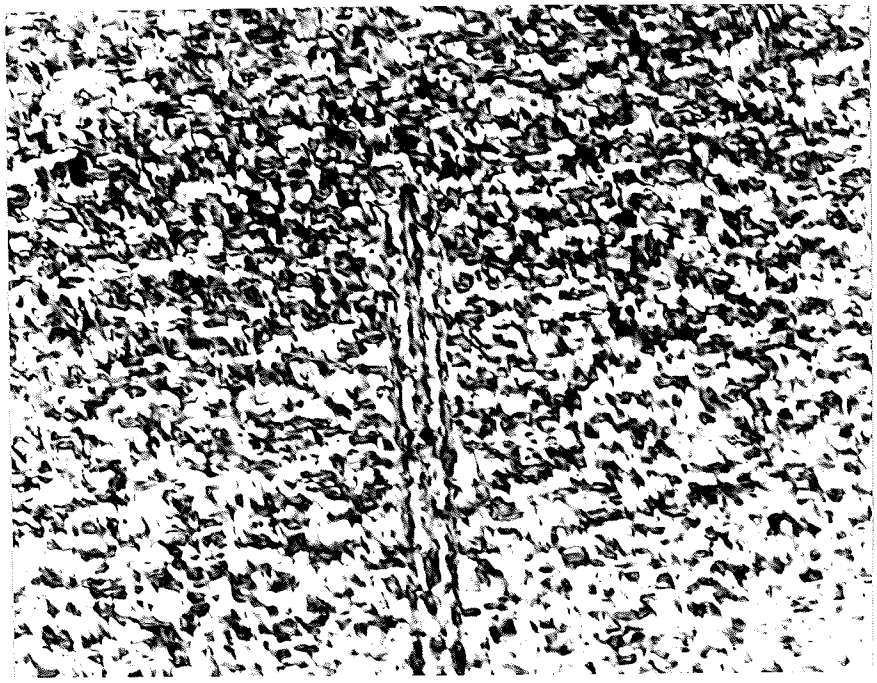

Figure 52: Dislocation structure and fine twins of specimen aged for 7 hrs at 998 K and crept at 873 K and a stress of 815 MN/m^2 for 21 hours.

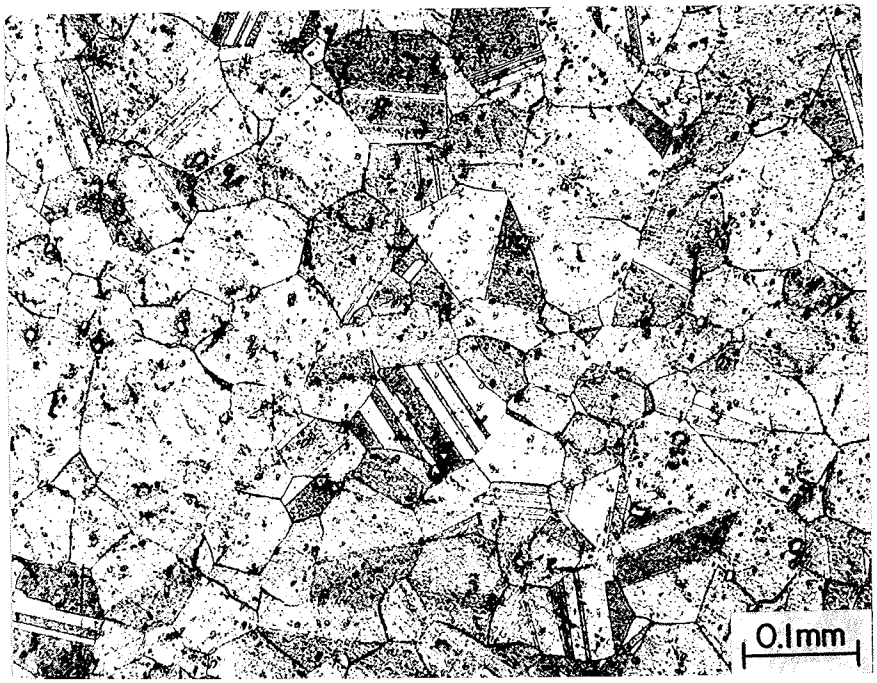

Figure 53: Deformation twins of specimen aged for 15 hrs at 998 K and tested at a stress range of 790 MN/m^2 → 620 MN/m^2 amd a temperature of 873 K.

B. Temperature

The decrease of σ_o with increasing testing temperature, as shown in Table 7 and Figure 36, can be attributed to the dependence of shear modulus on temperature. As discussed in Chapter 2, the threshold stress predicted from all the theoretical models is proportional to the shear modulus. Furthermore, from the energy point of view when the temperature increases more thermal energy is available to assist the applied stress to activate Frank-Read sources and Bardeen-Herring sources, or nucleate prismatic dislocation loops. Therefore, σ_o is expected to decrease with increase testing temperature.

5.3 Effect of particle size on creep behaviour.

5.3.1 Effect of particle size on steady state creep rate.

The experimental results given in Table 6 and Figure 43 show that the secondary creep rate, $\dot{\varepsilon}_s$, decreases with increasing particle size or interparticle spacing until a critical particle size is reached. The creep rate then increases with any further increase in particle size. This is in agreement with both the theoretical models of Ansell and Weertman[47] and McLean[22] and the results of several previous investigations[48,54,55]. It was found that in the present alloy the particle sizes in specimens with optimum creep resistance, $d\gamma'' = 23.2$ nm, $d\gamma' = 13.7$ nm (specimens aged for 10 hrs at 998 K) are slightly smaller than that for maximum room temperature yield strength, i.e., $d\gamma'' = 26.9$ nm, $d\gamma' = 15.7$ nm (specimens aged for 15 hrs at 998 K). This is similar to alloys of the Ni-Cr-Al-Ti system containing 10 - 20% γ' phase[100]. There are two possible reasons for this phenomenon. Firstly, the deformation mechanism of high temperature creep is different from that of room temperature tensile deformation. It has been observed[24,86] that in the underaged conditions particles are cut by moving dislocation during room temperature deformation, while in the case of high temperature creep, dislocations are believed to climb over the particles. Also, in the overaged condition, dislocations bow between the particles during both room temperature deformation and high temperature creep. However,

in the case of room temperature deformation, local stress concentrations due to dislocation pile-ups can result in crack initiation and failure of the material. During high temperature creep the stress concentration due to pile-ups can be relieved by the climb of the innermost loop and self annihilation to permit the next dislocation to bow[47]. Therefore, the optimum particle size for room temperature yielding is obtained when the particle size increases to a dimension where the applied shear stress for the dislocation to cut the particles is equal to that for the dislocation to bow between the particles. As a result, in the peak aged condition, dislocations are seen to cut the particles as well as bow between them[72]. According to Ansell and Weertman[47] optimum creep resistance is obtained when the particle size is such that the shear stress causes the dislocation to climb over the particles only. Therefore, this particle size is generally slightly smaller than that where a maximum in yield strength is observed. This is schematically shown in Figure 54. Secondly, although precipitates do not grow significantly when the specimen is held at 873 K for 20 - 30 hours, the applied stress at this temperature may promote their growth, as has been observed in the specimen aged for 25 hrs at 998 K and crept at 873 K at a stress of 720 MN/m^2 for 222 hrs. The particle size of

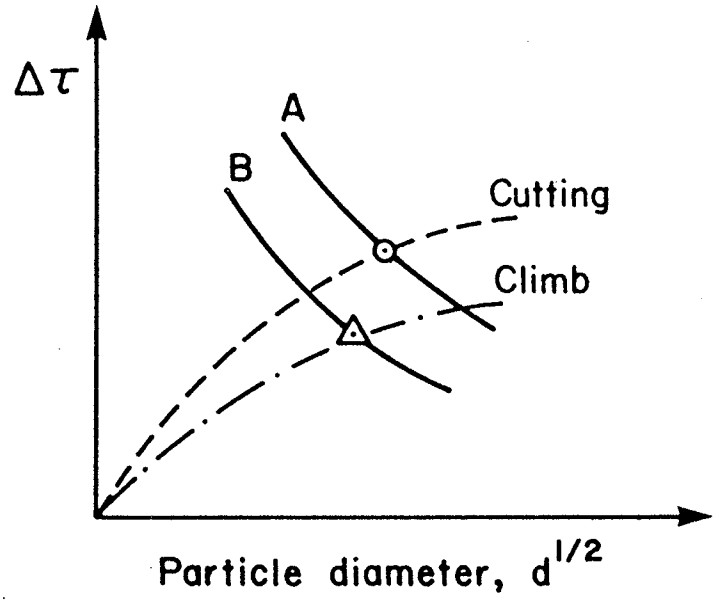

Figure 54. Schematic aging-hard[illegible] curves illustrating the particle size of [illegible]um room temperature yield strength ([illegible], and the particle size of the optimum high temperature creep resistance (△).
(A) Bowing at room temperature;
(B) Bowing at high temperature.

$d\gamma''$ = 40 nm is slightly larger than the precipitate size of specimen aged for 25 hrs at 998 K, where $d\gamma''$ = 32.4 nm. This is shown in Figure 46.

A discrepency was also observed between the experimental value of the exponent n and the theoretical value in the equation $\dot{\varepsilon}_s \alpha d^n$, where d is the particle diameter. That is, the value of n was between - 1.91 to - 2.51 for $\sigma_a \leq 765$ MN/m^2 and - 3.42 for σ_a = 815 MN/m^2 instead of - 2.0. This rapid decrease in creep rate with an increase in particle size or interparticle spacing may be a consequence not only of an increase in particle size and spacing but also of an increase in the volume fraction of precipitates. In an earlier study it was observed that the volume fraction of precipitate increased with aging time during the first four hours of aging at 998 K and then remained constant[92]. Therefore, it is probable that a part of the decrease in creep rate of specimens aged for up to four hrs is due to an increase in the volume fraction of precipitate. Secondly the big discrepancy in the value of n when σ_a was 815 MN/m^2, i.e., - 3.42 instead of - 2.0, may be explained as follows. In this situation the stress level may not be high enough for dislocations to bow between the very finely dispersed particles. Hov[illegible]ay be high enough for dislocation to cut particles or overrule the strain field of the particles by a small amount of localized bending (by either cross-slip or climb) to miss the particles so that the moving dislocation

glides continuously[18]. The finer the particles the easier the cutting or overriding process. This may be the reason for the high creep rate of specimens with very fine particles. For example, for a specimen aged for 1 hr at 998 K, the $\dot{\varepsilon}_s \propto d^{-2}$ relationship breaks down.

As described in Chapter 4, the value of the diffusion coefficient, D, can be calculated from the slope of $\dot{\varepsilon}_s \propto d^{-2}$ plots for the underaged specimens shown in Figure 43. This calculated value of diffusion coefficient was of the order of $10^{-21} cm^2/sec$ as shown in Table 15. This value is 2 to 3 orders of magnitude smaller than the diffusion coefficient of the matrix atoms[60]. Such a high magnitude of diffusion coefficient may be attributed to the following reasons. Firstly the deformation mechanism proposed by Ansell and Weertman's[47] model may not be true. Therefore the creep rate equation of $\dot{\varepsilon}_s = \pi b^3 \sigma D/2\ KTd^2$, which was derived from above model may not be reasonable for use in calculating the value D. Secondly, according to Harris[51] and Burton[52], during diffusional creep of two-phase alloys, the linear relationship between creep rate and applied stress is lost

the above creep rate equation is replaced by the equation

$$\dot{\varepsilon}_s = B\ D\ b^3(\sigma_a - \sigma_o)/d^2KT \qquad (2.17)$$

5.3.2 Effect of particle size on threshold stress.

The results in table 7 and Figure 37 show that the particle size affects the back stress. In the present investigation the effect of particle size on back stress has been studied only in the low stress region of $\sigma_a < 720$ MN/m^2, where diffusional creep processes predominate. The results show that the threshold stress, $\sigma_{o(th)}$ increases with increasing particle size in the underaged region and then decreases with further increase in particle size. In some regions however, where the γ" particle size is between 15 to 45 nm, the values of $\sigma_{o(th)}$ are not very sensitive to the particle size, i.e., the value of $\sigma_{o(th)}$ is between 564 and) MN/m^2. There are several theoretical models to predict he threshold stress during diffusional creep[51,52,67,69]. Ashby's grain boundary edge dislocation climb model predicted that $\sigma_{oA} = (2\Gamma/br_p)V^{1/2}$[67,69]. Harris[51,69] assumed that the particle/matrix interface is not a perfect source and sink for vacancies. Therefore, the stress concentration built up at particles due to the vacancy condensation on the surrounding regions of the interface can only be relaxed by the formation of prismatic dislocation loops. This model predicted that $\sigma_{oH} = (2\Gamma/br_p)\,V$. Burton's model[52] predicted $\sigma_{oB} = (\pi\,\Gamma^2/55\,b\,KT)V$, which was calculated by balancing the rate of nucleation of interfacial defects at the particles and the rate of vacancy condensation at the grain boundaries. G is the shear modulus, b is the Burgers vector, r_p is particle radius, V is the volume fraction of precipitates, and Γ is the dislocation line energy given by

$\Gamma = \alpha G b^2$, where $\alpha = 0.5 \sim 1$. Burton's model predicts that threshold stress is independent of particle size when $r_p > r_{Pcritical}$. This is not in agreement with experimental results of the present study. In order to compare the experimentally measured value of $\sigma_{o(th)}$ with the theoretical values, the calculated values of σ_{oA} and σ_{oH} as well as the measured values of $\sigma_{o(th)}$ are listed in Table 16. The data presented in Table 16 show that, in the underaged region and in the slightly overaged region the measured threshold stresses, $\sigma_{o(th)}$, are comparable to the values predicted by the model of Harris, σ_{oH} (for $d\gamma'' < 32.6$ nm and $d\gamma' < 18.4$ nm when specimens were aged at 998 K for less than 25 hrs). This implies that the prismatic dislocation loop formation mechanism is predominant in this particle size region. When particle sizes are greater than this value, i.e., the aging time is longer than 25 hrs at 998 K, the measured value of $\sigma_{o(th)}$ is comparable to the value predicted by Ashby's model σ_{oA}. This suggests that in the large particle size region, grain boundary edge dislocation climb may be the rate-controlling process. The rapid decrease of $\sigma_{o(th)}$ with decreasing particle size in the very small particle size region can be attributed to the small volume fraction of precipitates.

The results of this investigation show that the creep deformation behaviour and creep mechanism for Inconel 718 depend on many factors, such as, testing temperature, applied stress, particle size of γ'' and γ' phases, intrinsic

Table 16 The experimental measured back stress, $\sigma_{o(th)}$ and calculated σ_{oA} and σ_{oH} from Ashby's model and Harris' model. Specimens were tested at 873 K and stress range of 620 MN/m^2 ~ 720 MN/m^2.

aging time(hrs) at 998 K	particle size $d\gamma'$(nm)	measured σ_o(MN/m^2)	calculated σ^*_{oA} $\alpha = 0.5$	$\alpha = 1$	calculated σ^*_{oH} $\alpha = 0.5$	$\alpha = 1$
1	6.5	467	1457	2914	420	841
3	9.2	564	1355	2710	507	1014
5	11.0	590	1234	2468	502	1005
7	12.3	600	1103	2206	450	899
10	13.7	600	991	1982	404	808
15	15.7	576	864	1729	352	704
25	18.4	564	738	1476	301	602
50	23.0	538	590	1180	241	482
100	29.2	522	465	930	189	378
200	36.0	472	377	754	154	308
400	46.0	416	295	590	120	241

$b = 2.54 \times 10^{-10}$ m

$G = 65.6$ GN/m^2 [100] ($E = 25 \times 10^6$ psi $G = \frac{3}{8} E$)

* $V = 0.166$ [92] when aging time $t \geq 5$ hrs. $V_{1\ hrs} = 0.082$. $V_{3\ hrs} = 0.14$.

properties of matrix and γ'' and γ' precipitates, and the state of grain boundary. The high resistance to creep which is the main reason for the wide application of this alloy in high temperature applications is attributed to high values of the back stress.

CHAPTER 6 CONCLUSIONS

1. The steady state creep rate, $\dot{\varepsilon}_s$, of Inconel 718 decreases with increase in the particle sizes of the γ'' and γ' phases until critical particle sizes are reached. The creep rate then increases with further increase in particle sizes. The optimum particle sizes for high temperature creep are slightly smaller than that for room temperature yield strength. The low creep rate of peak aged material (aged ~ 10 hrs at 998 K) crept at high temperature is attributed to the optimum particle sizes of strongly bounded, coherent, ordered BCT γ'' and FCC γ' precipitates. The dependence of $\dot{\varepsilon}_s$ on particle size, $d\gamma''$, for the underaged condition agrees with Ansell and Weertman's as well as McLeans' theoretical model. The dependence of $\dot{\varepsilon}_s$ on particle size in the overaged condition agrees with Grant and McLean's stored energy model.

2. For the testing condition employed, i.e. a temperature range of 853 K to 943 K and an applied stress of 620 - 865 MN/m^2, the value of the apparent stress exponent, n_a, and activation energy, Q_c, for the creep rate equation

$$\dot{\varepsilon}_s = A\sigma_a^{n_a} \exp(-Q_c/RT)$$

were between 8.57 to 15.93 and 349.5 to 370.9 KJ/mol, respectively. The values of the effective stress exponent, n_e,

and activation energy, Q_e, for the creep rate equation

$$\dot{\varepsilon}_s = A_1 \left(\frac{Gb}{KT}\right)\left(\frac{\sigma_a - \sigma_o}{G}\right)^{n_e} \exp\left(-Q_e/RT\right)$$

were between 1.12 to 5.65 and 249.4 to 296.8 KJ/mol, respectively.

3. The values of effective stress exponent and activation energy show that the creep deformation mechanism of Inconel 718 alloy changes from linear law or diffusional creep ($n_e \simeq 1$) to dislocation power law creep ($n_e \simeq 3$ to 6) when the temperature or applied stress is increased. The experimental results also reveal that there is a transition region between the diffusional creep and the dislocation power law creep regions. This transition is attributed to the occurrence of non-uniform power law creep within the grains as the temperature or applied stress is changed gradually from the linear law creep region to the dislocation power law creep region.

4. The threshold stress, $\sigma_{o(th)}$, during diffusional creep and the back stress, σ_o, during dislocation power law creep for Inconel 718 have been found to be as high as 0.6 ~ 0.9 σ_a in the stress range of 620 to 865 MN/m^2 and in the temperature range of 853 to 943 K. The magnitude of the

applied stress, the testing temperature and the γ'' and γ' precipitate particle sizes affect the magnitude of the back stress for creep of Inconel 718 superalloy.

(a) In the diffusional creep region, there exists a threshold stress, $\sigma_{o(th)}$, which is independent of the applied stress, and in the dislocation power law creep region the back stress is proportional to the applied stress, i.e., $\sigma_o \alpha \sigma_a$.

(b) The back stress decreases with increase in temperature, which is attributed to the dependence of the shear modulus on temperature.

(c) The threshold stress increases with particle size in the underaged condition and decreases with increase in particle size in the overaged condition. A comparison of the theoretical values of back stresses calculated from Harris and Ashby's models, σ_{oH} and σ_{oA}, with the measured values of threshold stress, $\sigma_{o(th)}$, in the present investigation confirms that in the small particle region prismatic dislocation loop formation at the precipitate/matrix interface is the rate controlling process. In the large particle size region grain boundary edge dislocation climb over γ'' and γ' precipitates at grain boundaries is the rate controlling process.

REFERENCES

1. "Alloy and Microstructure Design" edited by J.K. Tien and G.S. Ansell. Academic Press, 1976.

2. K. Sadananda and P. Shaliman: Met. Trans. A, Vol. 8A, 1977, p. 439.

3. D.F. Paulonis, J.M. Oblak and D.S. Duvall: Trans. ASM., 1969, Vol. 62, p. 611.

4. M.C. Chaturvedi and Y. Han: Met. Sci., 1983, Vol. 17, p. 145.

5. Y. Han, P. Deb and M.C. Chaturvedi: Met. Sci., 1982, Vol. 16, p. 555.

6. O.D. Sherby and P.M. Burke: Progr. Mater. Sci., 1968, Vol. 13, p. 325.

7. A.K. Mukherjee: "Treatise on Materials Science and Technology". Vol 6 - Plastic Deformation of Materials, edited by R.J. Arsenault, 1975.

8. R. Lagneborg: International Met. Rev., 1972, Vol. 11, p. 130.

9. O.D. Sherby, J.L. Lytton and J.E. Dorn: Acta. Met., 1957, Vol. 5, p. 219.

10. H. Conrad: J. Metals, July 1964. p. 582.

11. S.N. Zhurkov and T.P. Sanfirova: Soviet physics - Tech. physics, 1959, Vol. 3, p. 1586.

12. T.A. Trozera, O.D. Sherby and J.E. Dorn: Trans. ASM., 1957, Vol. 49, p. 173.

13. N. Jaffe and J.E. Dorn: Trans. AIME., 1962, Vol. 224, p. 1167.

14. T.S. Lundy and J.F. Murdock: J. Appl. phys., 1962, Vol 33. p. 1671.

15. J. Weertman: J. Appl. phys., 1957, Vol. 28, p. 362.

16. J.P. Poirior: Metallurgica, 1978, Vol. 26, p. 629.

17. M.F. Ashby and H.J. Frost: "Constitutive Equations in Plasticity" edited by Ali. S. Argon, Cambridge, Mass. MIT Press, 1975.

18. F.R. Nabarro: Rep. Conf. Strength of Solids, London, p. 75, 1948.

19. C. Herring: J. Appl. phys., 1950, Vol. 21, p. 437.

20. R.L. Coble: idib, 1963, Vol. 34, p. 1679.

21. G.B. Gibbs: Phil. Mag. [8], 1966, Vol. 13, p. 589.

22. D. McLean: Met. Rev., 1962, Vol. 7, p. 481.

23. C.R. Barrett and W.D. Nix: Acta Met., 1965, Vol. 13, p. 1247.

24. J.W. Martin: "Micromechanisms in particle-hardened alloys", Cambridge Univ. Press, 1980.

25. G. Gernasconi and G. Piatti: "Creep of Engineering Materials and Structures", A.S.P. Ltd., London, 1979.

26. F. Garofalo: "Fundamentals of Creep and Creep-Rupture in Metals", 1965, New York, SC (Macmillan).

27. F. Garofalo: Trans. AIME., 1963, Vol. 227, p. 351.

28. F.H. Norton: "The Creep Steels at High Temperature". McGraw Hill, New York and London, 1929.

29. J.G. Harper and J.E. Dorn: Acta, Met., 1957, Vol. 5, p. 654.

30. C.R. Barrett and O.D. Sherby: Trans. AIME., 1965, Vol. 233, p. 116.

31. C.R. Barrett, AS.J. Ardell and O.D. Sherby: Trans. AIME, 1964, Vol. 230, p. 200.

32. J. Weertman: Trans. AIME., 1965, Vol. 233, p. 2069.

33. J. Weertman: J. Appl. phys., 1955, Vol. 26, p. 1213.

34. C.R. Barrett, J.L. Lytton and O.D. Sherby: Trans AIME., 1967, Vol. 239, p. 170.

35. AS.K. Mukherjee, J. E. Bird and J.E. Dorn: Trans. ASM., 1969, Vol. 62, p. 155.

36. H.J. McQueen and J.E. Hockett: Met. Trans., 1970, Vol. 1, p. 2997.

37. R.W. Bailey: J. Inst. Met., 1926, Vol. 35, p. 27. (quoted in Ref. 25).

38. E. Orowan: J. West Scotland Iron and Steet Inst., 1946 - 1947. Vol. 54, p. 45. (quoted in Ref. 5).

39. D. McLean: Rep. Prog. phys., 1966, Vol. 29, p. 1.

40. D. McLean and H.F. Hale: "Structural processes in Creep", 1961, p. 19, Iron and Steel Institute, London.

41. R. Lagneborg: Trans. ASME., April 1976, p. 1114.

42. N.F. Matt: A Discussion of some Models of Rate-Determining process in creep. Proc. Conf. on Creep and Fracture of Metals at High Temperatures, London, 1956, p. 21.

43. C.T. Sims and W.C. Hagel: "The Superalloys", 1972, John Wiley & Sons Inc. p. 101.

44. Second International Conference on the Strength of Metals and Alloys. 1970, Vol. 3, p. 1011 - 1027.

45. G.S. Ansell and F.V. Lenel: Trans Metall. Soc. AIME., 1961, Vol. 221, p. 452.

46. R. Lagneborg: Met. Sci. J., 1969, Vol. 3. P. 18.

47. G.S. Ansell and J. Weertman: Trans. Met. Soc. AIME., 1959, Vol. 215, p. 838.

48. A.H. Caluer and B.A. Wilcox: Met. Sci. J., 1967, Vol. 1, p. 86.

49. N.J. Grant: "The Strengthening of Metals", edited by Pecker, New York, 1964, p. 163.

50. J.E. Harris, R.B. Jones, G.B. Greenwood and M.J. Ward: J. Austraslian Inst. Metals, 1969, Vol. 14, p. 154.

51. J.E. Harris: Met. Sci. J. 1973, Vol. 7, p. 1.

52. B. Burton: Mat. Sci. Eng., 1973, Vol. 11, p. 337.

53. B. Burton: Met. Sci. J., 1971, Vol. 5, p. 11.

54. L.K. Singhal and J.W. Martin: Scripta Met., 1967, Vol. 1, p. 181.

55. P.L. Threadgill and B. Wilshire: Metal Sci., 1974, Vol. 8, p. 117.

56. K.E. Amin and J.E. Dorn: Acta. Metall., 1969, Vol. 17, p. 1429.

57. J.P. Dennison and R. Stevens: Scr. Metall., 1970, Vol. 4, p. 421.

58. K.R. William and J.R. McLauchlin: J. Mater. Sci., 1970, Vol. 5, p. 1063.

59. B.A. Wilcox, A.H. Clauer and W.S. Mccare: Trans. Metall. Soc. AIME, 1967, Vol. 239, p. 1791.

60. R.W. Lund and W.D. Nix: Acta Metall., 1976, Vol. 24, p. 469.

61.C. Carry and J.L. Strudel: ibid, 1978, Vol. 24, p. 859.

62. J.D. Parker and B. Wilshire: J. Met. Sci., 1975, Vol. 9, p. 248.

63. P.W. Davies, G. Nelines, K.B. Willams and B. Wilshire: ibid, 1973, Vol. 7, p. 87.

64. J.D. Parker and B. Wilshire: ibid, 1978, Vol. 12, p. 453.

65. D. Sidey and B. Wilshire: ibid, 1969, Vol. 3, p. 56.

66. O.D. Sherby: Acta. Met., 1962, Vol. 10, p. 135.

67. J.C. Gibeling and W.D. Nix: Mat. Sci. Eng., 1980, Vol. 45, p. 123.

68. M.F. Ashby: Scripta Met., 1970, Vol. 4, p. 171.

69. B. Burton and W.B. Beere: Met. Sci., 1978, Vol. 12, p. 71.

70. B. Burton: Mat. Sci. Eng., 1972, Vol. 10, p. 9.

71. A. Horsewell: Scr. Mettall., 1979, Vol. 13, p. 21.

72. M.F. Ashby: "Strengthening Methods in Crystals", edited by A. Kelly and R.B. Nicholson. p. 137, 1971, New York.

73. C.N. Ahlquist and W.D. Nix: Acta, 1971, Vol. 19, p. 373.

74. P. Ostrom and R. Lagneborg. Trans. ASME, April 1976, p. 114.

75. S.K. Mitra and D. McLean: Met. Sci. J., 1967, Vol. 1, p. 192.

76. R. Lagneborg: ibid, 1969, Vol. 3, p. 161.

77. G. Helmes and B. Wilshire: Scr. Metall., 1976, Vol. 10, p. 697.

78. W.J. Evans and G.F. Harrison: Met. Sci., 1976, Vol. 10, p. 307.

79. W.J. Evans and G.F. Harrison: Scr. Metall, 1975, Vol. 9, p. 239.

80. C.N. Ahlquist and W.D. Nix: Scr. Metall., 1969, Vol. 3, p. 679.

81. A.A. Solomon and W.D. Nix: Acta. Metall., 1970, Vol. 18, p. 863.

82. D.J. Lloyd and J.D. Embury: Met. Sci. J., 1970, Vol. 4, p. 6.

83. S. Purushothaman and J.K. Tien: Acta. Metall, 1978, Vol. 26, p. 519.

84. J.H. Hausselt and W.D. Nix: ibid, 1977, Vol. 25, p. 595.

85. B.A. Wilcox and A.H. Clauer: Trans. Met. Soc. AIME, 1966, Vol. 236, p. 570.

86. L.M. Brown and R.H. Ham: "Strengthening Methods in Crystals", edited by A. Kelly and R.B. Nicholson, ASP. London, 1972, p. 12.

87. R.S.W. Shewfelt and L.M. Brown: Philos. Mag., 1977, Vol. 35, p. 945.

88. J.K. Tien and R.P. Gamble: Metall. Trans., 1972, Vol. 3, p. 2157.

89. G.M. Pharr and W.D. Nix: Scr. Metall., 1976, Vol. 10, p. 1007.

90. R.S.W. Shewfelt and L.M. Brown, Philos. Mag., 1974, Vol. 30, p. 1135.

91. J.D. Whittenberger: Metall. Trans. A, 1977, Vol. 8, p. 1155.

92. YaFang Han: Master thesis, Univ. of Manitoba, Canada, 1982.

93. K.R. Williams and B. Wilshire: Met. Sci., 1983, Vol. 17, p. 145.

94. G.L. Kehl: "The principles of Metallurgraphic Laboratory practice", McGraw-Hill Book Company Inc., 1949, p. 293-298.

95. J.P. Dennison, R.J. Llewellyn and B. Wilshire: J. Inst. Metal, 1967, Vol. 95, p. 115.

96. Z. Herita and T.G. Langdon: Proceedings of the Second International Conference on Creep and Fracture of Engineering Materials and Structures, edited by B. Wilshire and D.R.J. Owen, Pineridge Press, 1984, p. 75-87.

97. J. Gittus: "Creep Viscoelasticity and Creep Fracture in Solid". London, Applied Science Publishers, 1975, p. 14 - 41.

98. J.M. Oblak, D.F. Paulonis and D.S. Duvall: Metall. Trans., 1974, Vol. 5, p. 143.

99. D. Hull: "Introduction to Dislocations". Pergamon Press, 1975, p. 188-190.

100. C.T. Sims and W.C. Hagel: "The superalloys", 1972, John Wiley & Sons Inc. p. 111.